

We are committed to providing [accessible customer service](#).

If you need accessible formats or communications supports, please [contact us](#).

Nous tenons à améliorer [l'accessibilité des services à la clientèle](#).

Si vous avez besoin de formats accessibles ou d'aide à la communication, veuillez [nous contacter](#).

# **Report on IP Geophysics at the Ranoke Project, Ontario**

Mulholland, Pickett & Morrow Townships,  
Porcupine Mining Division,  
Northeast Region, Ontario  
Map Sheet: 42112

**Exploration Plan Submission, PL-19- 000002**

Author:

Justin J. Daley, MSc, PGeo  
Exploration Manager & Chief Geologist  
VR Resources Ltd.

April 2021

VR RESOURCES LTD.  
1750 – 700 West Pender St.  
Vancouver, BC, Canada, V6C1G8  
Web: [www.vrr.ca](http://www.vrr.ca)



Report on Quantec Titan24 IP at Ranoke Project	2
--	---

## **Table of Contents**

List of Figures & Tables	2
Appendix A	2
Appendix B	2
<b>Summary</b>	3
Location and Access	4
Regional Geology and Exploration History	5
Property Exploration History	9
Property Geology	9
Exploration Model	10
Certificate	13
References	14

## **List of Figures & Tables**

Figure 1: Location and access to the Ranoke Property	5
Figure 2: Location of assessment report database drillholes	7
Figure 3: Regional geology map of Kapuskasing structural zone (KSZ)	8
Table 1: Summary of major geological/tectonic events shaping the study region.	9
Figure 4: Total magnetic field at Ranoke	100
Figure 5: Schematic section of the exploration target at Ranoke.	111

## **Appendix A**

CA01199T Quantec Summary Report

## **Appendix B**

Expense Report

### Summary

This report presents the Property and Geological background information that accompanies the logistics and geophysical analysis report in Appendix A for the Titan 24 DCIP survey completed from August 23 to September 8, 2019 over the Ranoke Property by Quantec Geoscience Ltd. on behalf of VR Resources. The goal of the survey was to map chargeability and resistivity as an analogue for potential disseminated sulfide mineralization on the Ranoke Property to define targets for drill testing.

The report describes the instrumentation, data acquisition and processing procedures, final data formats and contents of the digital archives, as well as the procedures for data analysis and interpretation. The final processed data are presented as pseudo-depth plots of apparent resistivity and chargeability, and the inversion models are presented in relation to the survey objectives and significance to future exploration.

A total of 3 profiles were surveyed. Data were processed and inspected for quality assurance on site and reviewed daily by the geophysicist in charge of the project. The 3 profiles were subsequently inverted to generate resistivity and chargeability models.

The final processed survey results delivered with the report include:

- GPS Data
- Multi-site ASCII survey files
  - Each file includes location (Latitude/Longitude, projected UTM and GRID coordinates)
- Direct Current (DC) and Induced Polarisation (IP) Data
  - CSV formatted files
  - Each file includes electrode locations (GRID coordinates), normalised Potential (V) and measured phase (radians or milliradians) for all readings on the line.
- 2D inversion models of all the profiles, for Resistivity, DC-referenced chargeability, and HS-referenced chargeability
  - Geosoft databases and maps files, PNG images.

**\*\*All maps, figures and coordinates are in UTM WGS84 Zone 17\*\***

## Location and Access

The Ranoke property is in the Moose River basin in northern Ontario, Canada. It is located between the Mattagami and Missinaibi rivers. The nearest town is Moosonee located on tide water some 111 kilometres to the northeast at James Bay. Cochrane is the regional services hub and is located 180 kilometres to the southeast, on the Trans-Canada Highway (Provincial HWY 11). The property is 15 kilometers west of the active ONR railway line which connects the town of Moosonee with the Cochrane on the Trans Canada Highway, thus providing port access to the James Bay region (Figure 1).

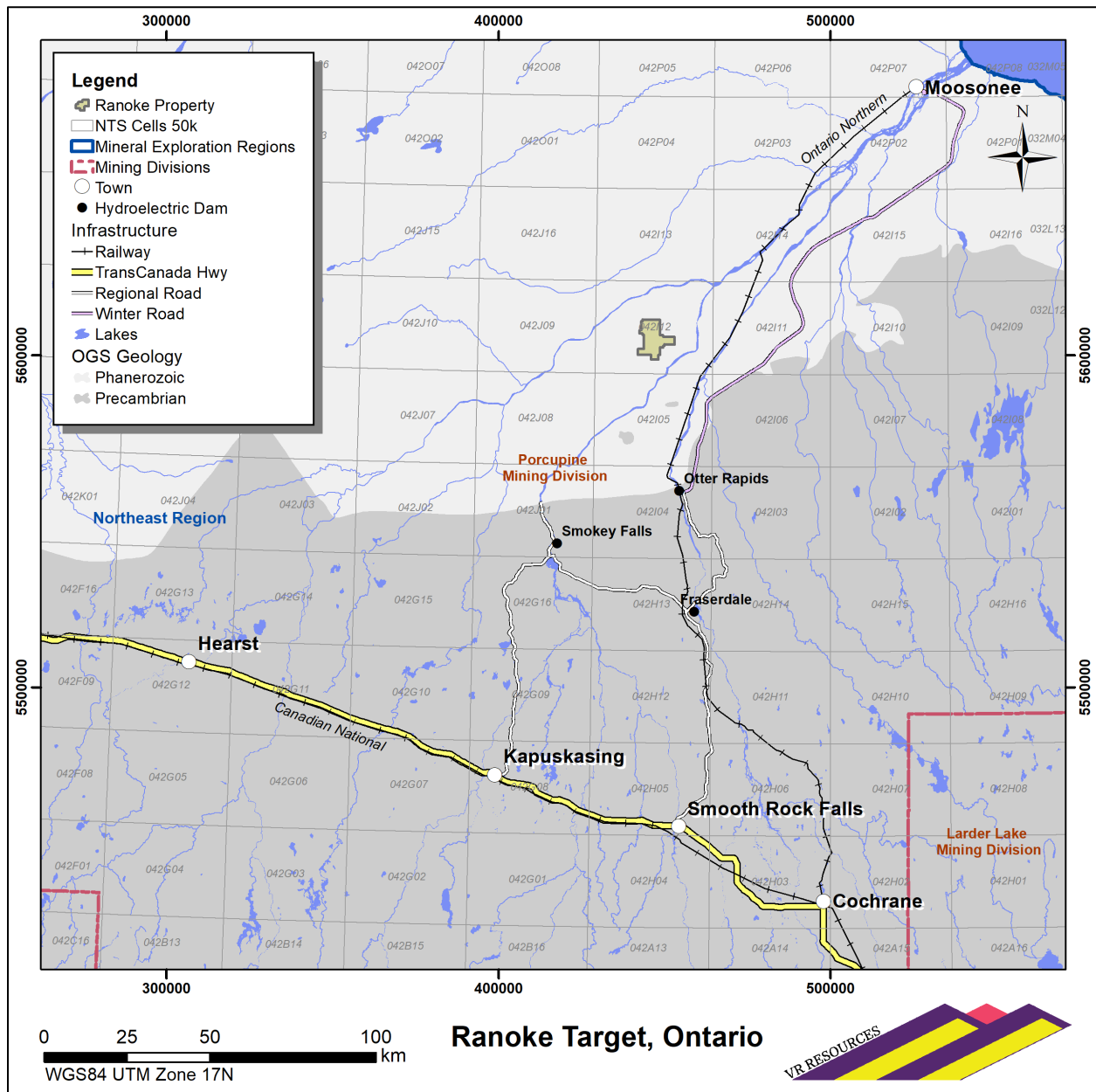


Figure 1: Location and access to the Ranoke Property

Otter Rapids Dam is an Ontario hydroelectric facility located on the Abitibi River about 50 kilometres to the south of the property. Provincial Highway 634 provides road access to Otter Rapids from Smooth Rock Falls, located at the junction of HWY 634 with the Trans-Canada Highway. Private ground just behind the ONR bunk house was rented from Villeneuve Construction and served as camp and helicopter base for crews during drilling. Helicopter access to the property from camp is about 50km each way

The Ranoke property is located in a boreal region of lowland muskeg, with black spruce and pine forest along river drainages. Topographic relief is minimal, and there is no outcrop in the lowland region; Ranoke is tens of kilometres north of the northern limit of exposed Archean Superior Province shield in northern Ontario.

## **Regional Geology and Exploration History**

The Moose River Basin has a varied, checkerboard history of mineral exploration for the past 100 years. Cretaceous coal seams were the focus at the turn of the previous century, while diamond exploration has dominated in the region during the past 60 years (Figure 2). This section was adapted from the 2006 Coral Rapids Assessment Report for Baltic Resources.

Overall, exploration in the region is hindered by the lack of outcrop in the boggy, lowland terrain, and by the cover of up to 400 metres of mid-Paleozoic (Devonian) marine shelf strata and Cretaceous in-land basinal strata overlying Archean basement. Archean VMS and Proterozoic orogenic gold deposits occur in the surrounding sub-provinces of the Superior craton, but there are no active base metal or precious metal mines in the Moose River Basin region. The Attawapiskat diamond mine (“Victor”) of DeBeer’s located well to the north along the Attawapiskat River has reached the end of its mine life after more than a decade in production.

The oldest mineral exploration in the Moose River region relates to coal, which is documented as far back as 1672 when the Abitibi River was part of an important fur trading route linking Hudson Bay with the Great Lakes. There are lignite occurrences exposed in the banks of the Abitibi River north of Coral Rapids. The coal seams were first studied in detail by the Geological Survey between 1871 and 1912. They extend westward from the Abitibi River within the confines a small Cretaceous successor basin named the Moose River Basin which is less than 50 kilometers in diameter. More than one hundred shallow drill holes were completed by the Ontario Department of Mines between 1926 and 1930 to evaluate the resource, leading ultimately to the completion of two shafts and some 389 metres of interconnecting drifts. Drilling resumed in the early 1950’s with the completion of an additional 182 holes. In 1981, the Ontario Energy Corporation re-visited the potential of the coal and evaluated lignite stratigraphy farther to the west, in the region between the Mattagami and Missinaibi rivers. Hundreds of shallow drill holes were completed on a lease which exceeded 1 million acres. Drill holes were completed around, but not on, VR’s current Ranoke copper-gold property.

Diamonds have been the focus of modern mineral exploration in the James Bay region. Exploration started in the 1960’s by DeBeers (Monoprose Canada), focused initially in the

Attawapiskat River region well to the north of the Moose River Basin, and built on the pioneering regional aeromagnetic program of the Geological Survey of Canada. Ongoing and extensive regional till and alluvium heavy mineral sampling and high-resolution magnetic surveys through the late 1980's eventually led to the discovery of numerous kimberlite pipes, including Victor.

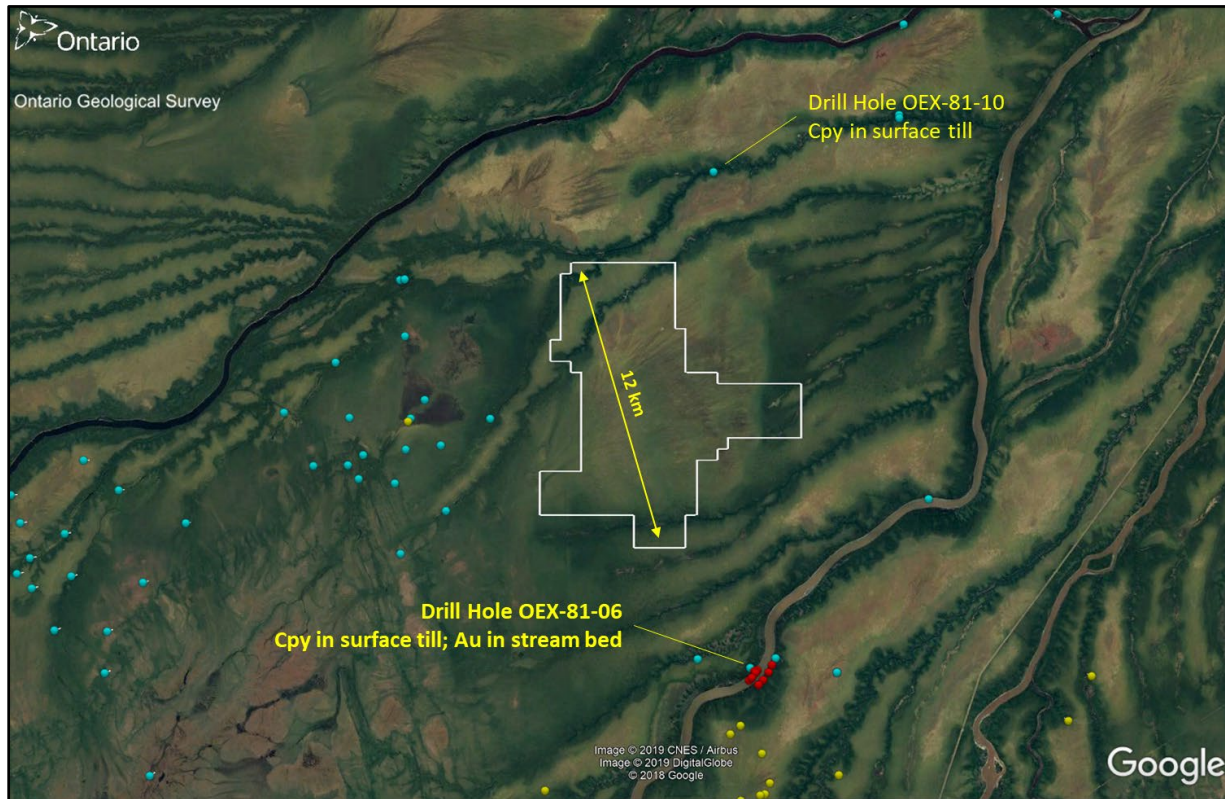


Figure 2: Location of assessment report database drillholes near the Ranoke Property. Teal pins to SW and NE of Ranoke represent drilling for coal by ONEXCO in 1981-1983, whereas red pins to south represent a soil auger campaign by them in 1982 following up on gold frains found in nearby heavy mineral separates from RC Drilling. Yellow pins to south represent kimberlite exploration during the 70s-90s.

The Ranoke property is near the southeastern margin of the Paleozoic Hudson Platform of Devonian marine strata. The property is within the Moose River Basin, a small, Cretaceous successor basin less than 50 kilometres across and located at the southeastern-most margin of the Paleozoic platform. Devonian and Cretaceous strata in the Moose River area were deposited on a gneissic crystalline basement of metamorphosed sedimentary assemblages and lesser volcano-plutonic complexes of the English River sub-Province, in what is believed to be the thickest part of the Archean Superior craton.

The Ranoke property occurs on the western margin of the Kapuskasing Structural Zone (KSZ), a crustal-scale shear zone which bisects the Superior craton in a complex, northeast-southwest trending zone of uplifted, high grade metamorphic rocks extending for more than 500 kilometres between Lake Superior and James Bay. There is believed to be more than 20 kilometres of

vertical crustal displacement along the KSZ. It is clearly defined by positive gravity and magnetic domains on regional geophysical maps.

The KSZ has a long-lived history of repeated ultra-basic, alkaline and carbonatite intrusions and kimberlite facies diatremes which collectively span 1.6 billion years of earth history, to as young as 125 million years ago. Intrusions in and around Coral Rapids and along the western margin of the KSZ where Archean rocks are exposed in major river drainages such as the Abitibi have been explored since the early 1960's, and many have been age-dated (Figure 3).

Selection Trust (later named Selco) began alluvial sampling in the KSZ region in 1962 and were joined by Esso Minerals in 1979. The first composite kimberlite – lamprophyry dyke was drilled in 1967, followed by drilling of the Valentine carbonatite complex in 1969. Between 1979 and 1983, the Selco – Esso partnership completed regional heavy mineral sampling of till and alluvium over an area exceeding 100,000 hectares, and an aeromagnetic program launched in 1980 led to the identification of numerous post-Paleozoic, pipe-like anomalies, of which 45 were drill-tested; most were ultra-basic and alkaline intrusions, non copper-bearing, and four were kimberlite-facies diatremes.

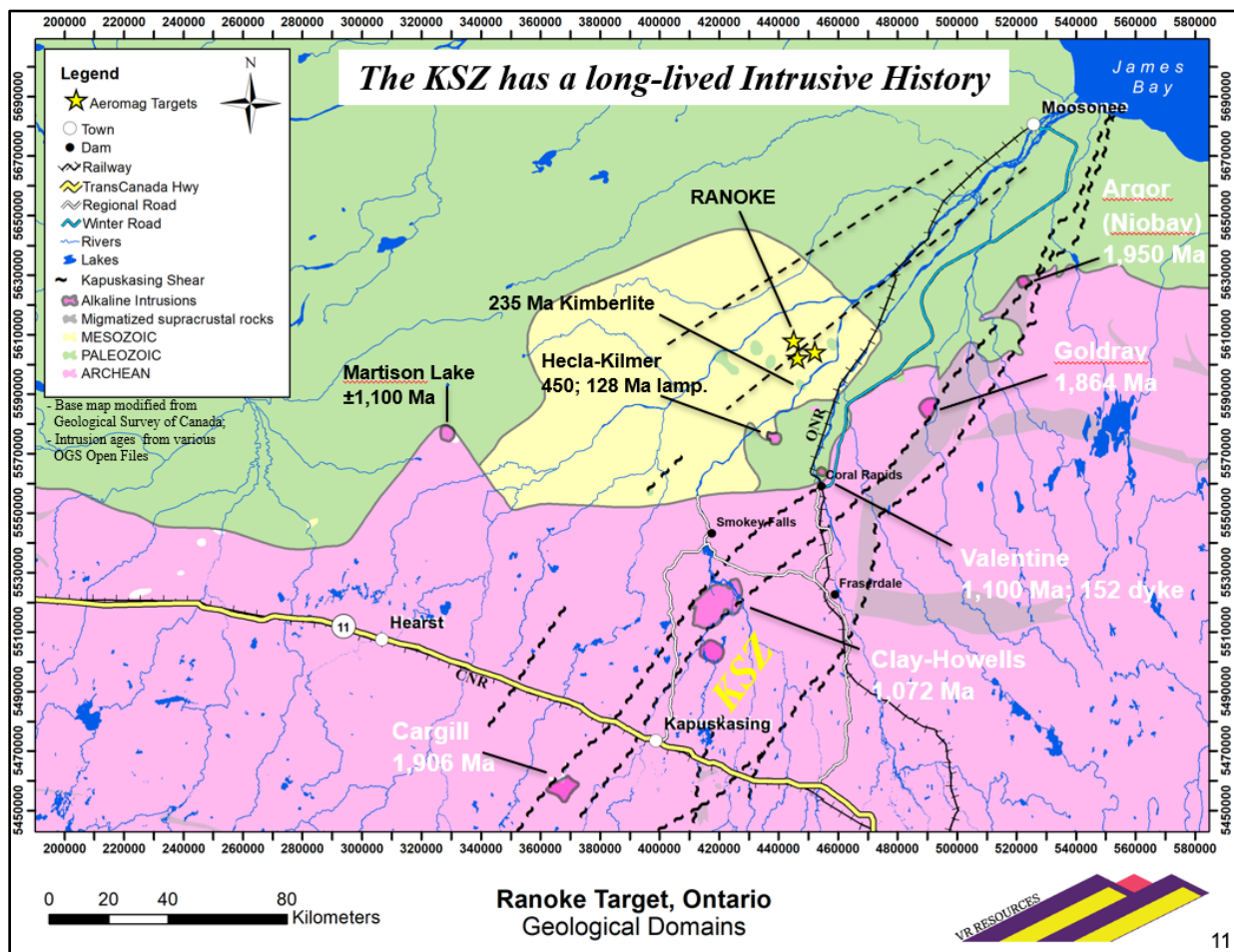


Figure 3: Regional geology map of Kapuskasing structural zone (KSZ) and James Bay Lowlands with alkaline and ultrabasic intrusions and their ages highlighted. The Ranoke target is noted by 3 gold stars indicating magnetic targets.



The Aquitane Company of Canada Ltd. completed airborne and ground geophysics between 1972 and 1974 to evaluate the hydro-carbon potential of Paleozoic strata, and twelve diamond drill holes to test for base metal, Mississippi Valley Type mineralization. A kimberlite west of Coral Rapids and south of Ranoke was also detected, delineated and drill-tested during this work. In 1978, Kerr-Addison Mines complete a series of reverse circulation drill holes near Coral Rapids to test exposed basal sandstone at the eastern edge of the Hudson Platform for uranium. These targets were re-visited and re-tested in 2006, during the re-surgent uranium exploration sector.

Regional-scale exploration in the KSZ - Moose River Basin region waned after 1983. Various small-scale airborne magnetic surveys and ground-based EM surveys, and local alluvium sampling programs were completed at the property-scale between 1983 and 2006, with the focus mostly on previously known, ultra-basic and alkaline intrusions and diatremes exposed at surface in and around Coral rapids, but also on limestone for industrial mineral applications.

Lastly, one high resolution airborne magnetic survey was completed north of Ranoke in 2014. The survey targeted kimberlite anomalies over an area of approximately 1,600 square kilometres.

Sixty years after modern mineral exploration arrived in the region, VR is focused on a specific, unexplored and untested geophysical anomaly and integrated target for a post-Archean intrusion or hydrothermal pipe with copper and gold located in a lowland terrain with no outcrop and no roads, and in a geologic domain where the Archean Superior shield is covered by a thin veneer of Paleozoic and Mesozoic rocks of the Hudson Platform and Moose River Basin respectively.

*Table 2: Summary of major geological/tectonic events shaping the study region. (Darbyshire et al., 2017)*

Date	Event
3–2.6 Ga	Assembly of Superior Craton
2.8–2.6 Ga	Kenoran Orogen completes assembly process
2.49–2.45 Ga	Hotspot influence and rifting on SE Superior margin leads to emplacement of Matachewan dyke swarm
2.2 Ga	Age of Southern Province; Nipissing Sills fed by distant Ungava plume
1.9–1.6 Ga	Penokean Orogen on southern margin of Superior Province; likely age of major uplift in Kapuskasing Structural Zone
~1.8 Ga	Trans-Hudson Orogen on northwest Superior margin
~1.1 Ga	Keweenaw Mid-Continent Rift on southern Superior margin
1.1–1.0 Ga	Grenville Orogen on southeast Superior margin
Late Proterozoic - Early Cambrian	Opening of Ottawa-Bonnechere Graben and Lake Timiskaming structural zone (Ontario/Quebec border region)
Phanerozoic	Development of Hudson Bay and Moose River intracratonic basins
180–134 Ma	Emplacement of kimberlites along track of Great Meteor hotspot

## Property Exploration History

The Ranoke target is previously unexplored: it is under cover, it is north of exposed Archean Superior Province shield, and it is north of road access in northern Ontario. The specific area of the Ranoke property does not appear to have been staked before, is not included in any mineral exploration assessment reports filed with the MENDM, and there are no historic drill holes located at Ranoke in the MENDM drill hole database (Figure 2).

## Property Geology

The overburden at the Ranoke Property begins around 210 metres depth at the Archean unconformity with the Upper Silurian Sextant Formation, comprising deep red limonitic sandstones at the weathered erosional contact and grades upward into a coarse reduced arenite. As the basin subsided and the sea prograded in the lower Devonian, clastics were replaced by carbonate muds and chemically precipitated carbonates with coral and stromatoporoid to form the Kwataboahagan Formation. The lower section contains chemically-deposited limestone, primary dolomite and thin muddy breccia. This breccia represents limy mud in evaporitic environments and dissolution features after induration. Several brecciated layers can be traced through several holes in the central and eastern areas of the basin. The upper part shows a definite marine influence and is well differentiated. While the lower part fluctuates from dolomitic to limy, the marine sequence with crinoids, corals and brachiopods is strictly limy.

The Moose River Formation, which conformably overlies the Kwataboahagan, is organic poor carbonate rocks developed with a reefal facies, rich in coral and stromatoporoids and very porous in the lower Murray Island beds. This features seems to have remained into the above formation (Williams Island) as well, though not as well marked. The Murray Island would rather represent a fore-slope with pelletoidal limestone, breccia and some wackestone. Towards the end of the Murray Island time, by reference to carbonate and biogenic sedimentation extended to the whole basin and tended to replace the clayish deposition of the underlying formation. The Williams Island Formation saw a quiet limy environment covering the general area, with its alternances of limestone, primary dolomite and some thin clay. The chemically deposited unfossiliferous strata suggested sabkha environment with its many intricate variations due to local geomorphic changes.

Unconformably overlying the Paleozoic strata at roughly 80m depth is a successor basin of unconsolidated Jurassic to Cretaceous muds, sands and local lignite coal deposition (however not observed in drilling at Ranoke). Recovery in this unit was very low, however plastic blue-grey muds were observed. Although not observed, regional drilling and reports from drillers suggests there were variably boulder-rich sandy tills from 50m to near surface where a layer of marine clay deposited from the post-glacially enlarged Hudson Bay.

The basement geology was the focus of geophysical targeting at the Ranoke property and consists primarily of undifferentiated Archean metasedimentary to metavolcanic paragneisses of the English River subprovince from within the deepest part of the Superior craton, a foliated probable-Archean granodiorite, as well as a wide (100's of metres) diabase/metabasalt intrusions that likely represents the 2.45 Ga Matachewan (NNW trending) and 2.2 Ga Biscotasing (ENE

Trending) dyke systems (See Table 1; Darbyshire et al., 2017, Hall & Davis, 2004) and occur as major structural and magnetic features that intersect on the property (Figure 4).

Variability in the depth to Paleozoic strata as well as changes in the regional TMI magnetic grain are interpreted to be caused by many generations of rifting along the KSZ (see Table 1). Normal faults appear to have formed along the planar margins of the Archean dykes that intersect within the property.

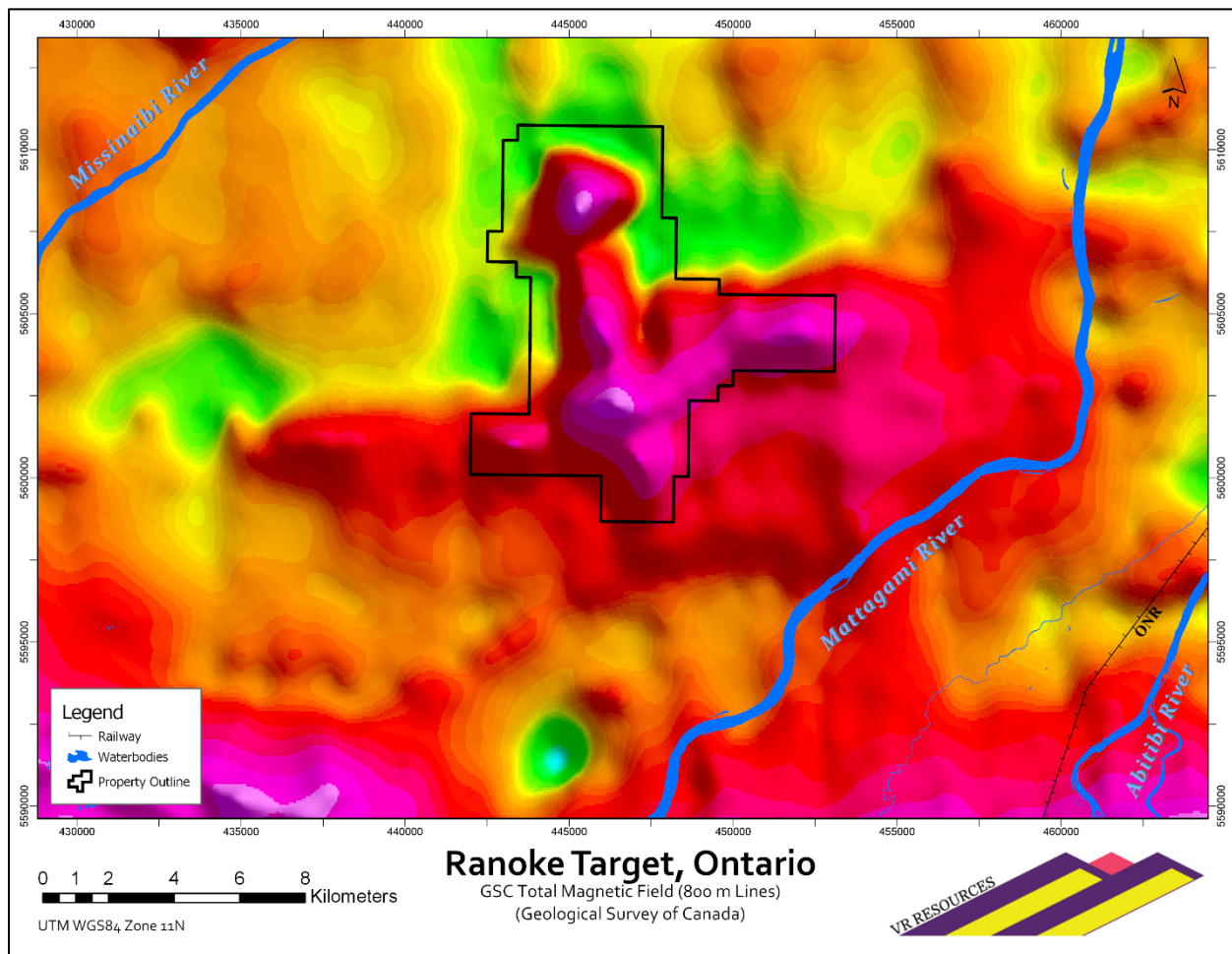


Figure 4: Total magnetic field at Ranoke showing staking over the high-magnetic complex inferred to be the intersection of Archean Mattachewan and Bisotasing dyke swarms. Structural planes along these dykes appear to have been reactivated by rifting providing a conduit for hydrothermal fluids and potential IOCG or carbonatite mineralization.

## Exploration Model

Ranoke is located immediately north of a robust copper-gold-fluorite heavy mineral anomaly evident in several rivers in the Coral Rapids area, based on a regional alluvium survey completed by the Ontario Geological Survey in 2001 and 2002. The unique mineral assemblage underscores

the potential for a buried carbonatite or IOCG deposit (iron oxide copper-gold) as the source of the geochemical anomaly.

The Ranoke property covers a well defined, high intensity magnetic complex approximately 12 x 12 kilometres in size and evident on regional-scale Geological Survey of Canada (GSC) aeromagnetic maps. The complex delineates a regional-scale structural intersection, and individual magnetic anomalies are locally discordant to the regional magnetic grain evident in Archean basement rocks. The high resolution airborne survey completed by VR in 2019 confirmed the location, geometry and intensity of the Ranoke complex evident on the historic GSC maps. The northern magnetic anomaly at Ranoke is both the largest, at > 2.3 km's in diameter, and the highest intensity, at > 1,000 nT. It has a vertical, pipe-like geometry with sharply defined margins and a central apex which is consistent across TMI, RTP and 1VD magnetic products.

The 2019 airborne survey by VR also confirmed the discrete gravity anomaly evident at Ranoke in historic, regional gravity data collected by the Geological Survey of Canada. A singular, 2.5 mgal gravity anomaly is apparent in the 13 x 14 km survey completed by VR. It is co-spatial with the central part of the Ranoke magnetic complex overall, but it is locally discordant to the large, circular magnetic pipe at the north end of the complex.

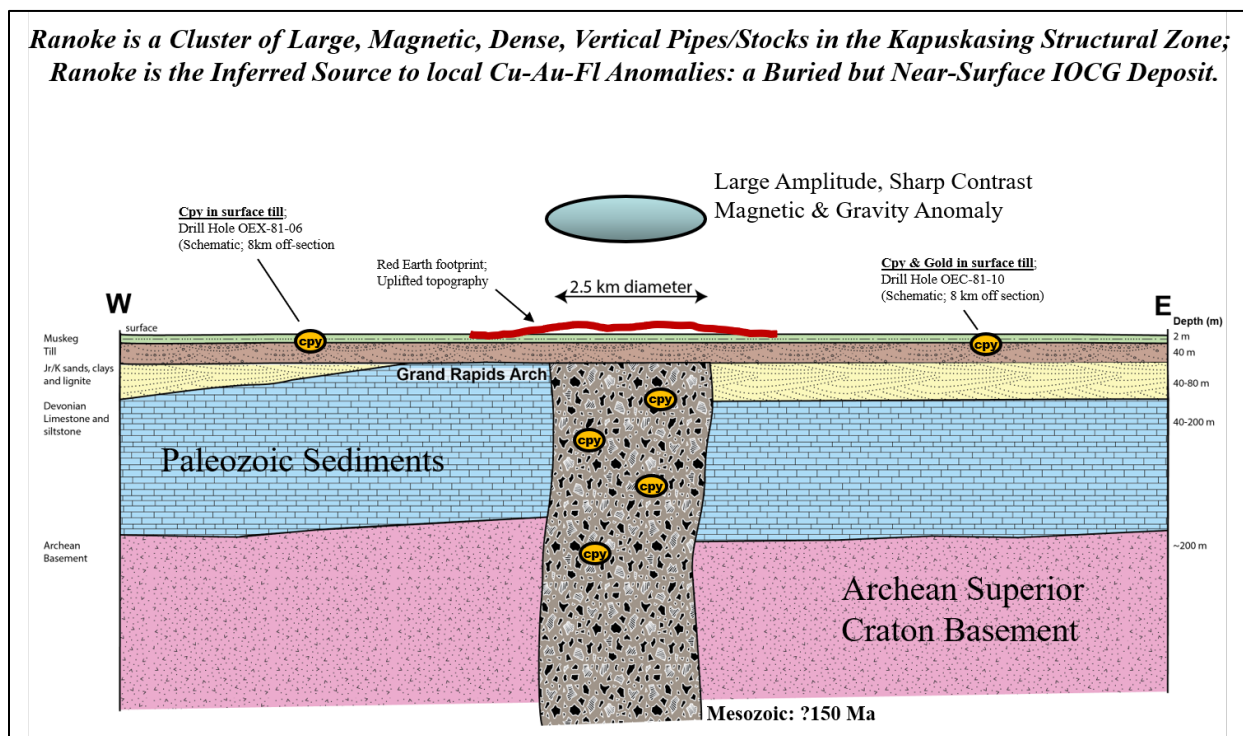


Figure 5: Schematic section of the exploration target at Ranoke.

The schematic cross-section shown in Figure 7 illustrates the target at Ranoke; a near-surface, large, vertical, magnetic, dense IOCG pipe or carbonatite intrusion. This cross-section is a representation of the discrete magnetic anomaly (pipe) at the northern end of the overall magnetic complex and structural intersection at Ranoke. This pipe is potentially the near-surface

but till-covered source to copper and gold grains observed in the unconsolidated overburden in nearby reverse circulation drill holes completed in the early 1980's during a reconnaissance evaluation of Cretaceous-aged coal seams in the Moose River Basin.

## Certificate

1. I, Justin J. Daley, reside at 451 Kingswood Rd., Toronto, Ontario, M4E3P4
2. I have a B.Sc. Honours in Geological Sciences from Queen's University in Kingston, ON (2012) and a M.Sc. in Geology (Mineral Exploration) from Laurentian University in Sudbury, ON (2017).
3. I am a registered Professional Geoscientist in the Province of Ontario as of November 2020, and was registered in the Province of BC for three years prior.
4. I have been involved in all aspects of mineral exploration for 10 years in the United States, Mexico, Chile, Peru, and across Canada in British Columbia, Saskatchewan, Yukon Territory and Ontario.
5. I have primarily worked within magmatic-hydrothermal systems, such as Cu-Mo-Au porphyries, Au-Ag epithermal deposits and iron-oxide copper gold deposits, for the last 10 years.
6. I am not aware of any material fact or of any material change with respect to the subject matter of this technical report, which has not been reviewed and might make the report misleading.
7. I am a non-independent person with respect to VR Resources, I own shares and have received option agreements with respect to my work with the company as "Exploration Manager & Chief Geologist" from 2017 to present.

Dated at Toronto, Ontario on June 8th, 2021

  
Justin J. Daley, PGeo



## References

Darbyshire, F. A., Eaton, D. W., Frederiksen, A. W., & Ertolahti, L. 2007. New insights into the lithosphere beneath the Superior Province from Rayleigh wave dispersion and receiver function analysis. *Geophysical Journal International*, 169(3), 1043-1068.

Halls, H. C., & Davis, D. W., 2004. Paleomagnetism and U Pb geochronology of the 2.17 Ga Biscotasing dyke swarm, Ontario, Canada: evidence for vertical-axis crustal rotation across the Kapuskasing Zone. *Canadian Journal of Earth Sciences*, 41(3), 255-269.

Meschede, M., 1986. A method of discriminating between different types of mid-ocean ridge basalts and continental tholeiites with the Nb 1bZr 1bY diagram. *Chemical geology*, 56(3-4), pp.207-218.

Mullen, E.D., 1983. MnO/TiO<sub>2</sub>/P<sub>2</sub>O<sub>5</sub>: a minor element discriminant for basaltic rocks of oceanic environments and its implications for petrogenesis. *Earth and Planetary Science Letters*, 62(1), pp.53-62.

Pearce, J., 1996. Sources and settings of granitic rocks. *Episodes*, 19, pp.120-125.

Salo, R. W., 2006. Diamond Drilling Report On The Coral Rapids Property For Baltic Resources Inc., OGS Assessment Report Database. Assessment File: 20000001302. AFRO Number: 2.31852. Resident Geologist District: Timmins. Resident Geologist Office File Number: T-5357

Winchester, J.A. and Floyd, P.A., 1977. Geochemical discrimination of different magma series and their differentiation products using immobile elements. *Chemical geology*, 20, pp.325-343.

# SUMMARY REPORT FOR A

## TITAN 24 DCIP SURVEY

OVER

### RANOKE PROPERTY

(COCHRANE, ON)

ON BEHALF OF

### VR RESOURCES



September 16, 2019  
CA01199T

Quantec Geoscience Ltd.  
146 Sparks Ave., Toronto, ON, M2H 2S4, Canada  
+1-416-306-1941



**QUANTEC**  
Geoscience



Report Disclaimer:

Quantec Geoscience Limited holds a Certificate of Authorization from the Association of Professional Geoscientists of Ontario (APGO) to perform the work presented in this report. Quantec employed qualified professionals to carry out the data analysis and interpretation presented in this geophysical report.

Statements made in this report represent opinions that consider information available at the time of writing the report. Although every effort has been made to ensure the accuracy of the material contained in this report, complete certainty cannot be guaranteed due to the interpretive nature of the work which may include mathematically derived solutions that are inherently non-unique. Therefore, the estimated physical parameters of the subsurface may have no direct relation to the possible economic value of any mineralization.

There is no guarantee or representation to the user as to the level of accuracy, currency, suitability, completeness, usefulness, or reliability of this information for any purpose. Therefore, decisions made based on this work are solely the responsibility of the end user. It is incumbent upon the end user to examine the data and results delivered and make Quantec aware of any perceived deficiencies.

## EXECUTIVE SUMMARY

This report presents the logistics and geophysical analysis summary of the Titan 24 DCIP survey completed from August 23 to September 8, 2019 over the Ranoke Property by Quantec Geoscience Ltd. on behalf of VR Resources.

The report describes the instrumentation, data acquisition and processing procedures, final data formats and contents of the digital archives, as well as the procedures for data analysis and interpretation. The final processed data are presented as pseudo-depth plots of apparent resistivity and chargeability, and the inversion models are presented in relation to the survey objectives and significance to future exploration.

A total of 3 profiles were surveyed. Data were processed and inspected for quality assurance on site and reviewed daily by the geophysicist in charge of the project. The 3 profiles were subsequently inverted to generate resistivity and chargeability models.

The final processed survey results delivered with the report include:

- GPS Data
  - Multi-site ASCII survey files
    - Each file includes location (Latitude/Longitude, projected UTM and GRID coordinates)
- Direct Current (DC) and Induced Polarisation (IP) Data
  - CSV formatted files
    - Each file includes electrode locations (GRID coordinates), normalised Potential (V) and measured phase (radians or milliradians) for all readings on the line.
- 2D inversion models of all the profiles, for Resistivity, DC-referenced chargeability, and HS-referenced chargeability
  - Geosoft databases and maps files, PNG images.

## TABLE OF CONTENTS

List of Figures .....	6
List of Tables .....	6
1. Introduction .....	7
1.1. Client Information.....	7
1.2. General Project Information .....	7
2. Survey Logistics .....	9
2.1. Access.....	9
2.2. Grid Area .....	9
2.3. Production Summary .....	9
2.4. Survey Coverage Summary .....	9
2.5. Quantec Personnel .....	11
2.6. Health, Safety, and Environment (HSE) .....	12
2.6.1. Hazard Assessment and Control .....	12
2.6.2. Systems and Procedures.....	12
2.6.3. Reporting .....	12
3. Survey Specifications .....	13
3.1. Instrumentation .....	13
3.2. Survey Layout.....	14
3.3. DCIP Survey Parameters .....	14
3.3.1. Geometry .....	14
3.3.2. Acquisition and Processing Parameters.....	15
3.3.3. Data Presentation .....	17
4. Comments on Measured Data .....	18
5. Inversion Procedures .....	19
5.1. DCIP Inversion Procedures.....	19
5.1.1. 2D inversion code .....	19
5.1.2. Data Pre-conditioning.....	19
5.1.3. 2D inversion parameters .....	20
6. Inversion Results .....	21
6.1. Effects of Logistical Restrictions on Data Quality for Inversion .....	21
6.1.1. Survey Configuration .....	21

6.1.2.	Limitations due to logistical restrictions.....	21
6.2.	Effects of Telluric Noise on Data Quality .....	21
6.2.1.	Telluric noise levels.....	21
6.3.	2D Section Views.....	22
6.3.1.	L1000E – DC resistivity model.....	23
6.3.2.	L1000E – DC-referenced chargeability model .....	24
6.3.3.	L1000E – HS-referenced chargeability model.....	25
6.3.4.	L2000N – DC resistivity model .....	26
6.3.5.	L2000N - DC-referenced chargeability model .....	27
6.3.6.	L2000N – HS-referenced chargeability model.....	28
6.3.7.	L3000N – DC resistivity model .....	29
6.3.8.	L3000N – DC-referenced chargeability model.....	30
6.3.9.	L3000N – HS-referenced chargeability model .....	31
6.4.	3D Views .....	32
6.4.1.	Resistivity models – view from top, look NNE .....	33
6.4.2.	Chargeability models, view from top, look NNE.....	34
6.4.3.	Resistivity models – view from top, look SW.....	35
6.4.4.	Resistivity models – view from top, look SW.....	36
7.	Conclusions and Recommendations.....	37
8.	Deliverables .....	38
8.1.	Field Data Archive .....	38
8.2.	Digital Archive Attached to the Report.....	39
APPENDIX A.	Production Summary .....	41
APPENDIX B.	Survey Coverage .....	42
APPENDIX C.	DCIP Pseudosections.....	43
APPENDIX D.	Instrument Specifications .....	52
APPENDIX E.	Quantec DCIP CSV File Format.....	57
APPENDIX F.	Quantec IP Processing .....	59
APPENDIX G.	References .....	63
APPENDIX H.	Inversion Sections.....	65

## LIST OF FIGURES

Figure 1-1: General location map. ....	8
Figure 2-1: DCIP survey coverage map. ....	10
Figure 3-1: Survey acquisition layout.....	14
Figure 3-2: Typical DCIP array configurations. ....	15
Figure 3-3: Example of spectral chargeability model and calculated Halverson-Wait decays. ....	17
Figure 4-1: Ap index for duration of the study .....	18
Figure 6-1: Resistivity and chargeability range used for sections.....	22
Figure 6-2: L1000E DC resistivity model .....	23
Figure 6-3: L1000E DC-referenced chargeability model .....	24
Figure 6-4: L1000E – HS-referenced chargeability model .....	25
Figure 6-5: L2000N – DC resistivity model.....	26
Figure 6-6: L2000N – DC-referenced chargeability model.....	27
Figure 6-7: L2000N – HS-referenced chargeability model.....	28
Figure 6-8: L3000N – DC resistivity model.....	29
Figure 6-9: L3000N – DC-referenced chargeability model.....	30
Figure 6-10: L3000N – HS-referenced chargeability model.....	31
Figure 6-11: Resistivity models with colour scale 10-5000 Ohm-m .....	33
Figure 6-12: Resistivity models with colour scale 10-1000 Ohm-m .....	33
Figure 6-13: DC-referenced chargeability model.....	34
Figure 6-14: HS-referenced chargeability model .....	34
Figure 6-15: Resistivity models with colour scale 10-5000 Ohm-m .....	35
Figure 6-16: Resistivity models with colour scale 10-1000 Ohm-m .....	35
Figure 6-17: DC-referenced chargeability model.....	36
Figure 6-18: HS-referenced chargeability model.....	36

## LIST OF TABLES

Table 8-1: Contents of the digital archive attached to the report.....	39
--	----

## 1. INTRODUCTION

This report presents the summary of the Titan 24 DCIP survey completed from August 23 to September 8, 2019 over the Ranoke Property by Quantec Geoscience Ltd. on behalf of VR Resources.

### 1.1. CLIENT INFORMATION

Name: VR Resources

Address: 1750 – 700 West Pender St.  
Vancouver, BC  
V6C 1G8  
Canada

Representative: Justin Daley  
Phone: +1-604-865-5119  
Email: [jdaley@vrr.ca](mailto:jdaley@vrr.ca)

### 1.2. GENERAL PROJECT INFORMATION

Quantec Project Manager: Kevin Blackshaw

Quantec Project Number: CA01199T

Report Prepared by: Ryan Fearon, José Antonio Rodríguez

Project Name: Ranoke Property

Survey Type: Titan 24 DCIP

General Location: Approximately 180 km North of Cochrane (see Figure 1-1).

Lat /Long: 50°36'04"N, 81°49'6"E

UTM: 442078 E, 5605793 N

Datum: WGS84, UTM Zone 17N

Survey Period: From August 23 to September 8, 2019

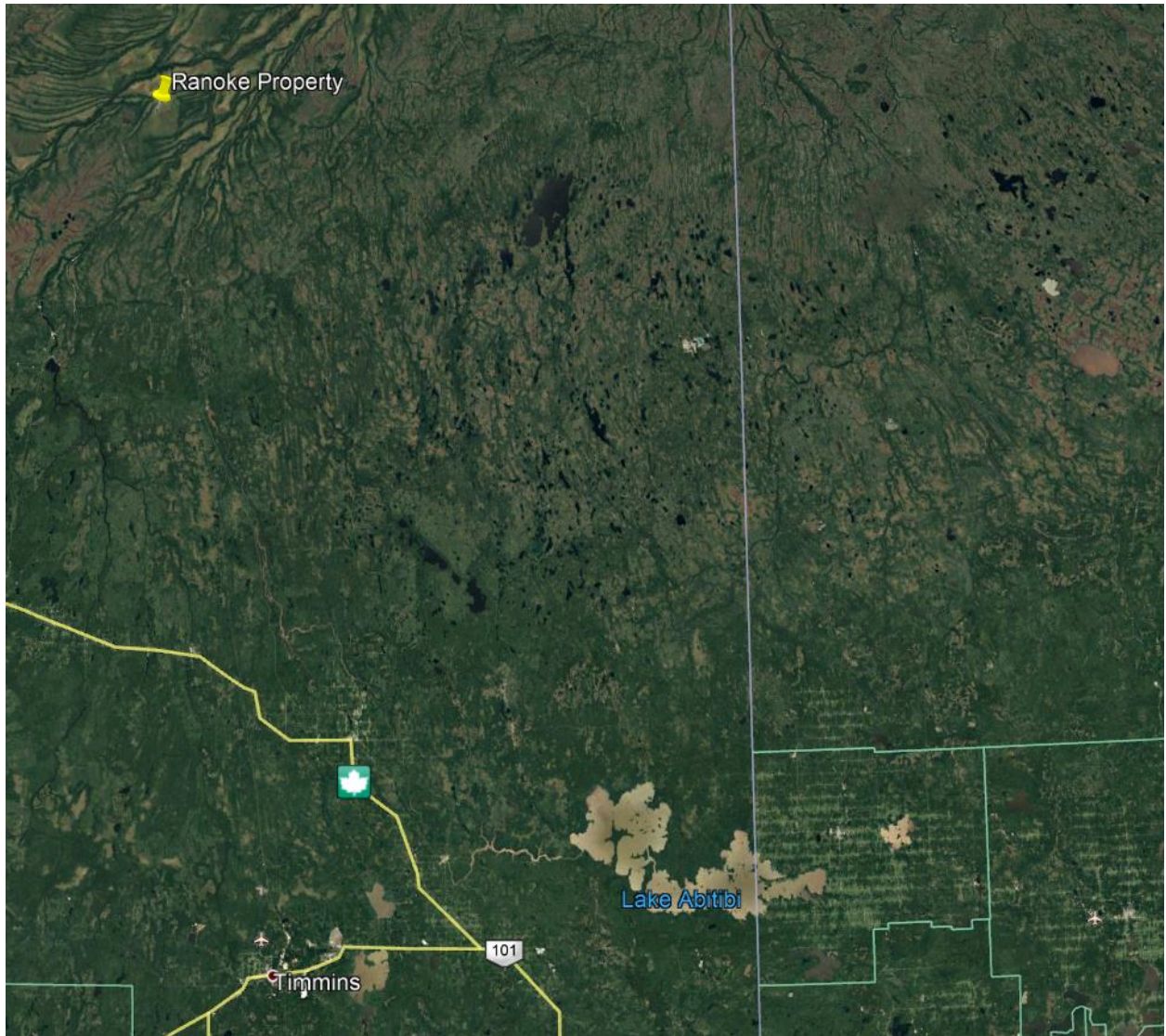


Figure 1-1: General location map.

## 2. SURVEY LOGISTICS

### 2.1. ACCESS

Base of Operations:	Client camp and Cochrane, ON
Mode of Access:	Helicopter, Foot

### 2.2. GRID AREA

Established by:	Client
Grid Coordinate Reference System:	Grid referenced to UTM coordinates
Datum and Projection:	WGS 84, UTM Zone 17N
Grid Azimuth:	Grid N is 345° and 65° True
Magnetic Declination:	10°E
Site Location:	Handheld GPS

### 2.3. PRODUCTION SUMMARY

Details of Survey Production:	See APPENDIX A
Survey Period (Total):	From August 23 to September 8, 2019 17 days
Survey Days (Read Time):	14 days
Safety Induction:	0 days
Weather Days:	1 days
Mob Days:	2 days

### 2.4. SURVEY COVERAGE SUMMARY

Details of Survey Coverage:	see APPENDIX B
-----------------------------	----------------



2D DCIP Survey:

Lines Acquired:

3 lines covering a total of 17 km

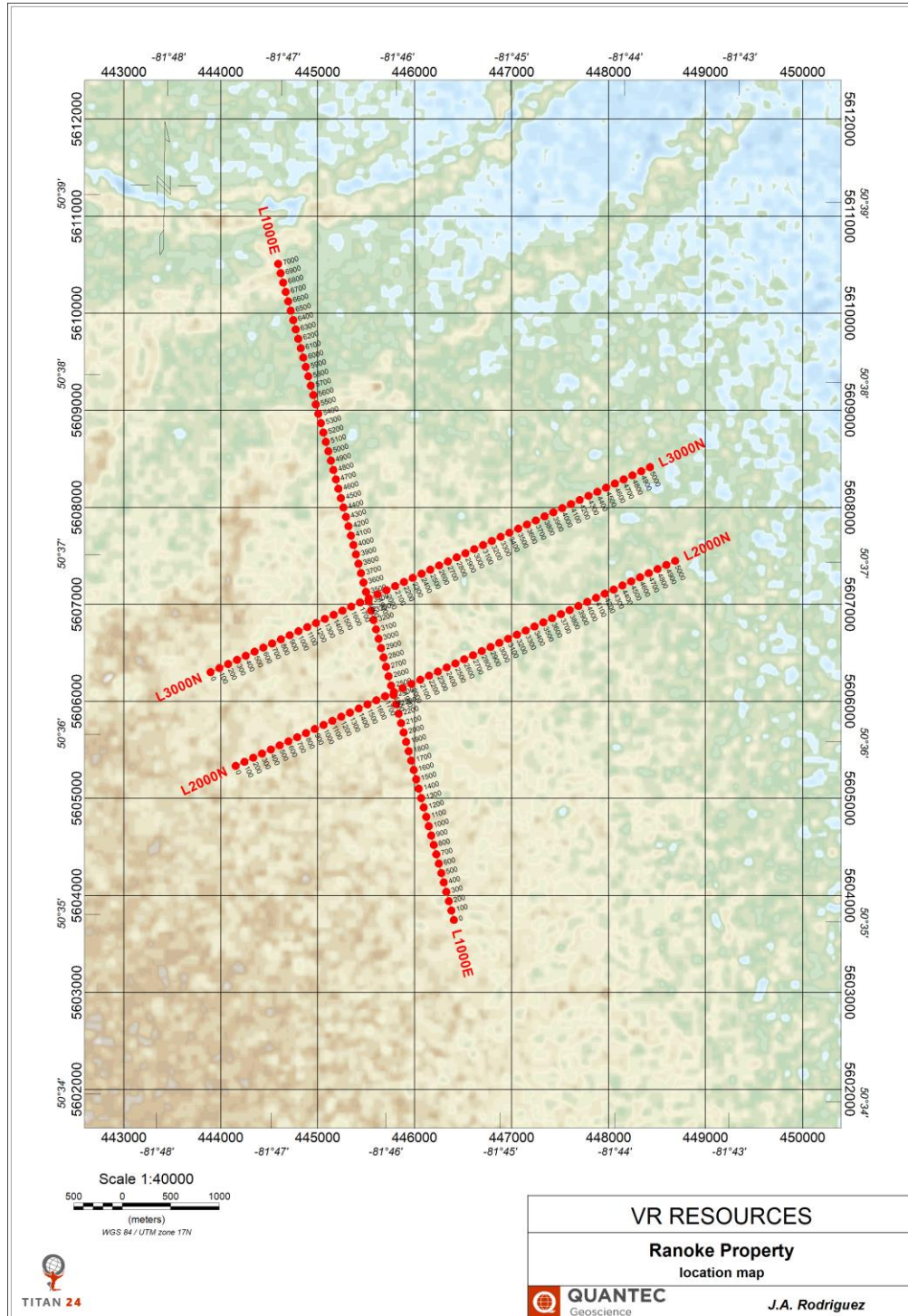


Figure 2-1: DCIP survey coverage map.

**2.5. QUANTEC PERSONNEL**

Project Manager:	Kevin Blackshaw
Field Operations Manager:	Neil Maukonen
Project Geophysicists:	José Antonio Rodriguez Mehran Gharibi
Field HSE Coordinator:	Neil Maukonen
Office Data Processor:	Ryan Fearon
System Operators:	Donald McLaren Ben Dubois Ryan Hrkac Alain Dufour Brooke Courchesne Andrew Casson

## **2.6. HEALTH, SAFETY, AND ENVIRONMENT (HSE)**

Quantec Geoscience is committed to conducting its activities in a manner that will safeguard and protect the health and safety of all Quantec personnel, clients, the public and the environment.

### **2.6.1. Hazard Assessment and Control**

Prior to mobilization, Quantec HSE compiled a hazard inventory for the project and risk assessments were completed for the tasks involved in conducting the work. On the basis of the risk assessments, corresponding Job Safety Analyses (JSA) were prepared defining safe work procedures.

### **2.6.2. Systems and Procedures**

All personnel were equipped with any personal protective equipment (PPE) required for the work.

One Quantec crew member was assigned as an HSE coordinator to assist the Field Manager with implementation of HSE procedures and reporting.

Daily safety meetings of Quantec personnel were conducted each morning prior to commencement of work to review safe work procedures and discuss any prior incidents, daily plans and potential hazards.

Vehicle circle checks were completed by drivers before departure.

### **2.6.3. Reporting**

Daily reports were sent by email to both Quantec and the client representative, including:

- Daily operations plan for each acquisition team.
- Minutes of Quantec crew daily Safety meetings.
- Incident Reports if required.

### 3. SURVEY SPECIFICATIONS

#### 3.1. INSTRUMENTATION

Receiver System:	RT120Q Quantec distributed array acquisition system
Synchronisation:	GPS clock (10 ns precision)
Receiver Electrodes:	Ground contacts using stainless steel rods

#### DCIP Specific

Transmitter:	GDD TxII-5000 (5 kW) with frequency/waveform control using Central Recording Unit (CRU) and Current Monitor (CM)
Transmitter Electrodes:	4 x 1.2 cm diameter 1 m long stainless-steel rods
Power Supply:	Honda 6500 W generator

See APPENDIX D for more detailed information.

### 3.2. SURVEY LAYOUT

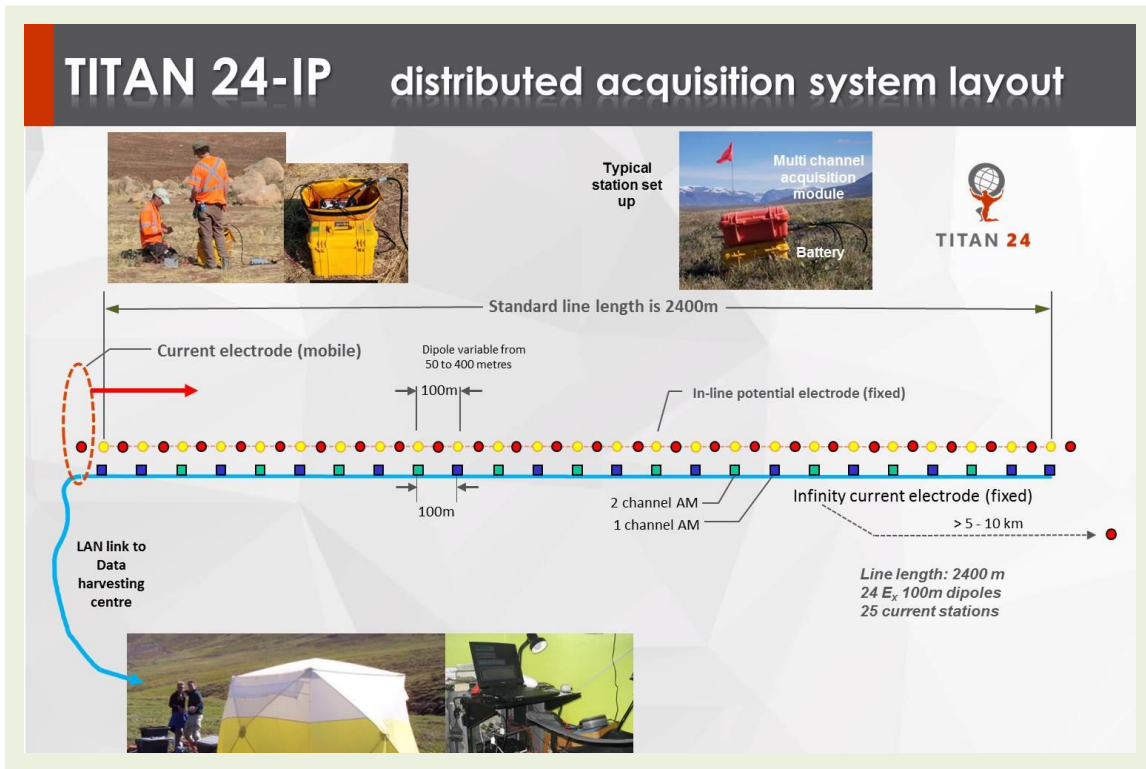


Figure 3-1: Survey acquisition layout.

### 3.3. DCIP SURVEY PARAMETERS

#### 3.3.1. Geometry

Dipole Length: 200 m

Layout Configuration: Pole-Dipole-Dipole array

Dipole-Dipole array

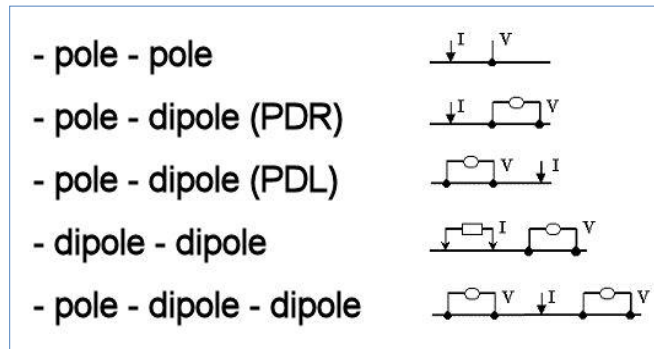


Figure 3-2: Typical DCIP array configurations.

Receiver Layout:	Continuous in-line dipoles
Transmitter Layout:	Current electrodes at midpoints between potential electrodes; N-spacing (Pn-Cn) = 0.5 to 23.5.
Infinite Pole Location:	<b><u>L1000E</u></b>  Measured using dipole-dipole and gradient array  <b><u>L2000N</u></b>  Grid: 2585E, 6504N UTM: 444594E, 5610508N (WGS84, UTM Zone 17N)  <b><u>L3000N</u></b>  Grid: 2410E, 6520N UTM: 444594E, 5610508N (WGS84, UTM Zone 17N)

### 3.3.2.Acquisition and Processing Parameters

Spectral Domain:	Tx = Frequency domain square wave current Rx = Full waveform time series acquisition Data processing and output in frequency domain.
Transmitter Waveform:	30/256 Hz square wave at 100% duty cycle (~4.3 s ON pos-neg)
Transmitter Output Current:	Approximately 0.15 A to 5.0 A

Sampling Rate:	240 samples/s (60 Hz)
Tx-Rx Synchronization:	Using current monitor (CM) with 10 $\mu$ s time accuracy and GPS clock
Time Series Stacking:	20 to 40 cycles (full-waveform)
Read Time:	Approximately 3.0 minutes per event
Processing:	Quantec proprietary QuickLay software (ver.5.4.7): 1) Time series stacking 2) Robust statistics 3) Current waveform deconvolution 4) Digital filtering (60 Hz + harmonics) 5) Spectral model decay curve fitting
Spectral Chargeability Model:	Halverson-Wait <sup>1</sup> (see APPENDIX F for details)
Time Domain Decay Window:	Start time: T0 = 0.8 seconds End time: TF = 1.8 seconds

---

<sup>1</sup> The Halverson-Wait model chargeability (Halverson et al., 1981) is similar to and improves upon the frequency domain Cole-Cole model (Pelton et al., 1978) described in the time domain by Johnson (1984).

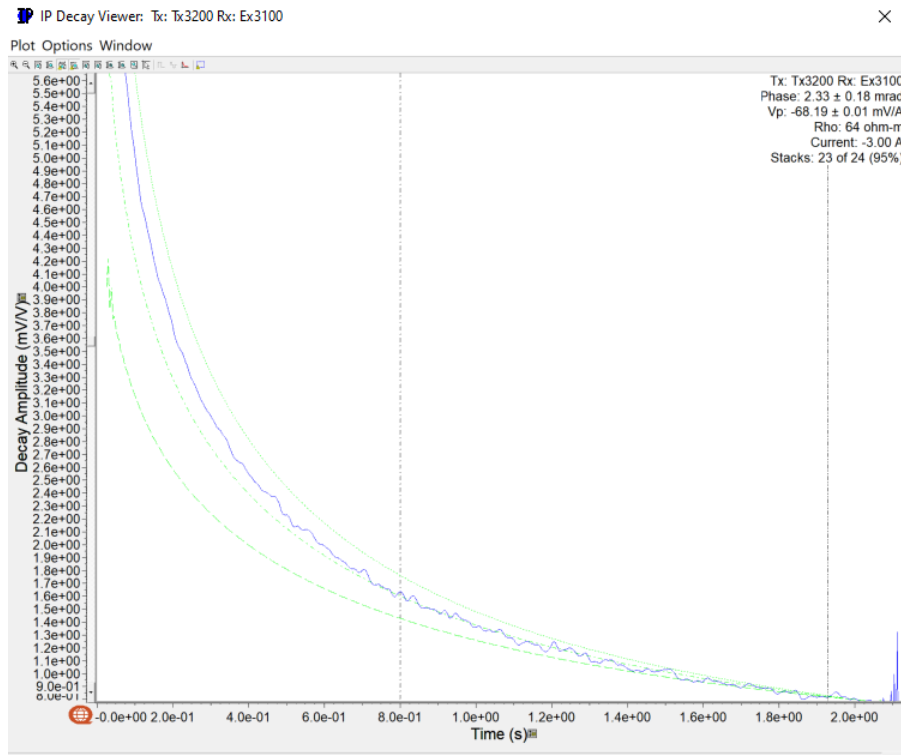


Figure 3-3: Example of spectral chargeability model and calculated Halverson-Wait decays<sup>2</sup>.

### 3.3.3. Data Presentation

Accuracy:	Measured average error (from CSV files) using Halverson-Wait model calculation.
	Voltage errors            0.0001 V/A (average)
	Phase errors                95% less than 1.0 mrad
Pseudo-Section Plots:	In-line DC (apparent resistivity) and IP (phase) presented in APPENDIX C.

<sup>2</sup> Halverson-Wait (HW) model parameters calculated in frequency domain, with hatched green lines corresponding to theoretical HW decay with spectral r-factors of 0.1, 1.0 (default) & 10, k-factor of 0.2 (default).



#### 4. COMMENTS ON MEASURED DATA

Due to the excellent communication provided by VR Resources at project start-up with respect to their survey objectives and constraints we were able to achieve the best quality data within our client’s budget and the field conditions.

Strong telluric activity was a constant issue during the acquisition period of this survey, several array configurations were tested to determine the best approach to penetrate our signal through the overburden.

##### Line 1000E

Line was read using dipole-dipole array as well as testing a gradient array to simulate a pole-dipole-pole array. The PDP method was collected with poles at the ends of the line which acted as the infinite.

We were able to observe between depths of ~200 and 300m using the dipole-dipole array, due to signal attenuation. With the efforts in field and processing we were able to observe a high-resistivity feature from ~1900 to 3500N on the PDP data, which corresponds with a moderate chargeability feature.

##### Line 2000N

This line was acquired using pole-dipole-pole array in view of the success from L1000E tests. The infinite pole was located at the North end of L1000E.

Acquisition was strongly affected by extreme telluric noise due to a geomagnetic storm during the first two days of acquisition (see Figure 4-1). Following a weather day to wait out the storm, the line was read a third day with improvement.

See Ap index below in Figure 4-1.

##### Line 3000N

This line was acquired using pole-dipole-pole array configuration in view of the success from L1000E tests. The infinite pole was located at the North end of L1000E.

Overall due to lower telluric activity, the results were comparable to those observed on day 3 of L2000N.

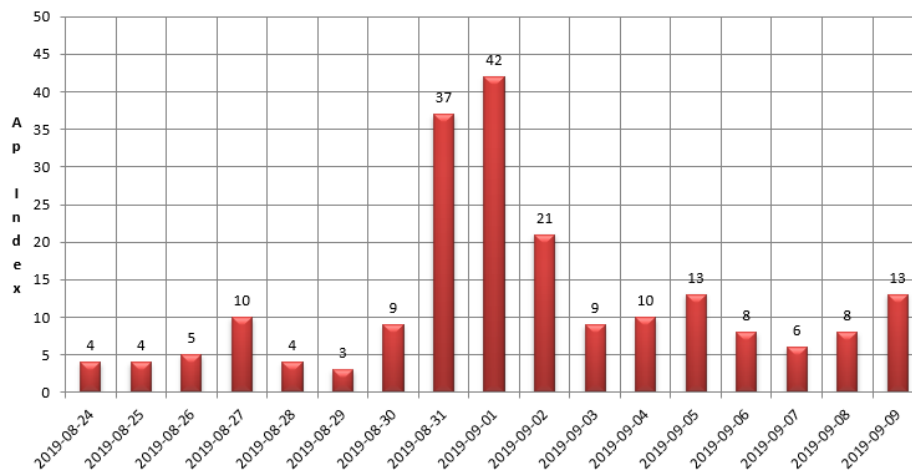


Figure 4-1: Ap index for duration of the study

## 5. INVERSION PROCEDURES

### 5.1. DCIP INVERSION PROCEDURES

DCIP is an electrical method that uses the injection of current and the measurement of voltage difference along with its rate of decay to determine subsurface resistivity and chargeability respectively. Depth of investigation is mainly controlled by the array geometry but may also be limited by the received signal (dependent on transmitted current) and ground resistivity. Chargeability is particularly susceptible to data with a low signal-to-noise ratio. The differences in penetration depth between DC resistivity and chargeability are a function of relative property contrasts and relative signal-to-noise levels between the two measurements. A detailed introduction to DCIP is given in Telford, et al. (1976).

The primary tool for evaluating data is through the inversion of the data in two or three dimensions. An inversion model depends not only on the data collected, but also on the associated data errors in the reading and the “model norm”. Inversion models are not unique and may contain “artefacts” from the inversion process. The inversion model may not accurately reflect all of the information apparent in the actual data. Inversion models must be reviewed in context with the observed data, model fit, and with an understanding of the model norm used.

#### 5.1.1. 2D inversion code

The 2D DC and IP inversions are carried out along lines to produce cross-sections of the resistivity and chargeability variations along those survey lines. The UBC DCIP2D inversion suite (Oldenburg and Li, 1994) utilizes the parallel computing library *OpenMP* (UBC-GIF-v5) to perform forward modeling and inversion of DC resistivity and IP data over a 2D distribution of electrical conductivity and chargeability; Two primary programs are:

- DCINV2D: a program to invert DC potentials to recover a 2D conductivity model.
- IPINV2D: a program to invert IP data to recover a 2D chargeability model.

#### 5.1.2. Data Pre-conditioning

The DC and IP data were pre-conditioned individually prior to the inversion to reject outliers and to facilitate the convergence of the optimization process.

The error of each data point is adjusted for the inversion process using a general error equation where an error estimate as a percentage of the observed data (Vp or phase) is added to the estimated data acquisition error and to a floor value similar to:

$$errors \begin{pmatrix} Vp \\ IP \end{pmatrix} = A\% \left| \frac{Vp}{IP} \right| + B \times \text{Acq\_Error} \begin{pmatrix} Vp \\ IP \end{pmatrix} + C \text{ (floor)}$$

A subset of the total measured data points is then pre-selected based on several criteria related to the measured values (i.e., Vp or phase), and their respective observed and calculated errors.

For this project, an error estimate of 5% has been used for the DC and IP data.

### 5.1.3. 2D inversion parameters

The DC and IP inversions use the same mesh. The horizontal mesh is set as 2 cells between electrodes. The vertical mesh is designed with a cell thickness starting from 25 m for the first 1325 metres, and then increases logarithmically with depth. The inversions were generally run for a maximum of 100 iterations.

The DC data is inverted using an unconstrained 2D inversion with a homogenous half-space of average input data as starting model.

For IP inversions, the apparent chargeability  $\eta$  is computed by carrying out two DC resistivity forward models with conductivity distributions  $\sigma(x_i, z_j)$  and  $(1 - \eta)\sigma(x_i, z_j)$  (Oldenburg and Li, 1994), where  $(x_i, z_j)$  specifies the location in a 2D mesh. The conductivity distributions used in IP inversions can be the inverted DC model or a half space of uniform conductivity. Two IP inversions are then calculated from the same data set and parameters using different reference models. The first inversion of the IP data uses the previously calculated DC model as the reference model and is labelled the ***IP\_dcref*** model. The second IP inversion uses a homogeneous half-space resistivity model as the reference model and is labelled ***IP\_hsref*** model. This model is included to test the validity of chargeability anomalies, and to limit the possibility of inversion artefacts in the IP model due to the use of the DC model as a reference.

## 6. INVERSION RESULTS

### 6.1. EFFECTS OF LOGISTICAL RESTRICTIONS ON DATA QUALITY FOR INVERSION

#### 6.1.1. Survey Configuration

The project was originally conceived to be a *dipole-dipole* (DPDP) survey with dipole spacing of 200m. However, the first attempts to obtain DPDP data on L1000E proved that the DPDP configuration did not allow the collection of valid data for n-spacing greater than n=5, approximately. This was confirmed both by field inspection of the decay curves in the IP data, and by a depth of investigation analysis using the UBC inversion code on a test data set. We believe that the DPDP configuration limited the penetration of current through the conductive overburden. For this reason, another attempt was made to obtain data under pole-dipole configuration, with infinite stations located 100m from the North and South extremes of L1000E, in order to obtain greater depth of investigation. This configuration allowed the crew to observe valid IP data above telluric noise level to spacings of approximately n=15. The data using the North and South infinities were merged and inverted together to produce a single pole-dipole data model for L1000E. The maximum n-spacing used for modeling purposes was 15.

After gaining experience on L1000E, the infinite station at the north end of L1000E was used to collect PDP data for both L2000N and L3000N. This location allowed an infinite 4700m distant at the nearest point for L2000N, and 3700m distant at the nearest point for L3000N.

#### 6.1.2. Limitations due to logistical restrictions

Ideally, the infinite station should be located some 10 km away for a PDP survey of this dimension. Due to practical limitations, this was not possible, so there may be some bias in the data due to the nearer-than-ideal infinite station location. However, this bias is estimated to be small, and would not change the conclusions of this study.

### 6.2. EFFECTS OF TELLURIC NOISE ON DATA QUALITY

#### 6.2.1. Telluric noise levels

Telluric noise is caused by geomagnetic variations in the Earth's upper atmosphere, caused mainly by the interaction of the Solar Wind with the Earth's magnetic field. The noise appears in the data as currents that are unrelated to the currents that the geophysical survey instruments inject into the ground, and therefore contaminate the DCIP data.

Figure 4-1 shows the Ap index for several dates encompassing the duration of the survey. Note that between August 31 and September 2 there was a geomagnetic storm that caused very large telluric noise levels in the DCIP data.

Data were collected for L2000N on August 31, and again on September 1, but the telluric noise levels on both days were too high for the data to be used for inversion. On September 21, the crew stood by to allow the geomagnetic storm to pass, and field work resumed on September 3 for L2000E. L3000E data were acquired on September 6. Data from the final acquisition runs were deemed acceptable in terms of noise levels, and subsequently were used to a maximum n-spacing of 15 in the inversions.

### 6.3. 2D SECTION VIEWS

The results of the 2D inversions of the DC and IP data for L1000E, L2000N, and L3000N are presented on a line per line basis as cross-sections. Figure 6-1 presents the resistivity and chargeability ranges used in plotting.

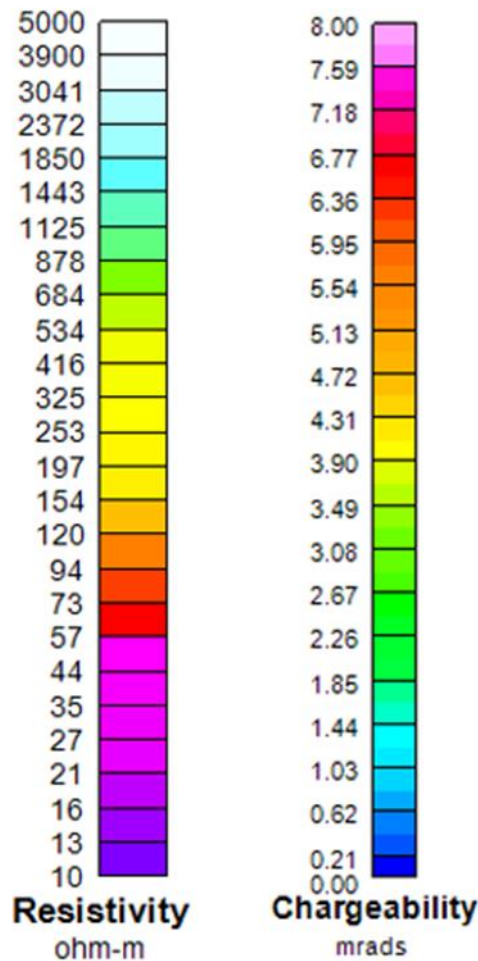


Figure 6-1: Resistivity and chargeability range used for sections

6.3.1. L1000E – DC resistivity model

We observe a high-resistivity anomaly between stations 4000 and 1900, below -250m elevation.

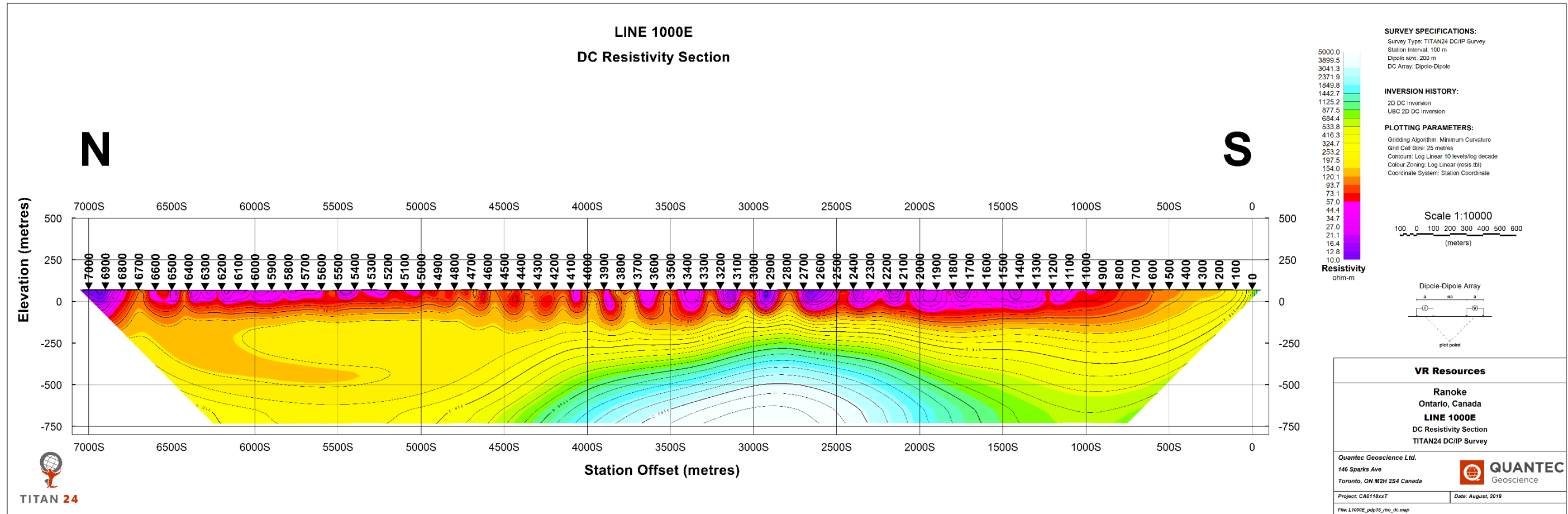


Figure 6-2: L1000E DC resistivity model

6.3.2. L1000E – DC-referenced chargeability model

There is a moderate chargeability feature centered around station 3000, roughly corresponding to the high-resistivity anomaly. Some chargeability extends further to the north.

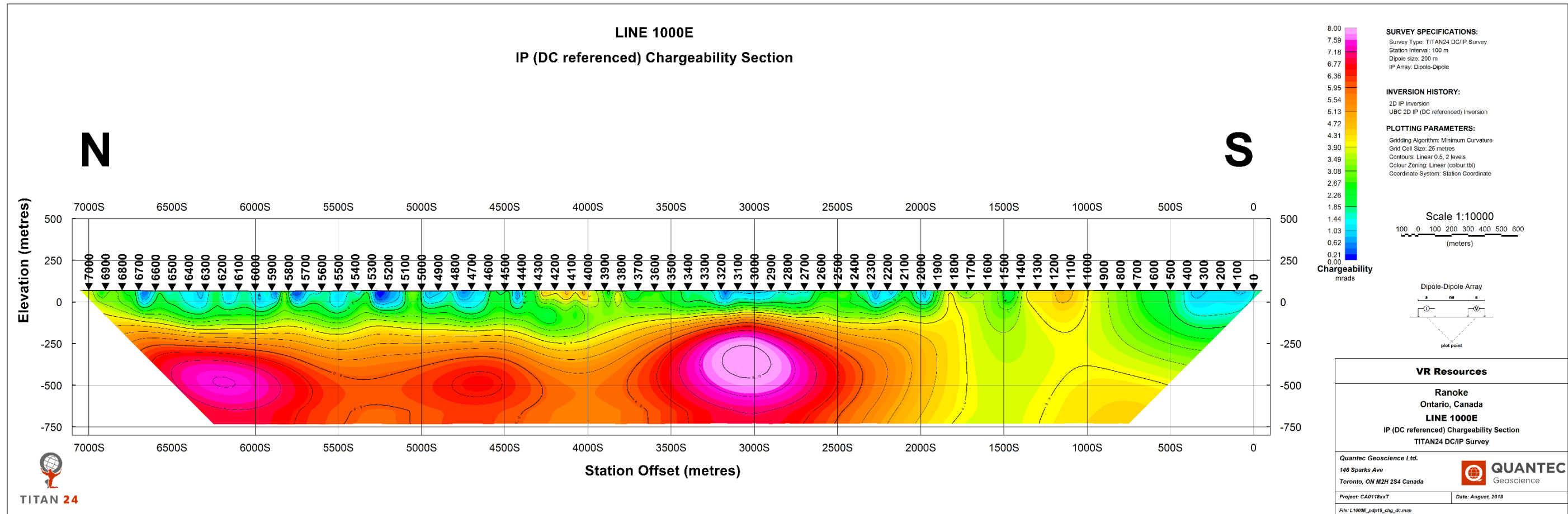


Figure 6-3: L1000E DC-referenced chargeability model

6.3.3. L1000E – HS-referenced chargeability model

Shows chargeability generally higher with depth below ~250m elevation, between stations 6500 and 2700. Some chargeability extends to the north.

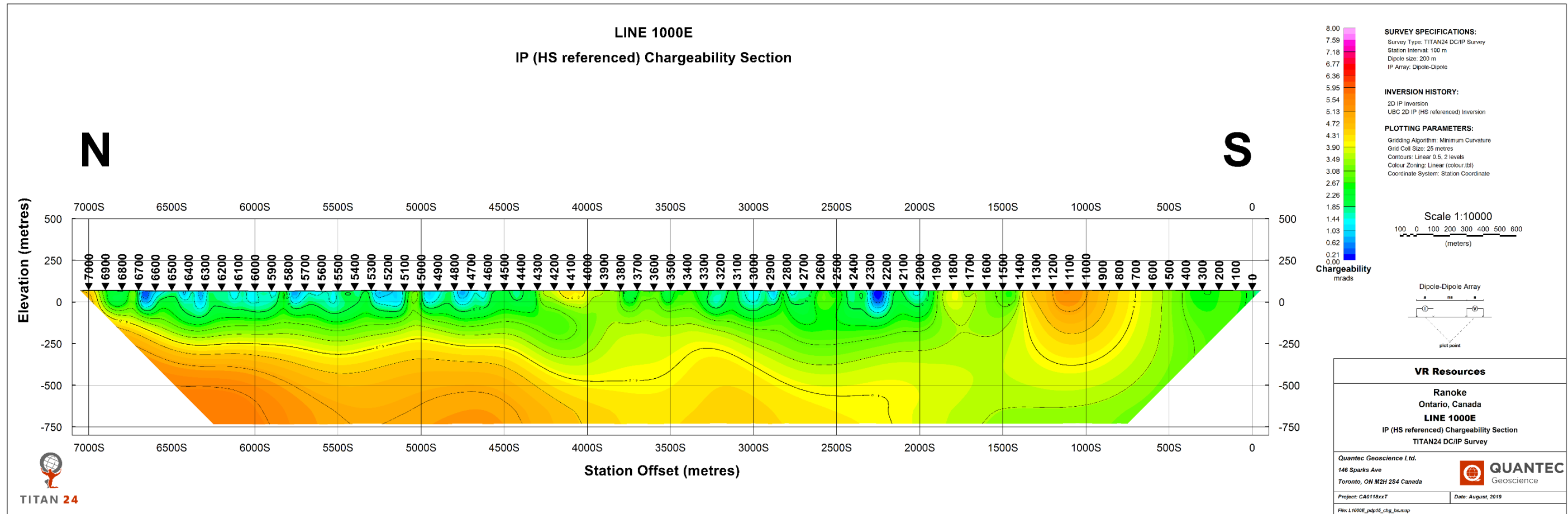


Figure 6-4: L1000E – HS-referenced chargeability model



6.3.4. L2000N – DC resistivity model

We observe a high-resistivity anomaly that corresponds in location and depth to the one observed in L1000E.

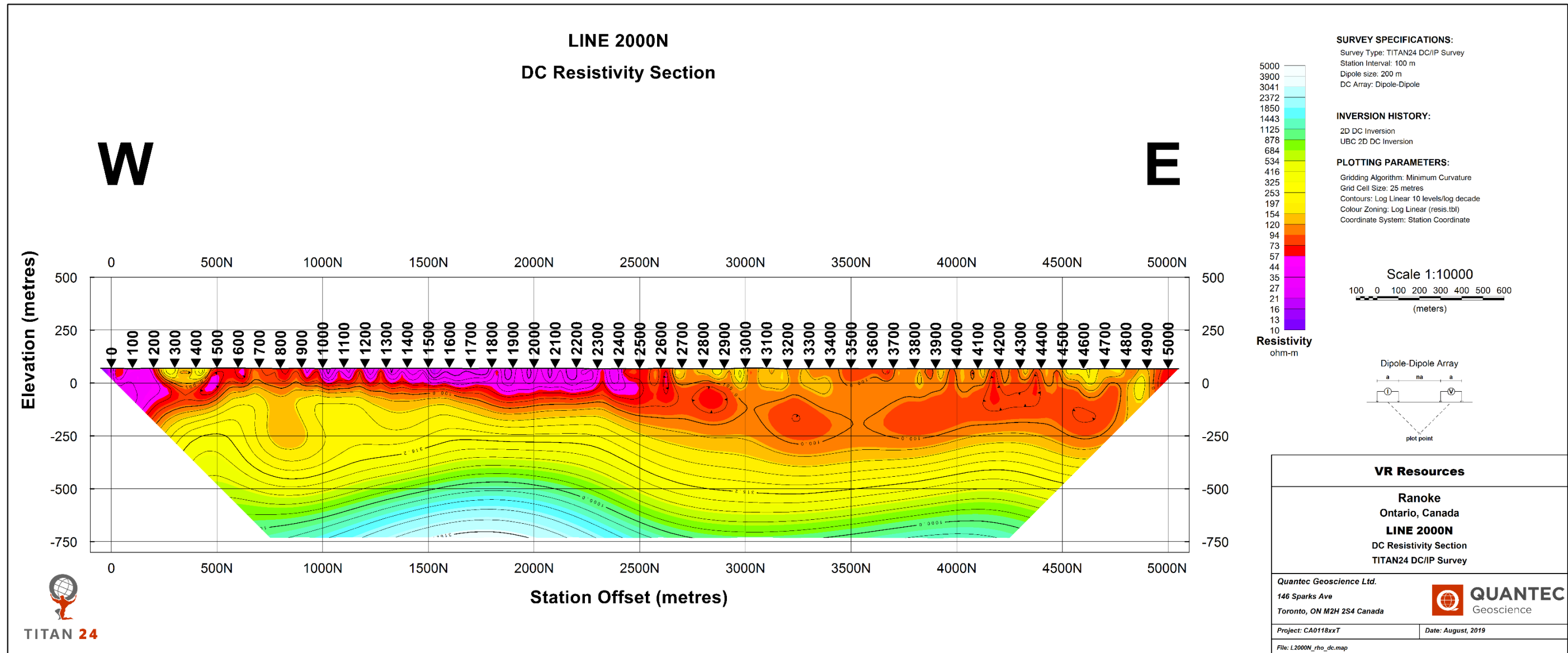


Figure 6-5: L2000N – DC resistivity model

6.3.5. L2000N - DC-referenced chargeability model

The moderate chargeability feature around station 1900 correlates with the one observed in L1000E.

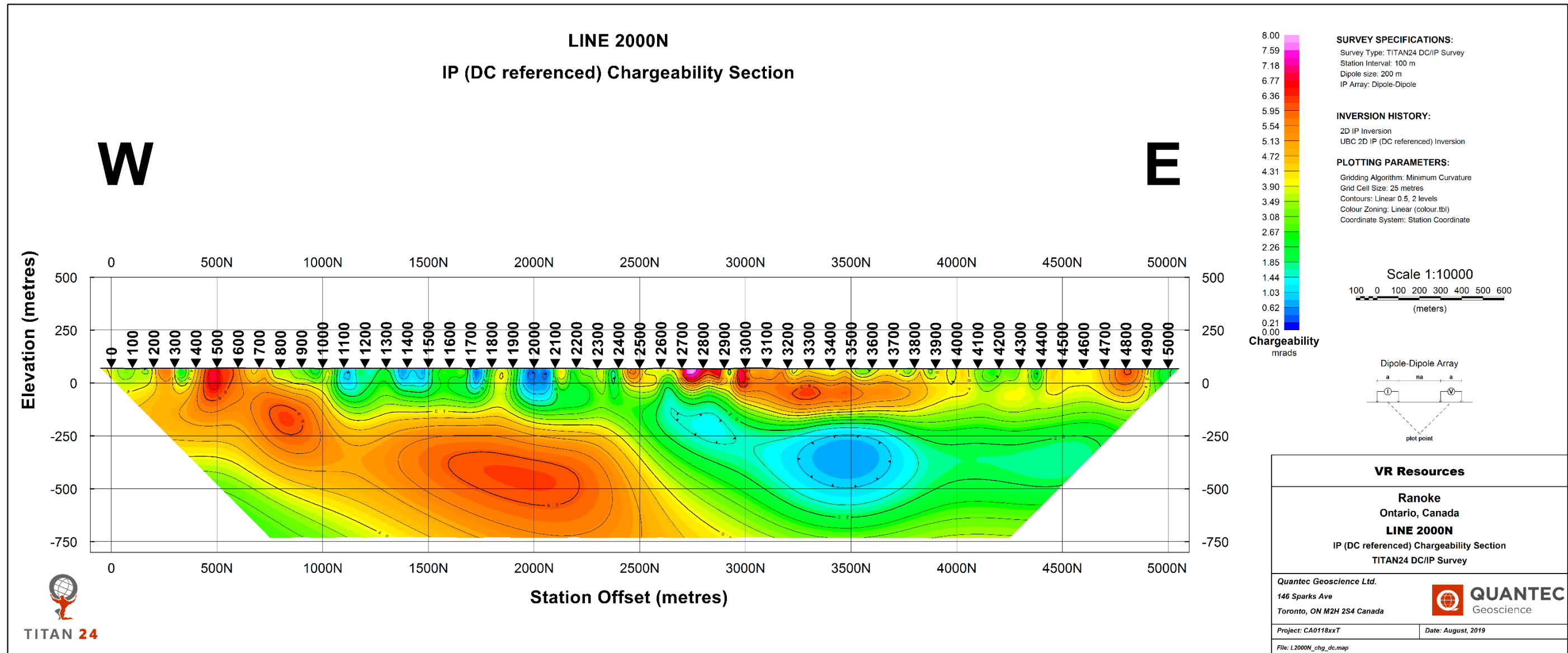


Figure 6-6: L2000N – DC-referenced chargeability model

6.3.6. L2000N – HS-referenced chargeability model

The moderate chargeability feature observable in the DC-referenced chargeability section is observable here, also.

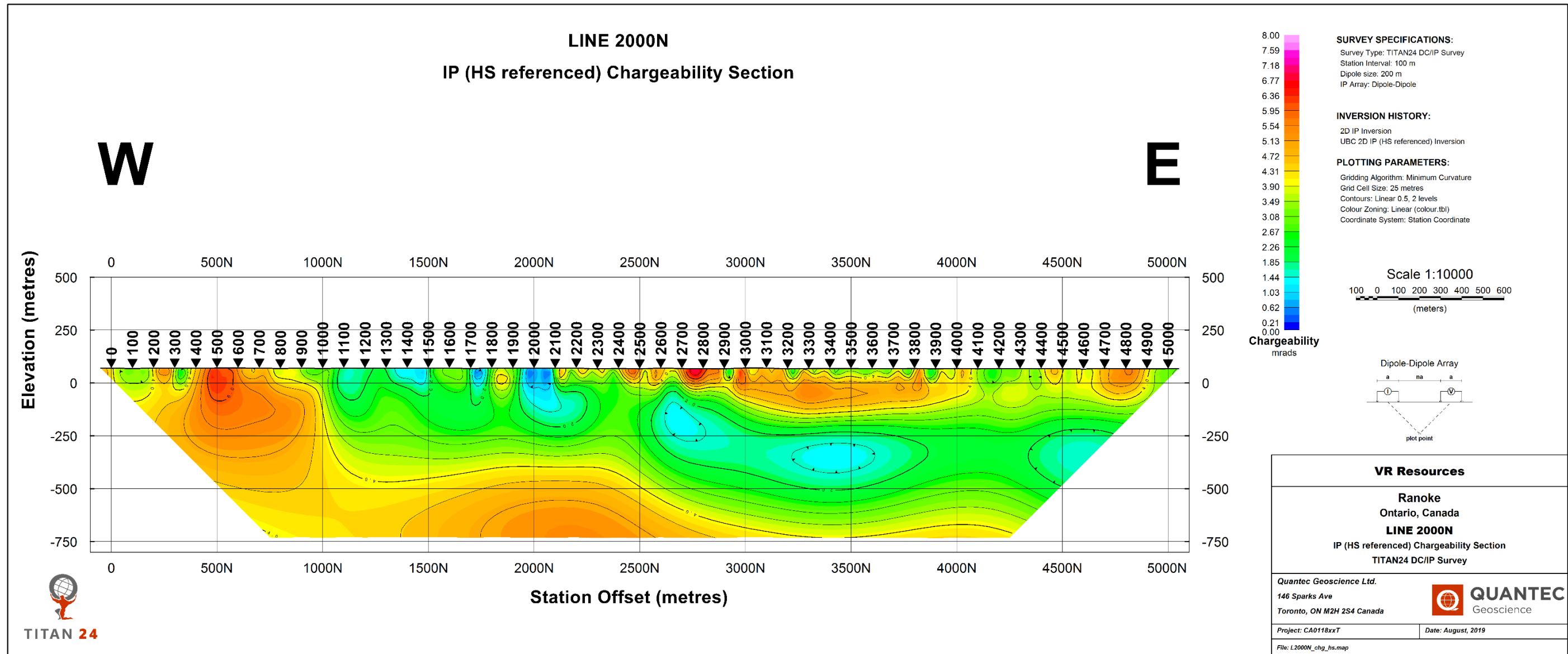


Figure 6-7: L2000N – HS-referenced chargeability model

6.3.7. L3000N – DC resistivity model

Similar to L2000N, the high-resistivity feature is observed between stations 1200 and 2200.

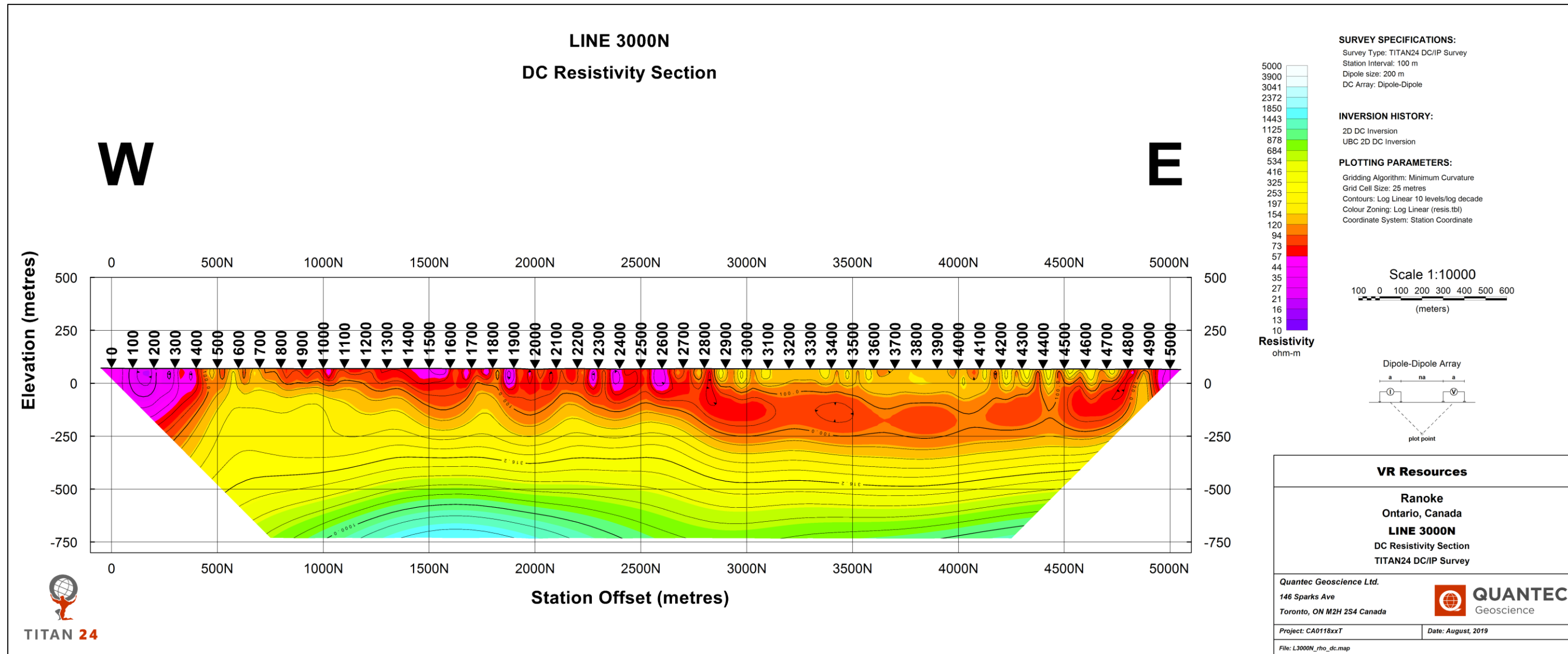


Figure 6-8: L3000N – DC resistivity model

6.3.8. L3000N – DC-referenced chargeability model

Similar to L2000N, the moderate chargeability feature corresponds with the one observed in L1000E.

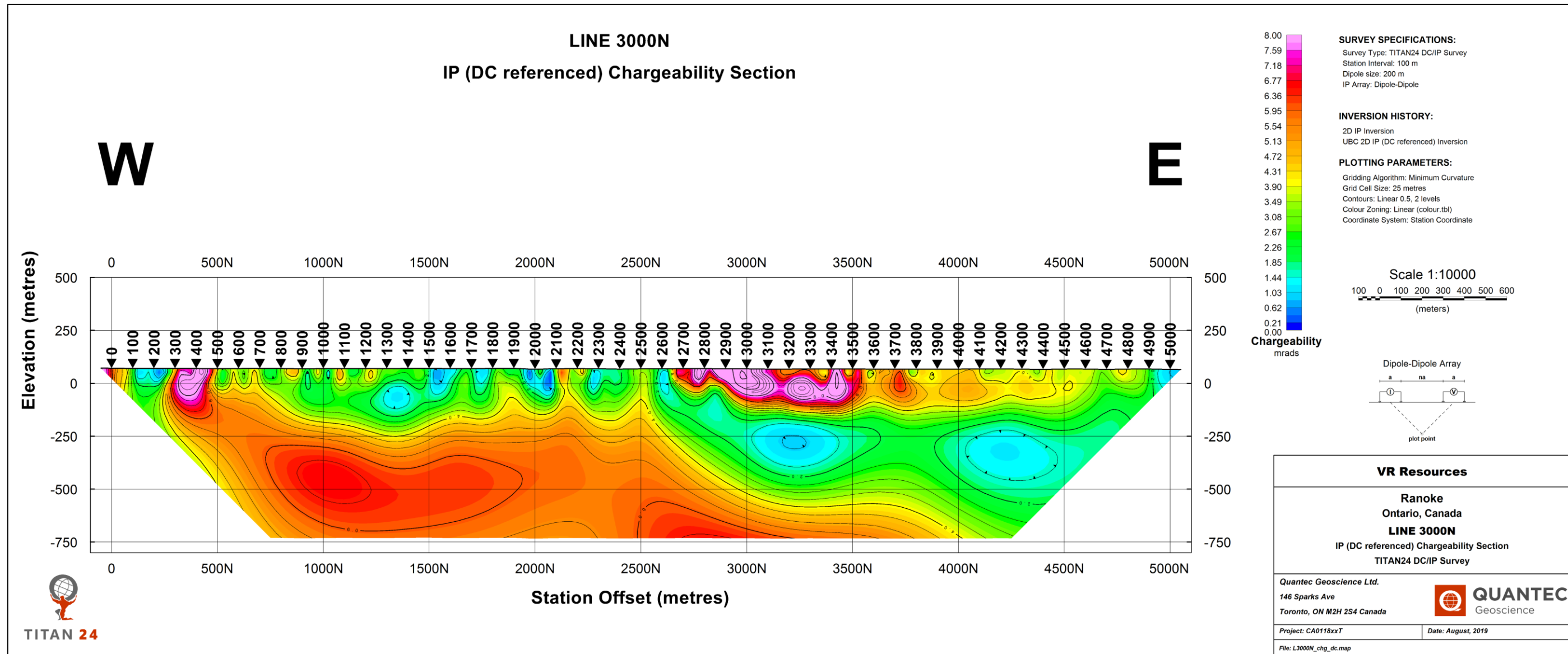


Figure 6-9: L3000N – DC-referenced chargeability model

6.3.9. L3000N – HS-referenced chargeability model

Similar to the DC-referenced chargeability section, but with a more pronounced chargeability gap between stations 2000 and 2500.

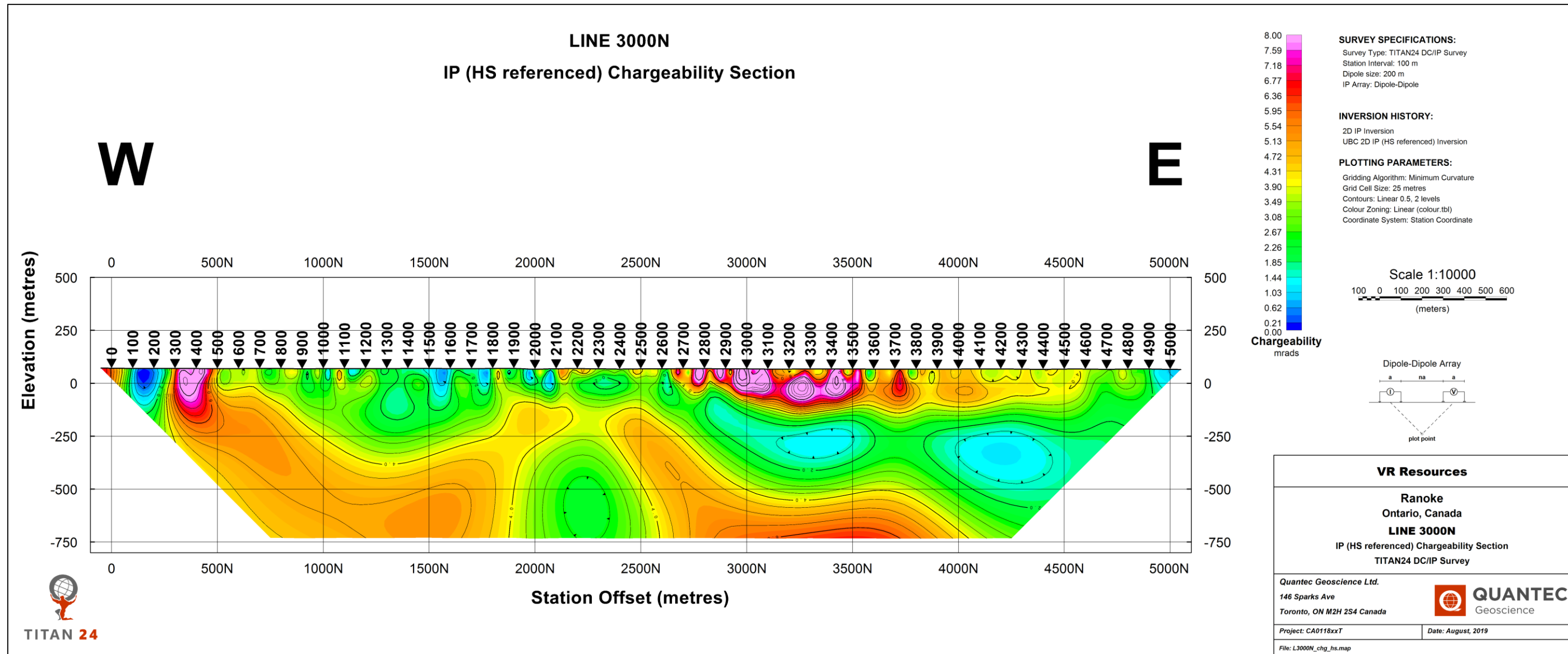


Figure 6-10: L3000N – HS-referenced chargeability model

#### **6.4. 3D VIEWS**

The georeferenced models can be displayed in 3D views to check the correlation of the models for the different lines at the intersection points. In general, there is good correspondence between the lines, in both the location and the magnitude of the main features, in all three models (DC resistivity, DC-referenced chargeability, and HS-referenced chargeability).

The resistivity models are shown in 3D first with the same resistivity colour scale as the sections, then with an alternate colour scale, going from 10 to 1000 Ohm-m, in order to better highlight the resistivity high-contrast zone around 500 Ohm-m.

6.4.1. Resistivity models – view from top, look NNE

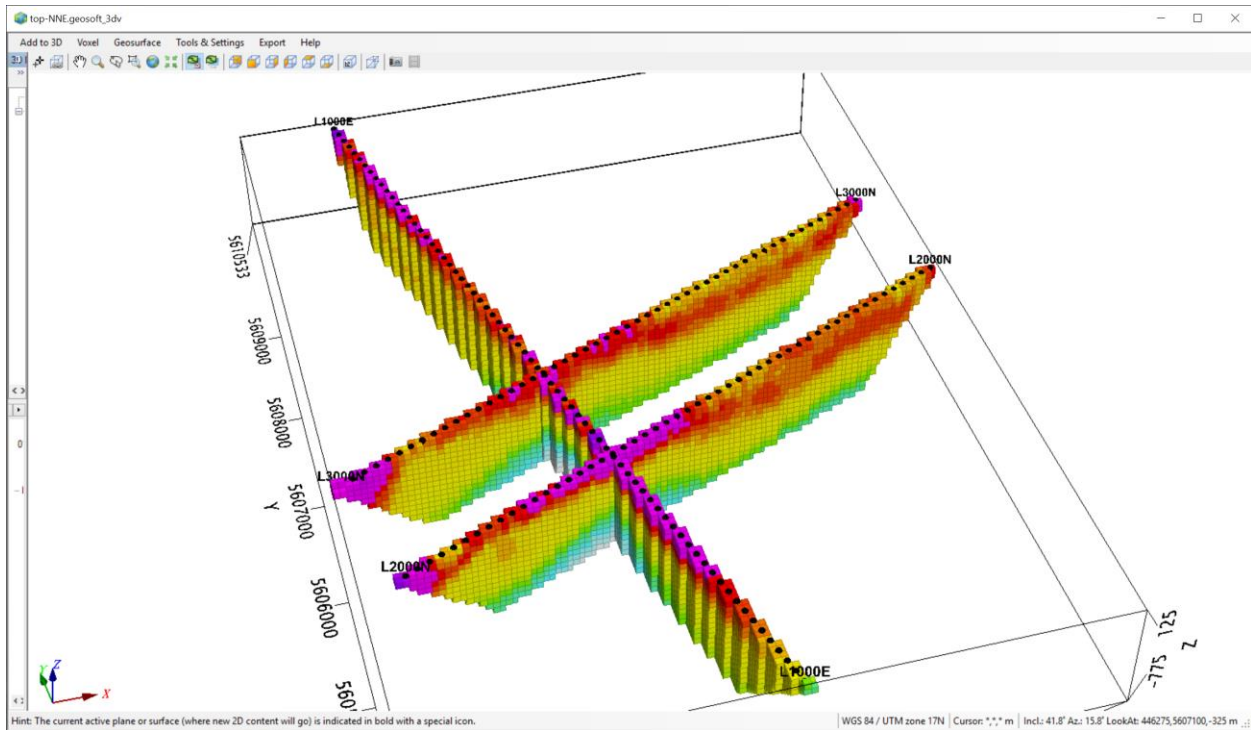


Figure 6-11: Resistivity models with colour scale 10-5000 Ohm-m

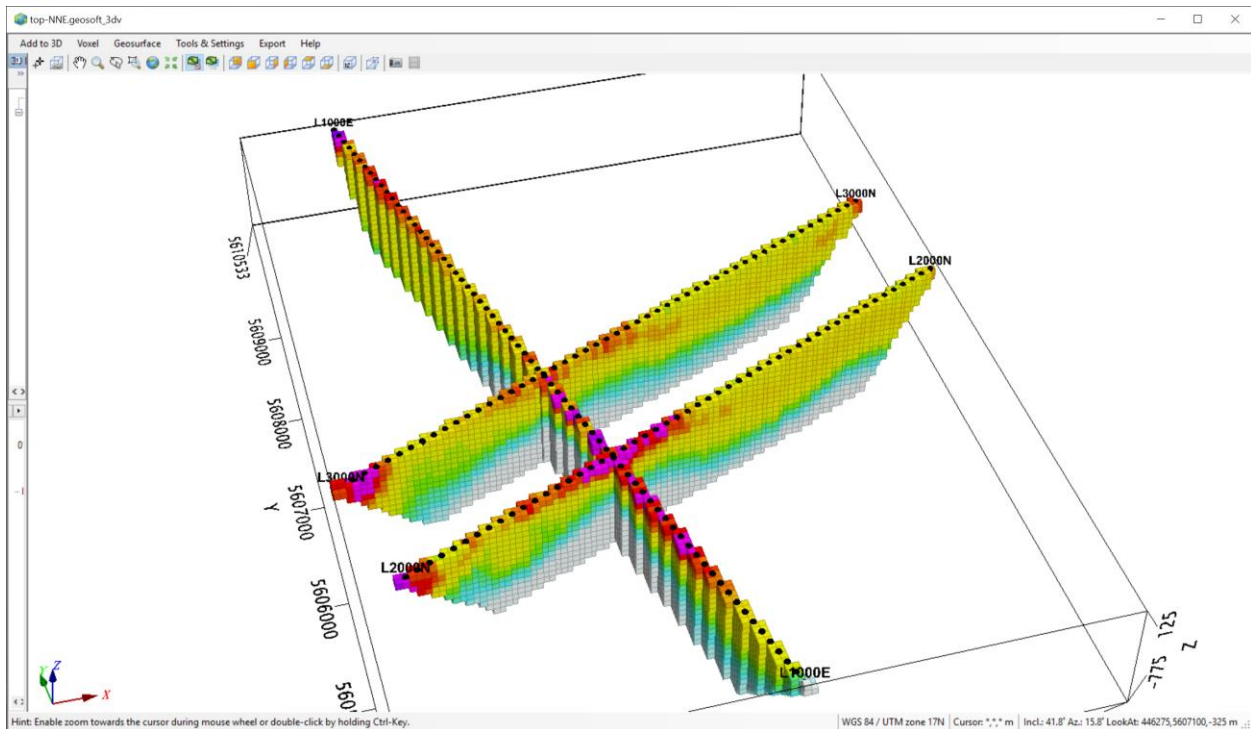


Figure 6-12: Resistivity models with colour scale 10-1000 Ohm-m



6.4.2. Chargeability models, view from top, look NNE

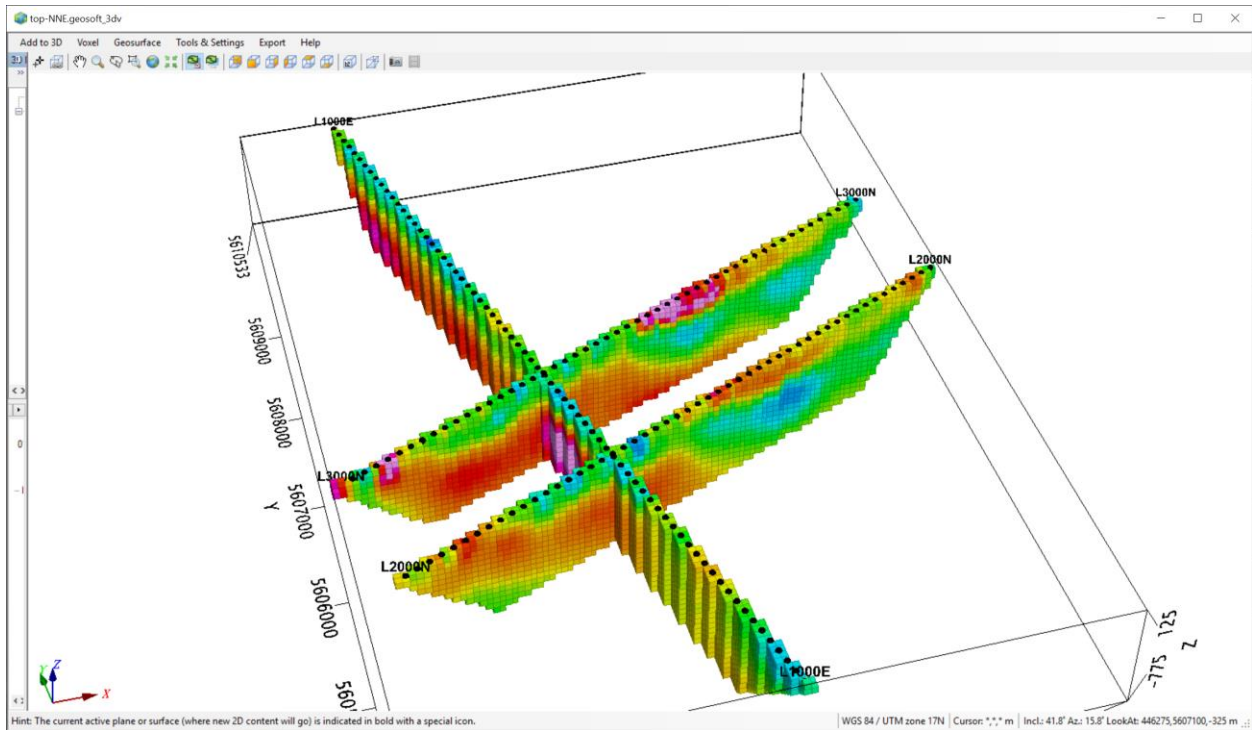


Figure 6-13: DC-referenced chargeability model

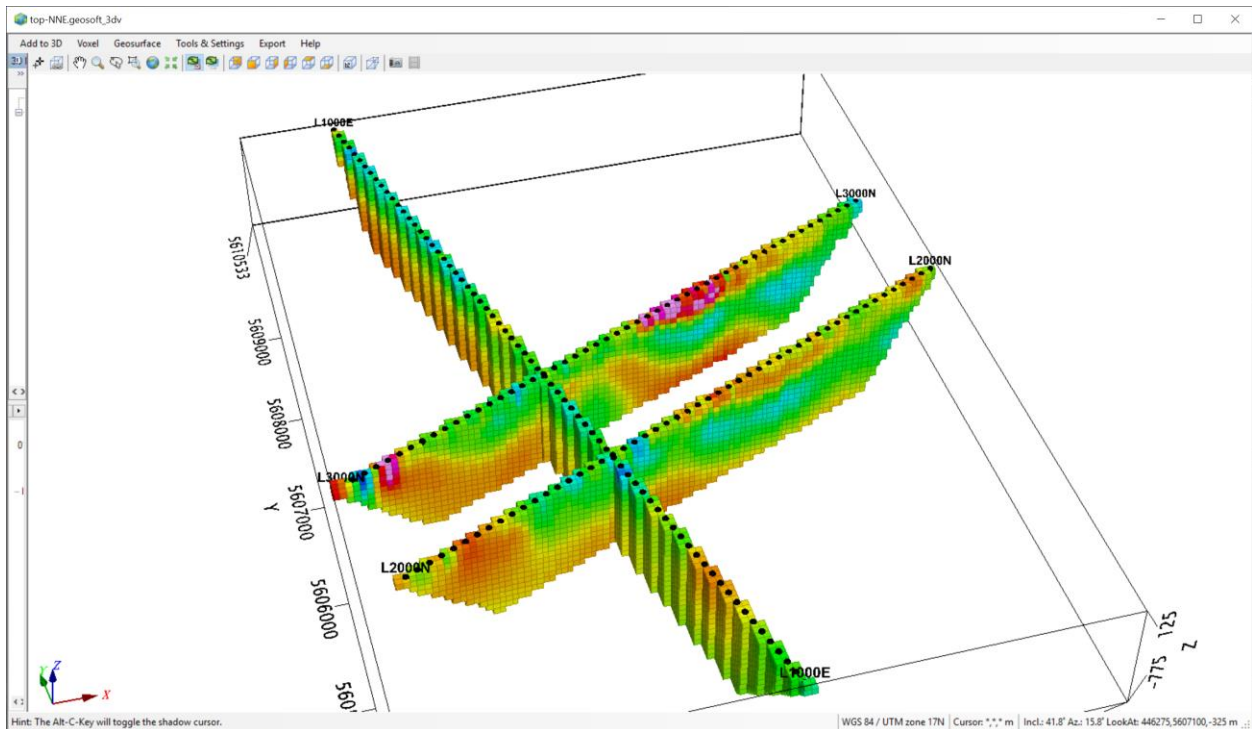


Figure 6-14: HS-referenced chargeability model

6.4.3. Resistivity models – view from top, look SW

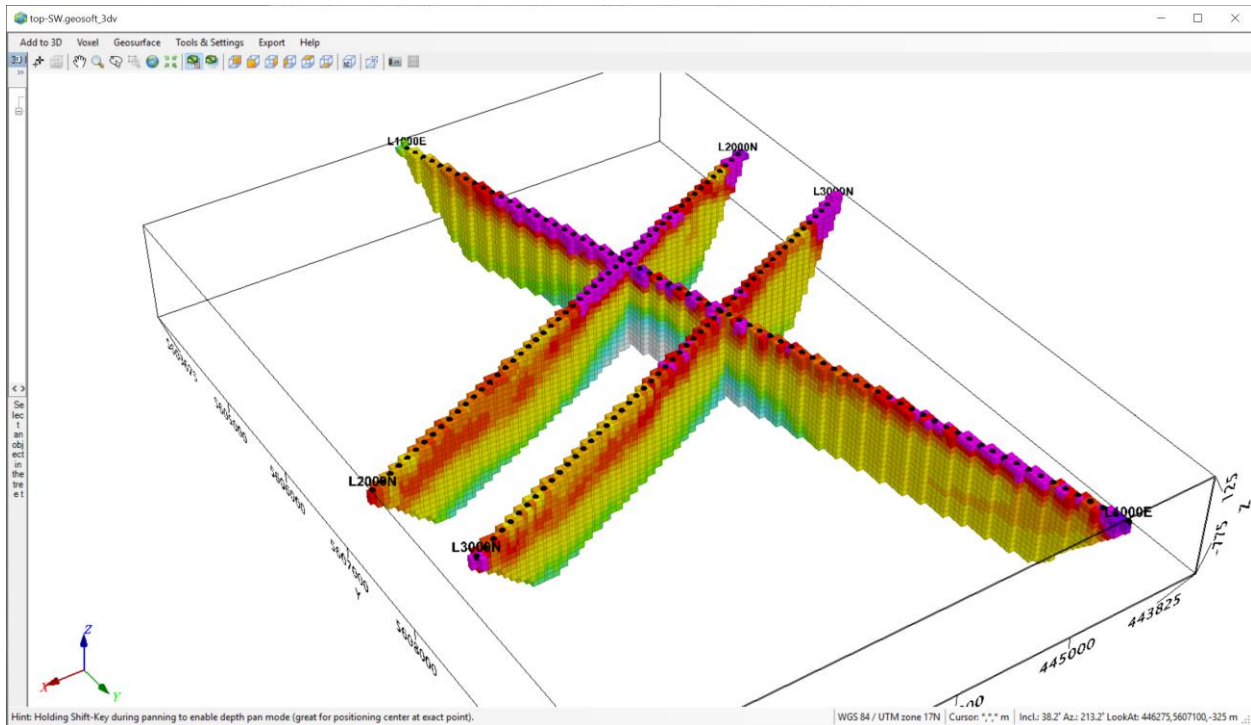


Figure 6-15: Resistivity models with colour scale 10-5000 Ohm-m

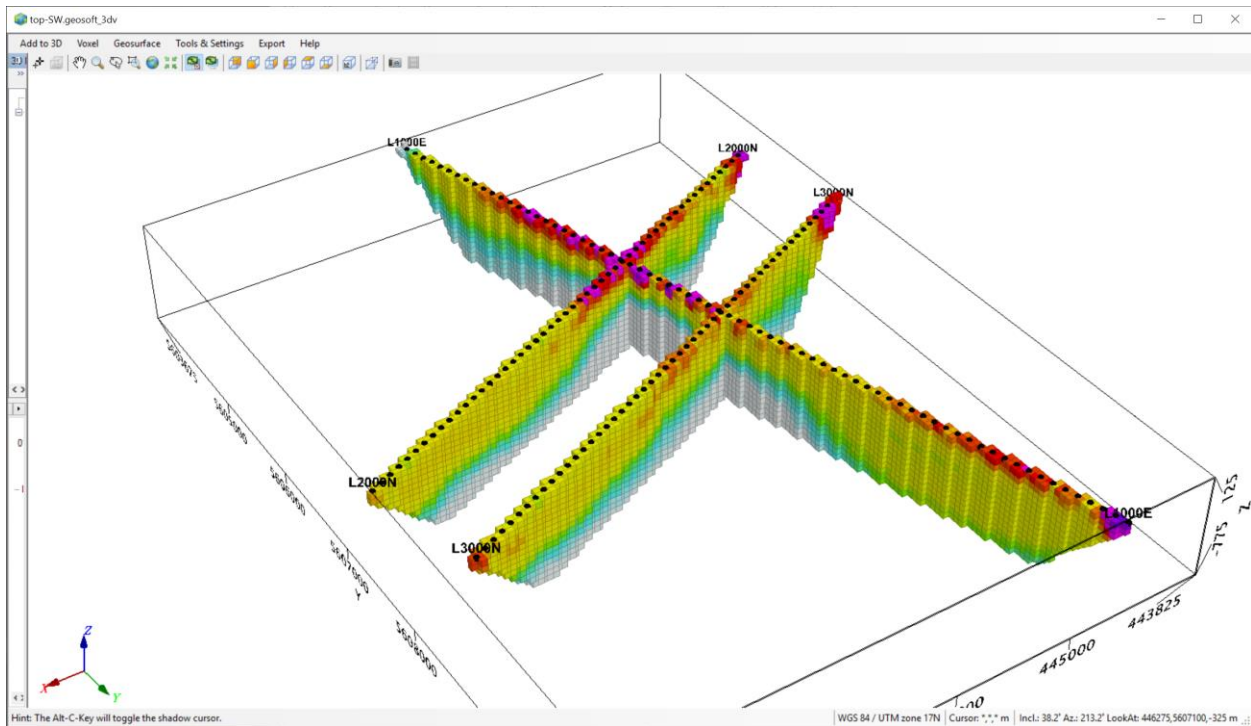


Figure 6-16: Resistivity models with colour scale 10-1000 Ohm-m

6.4.4. Resistivity models – view from top, look SW

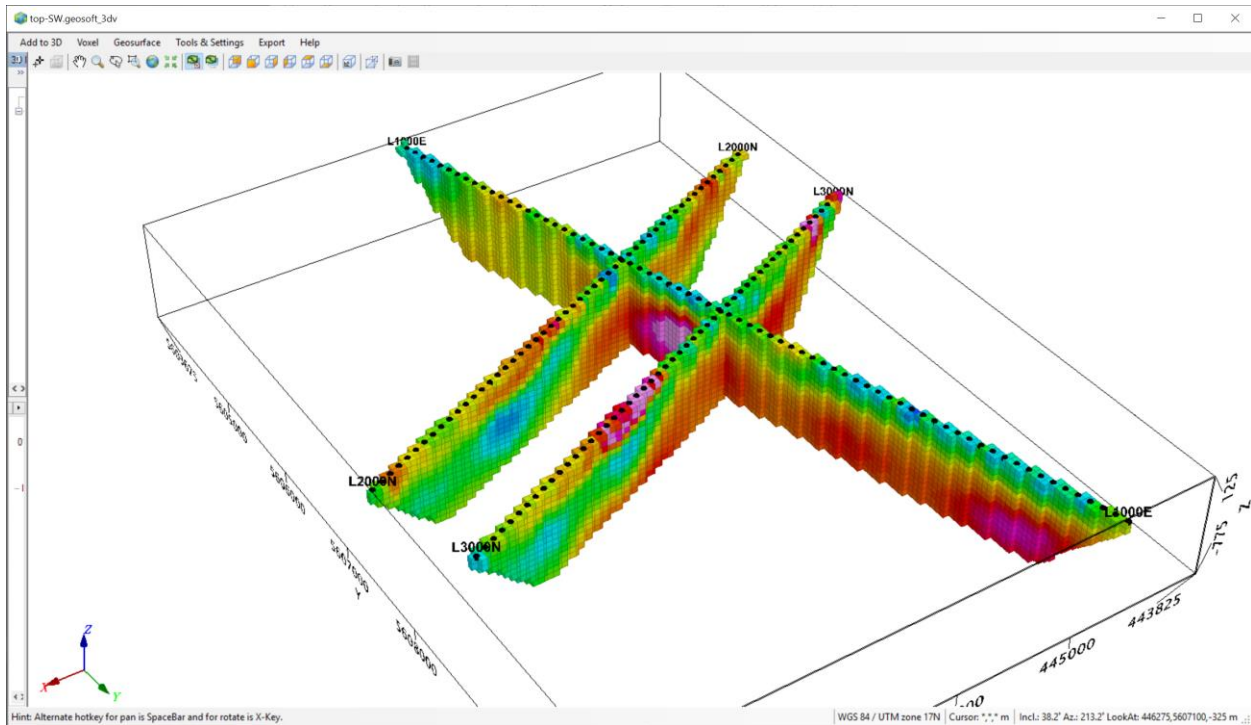


Figure 6-17: DC-referenced chargeability model

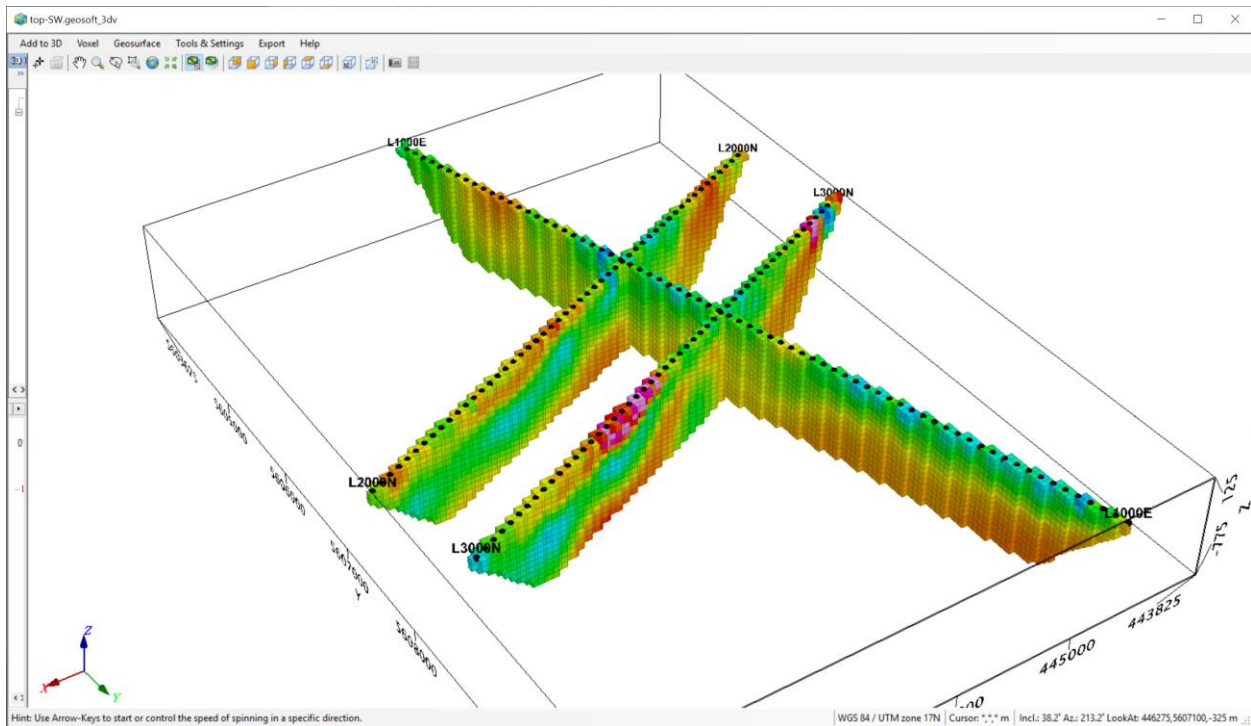


Figure 6-18: HS-referenced chargeability model

## 7. CONCLUSIONS AND RECOMMENDATIONS

This report presents the inversion results of the TITAN 24 DCIP survey completed from August 26 to September 7, 2019 over the Ranoke Project by Quantec Geoscience Ltd. on behalf of VR Resources Ltd.

The objective of the survey was to explore the possible occurrence of a chargeability feature associated with a high-gravity anomaly roughly 4 km in diameter, centered around 445786E, 5606127N (UTM Zone 17, WGS 84).

Three TITAN 24 DCIP lines were surveyed, L1000E with an azimuth of 345°, and lines L2000N and L3000N with an azimuth of 65°. The intersection points of L1000E with the other two lines are near the centre of the high gravity anomaly. Data were processed and inspected for quality assurance on site and reviewed daily by the geophysicist in charge of the project. Detailed information on the survey logistics, acquisition parameters, processing procedures, as well as presentation of the final processed data and digital archive formats are provided in this report. The measured data were analysed using 2D inversions, and the results are presented as 2D cross-sections of the resistivity and chargeability for each line.

The main feature observed in all three lines corresponds to a high-resistivity feature below approximately 250m depth, associated to a moderate chargeability feature, which correlate well with the high gravity zone. The resistivity feature extends approximately between stations 1900 and 4000 on L1000E, stations 1200 and 2500 on L2000E, and stations 1200 and 2000 on L3000N. L3000N shows a 500m gap in chargeability between stations 2000 and 2500, to the east of L1000E, which is not observed in the other sections, but is particularly evident in the HS-referenced chargeability section.

The moderate chargeability observed in all three lines could be caused by a chargeable mineral body, or alternatively it could originate from the resistivity contrast observed in the main anomaly at ~250 to 300m depth in the resistivity section. The similarities between the DC-referenced and HS-referenced chargeability models are such that it is not possible to determine the source of chargeability from the DCIP data.

On L1000E, a lower chargeability zone extends further to the north of the main feature, without a corresponding high in the resistivity. The source of this moderate chargeability does not appear to be directly related to the main high-resistivity feature observed in all the sections.

The L2000N resistivity section shows a moderate-to-low resistivity shallow feature below station 800, and this seems to be related to a non-symmetrical chargeability feature of moderate chargeability near the surface to the west side of the resistivity anomaly, and lower, deeper chargeability to the east. This may be indicative of a structure that serves as a boundary between different rock types, and charge accumulates preferentially on one side. An extension of the same feature may be occurring in L3000N, below station 400.

If further detailed DCIP studies are pursued in this area, it is recommended that they are done during the winter months, and with a full pole-dipole configuration, which would both improve the data quality and facilitate the access. This is because the frozen ground will not attenuate the signal as much as the muskeg in the summertime, and also distant stations can be accessed readily with snowmobiles, facilitating the installation of a distant infinite. Additionally, the acquisition of magnetotelluric (MT) data in conjunction with DCIP would allow observation of deeper phenomena, and may help identify intrusive structures that originate at great depths.

## 8. DELIVERABLES

The final deliverables include the following:

- GPS Data
  - Multi-site ASCII survey files
    - Each file includes location (Latitude/Longitude, projected UTM and local GRID coordinates) and elevation details
- Direct Current (DC) and Induced Polarisation (IP) Data
  - CSV formatted files
    - Each file includes electrode locations (GRID coordinates), normalised Potential (V) and measured phase (radians or milliradians) for all readings on the line.
- 2D inversion models of all the profiles, for Resistivity, DC-referenced chargeability, and HS-referenced chargeability
  - Geosoft databases and maps files, PNG images

### 8.1. FIELD DATA ARCHIVE

The raw field data are delivered on a hard disk drive and comprise the following:

Time Series:	Raw event files (e.g., Eventxxxx.dat), provided with log files having information on the location and time of the event (Quicklay digital format).
Processed DCIP Data:	Daily processing runs in QuickLay digital format saved as '.IP' files (results also saved as CSV files) linked with '#.Responses' folders that contain individual TxRx processed results (.mat files); Final processed results of DCIP data in ASCII (comma delimited) file format from QuickLay, containing final processed voltage and phase data. Description of the Quantec CSV file format is provided in APPENDIX E.

**8.2. DIGITAL ARCHIVE ATTACHED TO THE REPORT**

The digital archive accompanying this report contains the final processed data, including survey files, processing notes and a copy of this report. The digital archive is delivered on DVD.

Table 8-1: Contents of the digital archive attached to the report.

Directory	Contents
\Report	Summary report (.PDF)
\Data\Line#\DCIP	Final processed DCIP data (.CSV)
\Data\Line#\GPS	Location data
\Geosoft\BaseMaps	Base maps, location database, etc.
\Geosoft\Models	Section maps, model databases, PNG files, etc.

---

Respectfully submitted September 16, 2019 by Ryan Fearon, José Antonio Rodríguez

Quantec Geoscience Limited



## APPENDIX A. PRODUCTION SUMMARY

QUANTEC GEOSCIENCE LTD.				
Production Summary				
<b>Survey:</b>	Titan IP		<b>Client:</b>	VR
<b>Specs:</b>	Pole-dipole, Dipole-dipole a=200m		<b>Project Name:</b>	Ranoke
			<b>Project Number:</b>	CA01199T
Task	Date	Line	Survey Coverage (Km)	Daily Field Activity
Mob	23-Aug			Mob to Cochrane
Setup	24-Aug	L1000E		Sling gear to grid, set up approximately 2.4 km and doghouse.
Setup	25-Aug	L1000E		Finished setup from 7000N to 2400N.
Survey	26-Aug	L1000E	3.4	Rain all day. Survey dipole-dipole for half of line. Set up to 1600N. Strong tellurics all day.
Survey	27-Aug	L1000E	3.6	Survey southern half of line with dipole-dipole. Finished seup to 0N.
Survey	28-Aug	L1000E	6	Set up electrodes 100m off ends of line. Survey gradient. Survey pseudo-pole-dipole using electrodes on ends of line
Survey	29-Aug	L1000E		Pick up 5 km of L1000E
Survey	30-Aug	L2000N		Late start due to weather/visibility, arrive at noon. Start setup on L2000N, aproximatley 4km complete.
Survey	31-Aug	L2000N	5	Finished setup and survey line with Pole-dipole. Strong tellurics.
Survey	01-Sep	L2000N		Resurvey L2000N, pickup gear on north end of Line 1000E
Weather	02-Sep			Strong tellurics and rain, standby for weather.
Survey	03-Sep	L2000N		Resurvey L2000N tellurics settling down a bit.
Survey	04-Sep	L2000N		Pick up gear and start move to L3000N
Survey	05-Sep	L3000N		Weather delay in morning at Abitibi Canyon. Move all gear and doghouse to L3000N. Set up line
Survey	06-Sep	L3000N	5	Weather delay in morning between Cochrane and Otter Rapids. Survey L3000N
Survey	07-Sep	L3000N		Weather delay in morning in Cochrane. Pick up all gear and sling to Otter Rapids
Demob	08-Sep			Demob to Toronto



## APPENDIX B. SURVEY COVERAGE

### B.1. PROFILES

Line	Grid Coordinates		UTM Coordinates (WGS84, Zone 17N)			
	Start	End	Start		End	
			Easting	Northing	Easting	Northing
L1000E	0N	7000N	446405	5603746	444594	5610508
L2000N	0E	5000E	444156	5605333	448687	5607446
L3000N	0E	5000E	443897	5606299	448428	5608412

Note: information reported is first and last **receiver** electrode of each line.

#### B.1.1. DCIP Array

Line #	Spread #	Receiver		Current		Coverage	
		Start	End	Start	End	(1)	(2)
L1000E	n/a	0N	7000N	100N	6900N	7	6.8
L2000N	n/a	0E	5000E	100E	4900E	5	4.8
L3000N	n/a	0E	5000E	100E	4900E	5	4.8

(1) distance (km) from first to last **receiver** electrode of each spread;

(2) distance (km) from first to last electrode of each spread, including any current extensions.

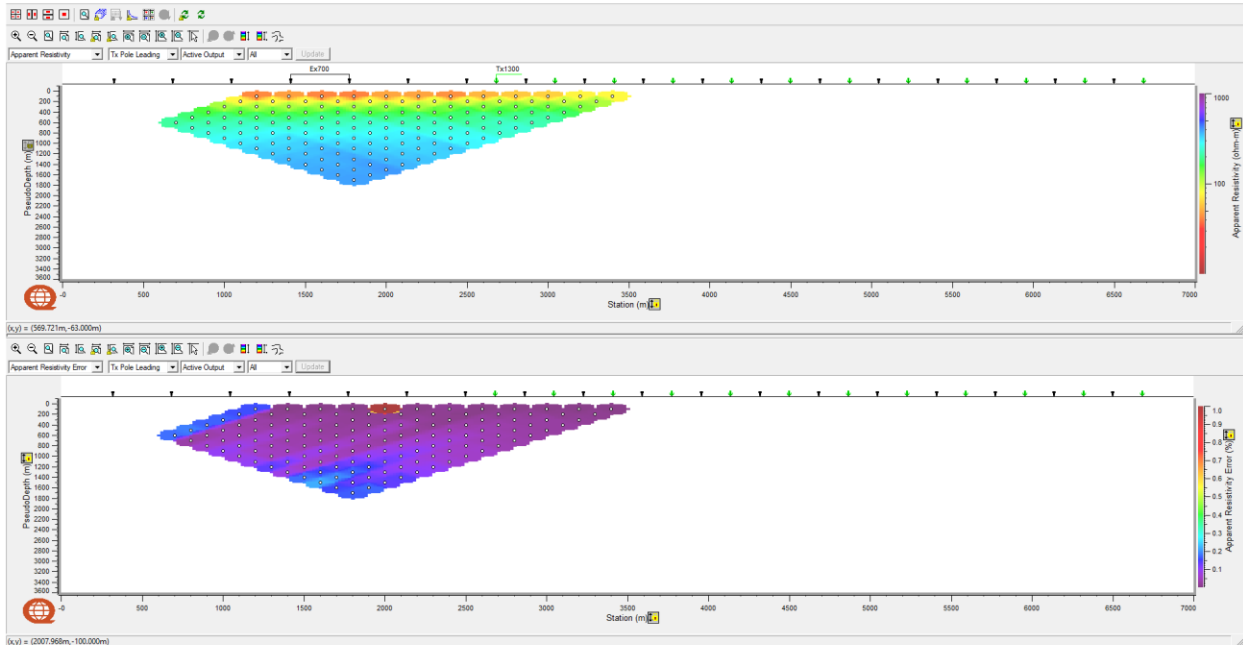
## **APPENDIX C. DCIP PSEUDOSECTIONS**

This section presents pseudosections of the final processed DCIP data on a line-by-line and spread-by-spread basis as:

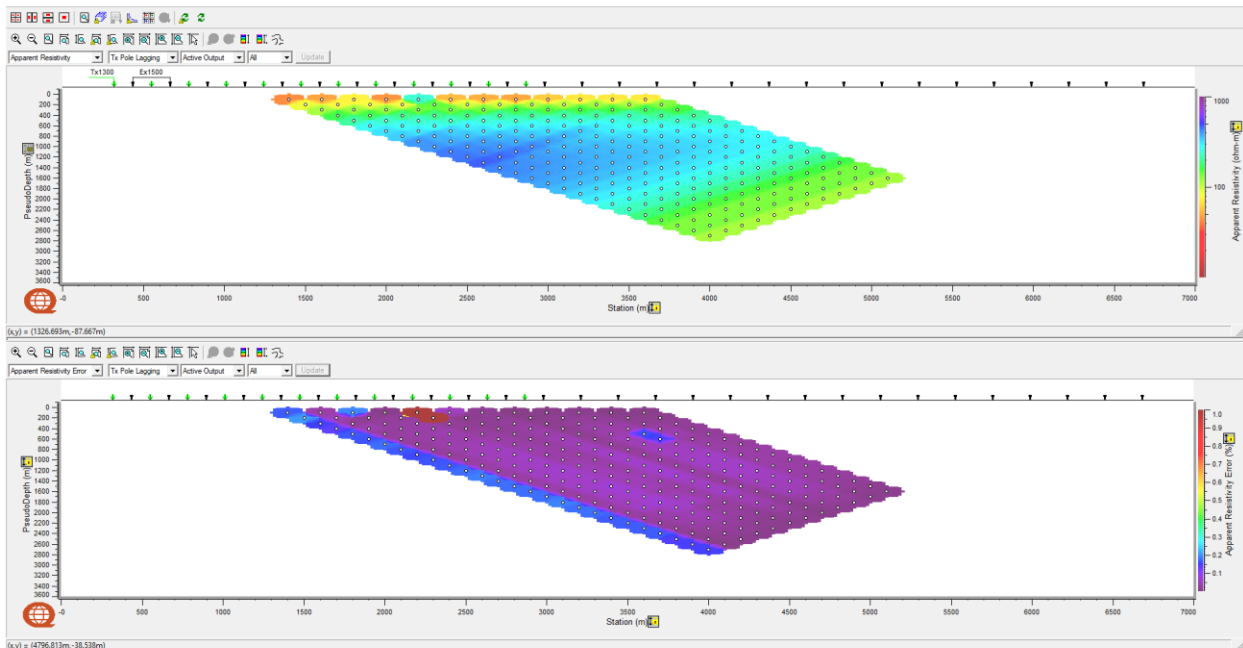
1. Observed Apparent Resistivity ( $\Omega\cdot\text{m}$ ) and Voltage Errors (%)
  - a. Transmitter (Tx) pole leading (i.e., right of) Receiver (Rx) dipoles
  - b. Transmitter (Tx) pole lagging (i.e., left of) Receiver (Rx) dipoles
2. Observed IP (mrad) and IP Errors (mrad)
  - a. Transmitter (Tx) pole leading (i.e., right of) Receiver (Rx) dipoles
  - b. Transmitter (Tx) pole lagging (i.e., left of) Receiver (Rx) dipoles

**C.1. LINE 1000E – NORTH INFINITE**

**C.1.1. Observed Apparent Resistivity ( $\Omega\cdot m$ ) and Voltage Errors (%)**

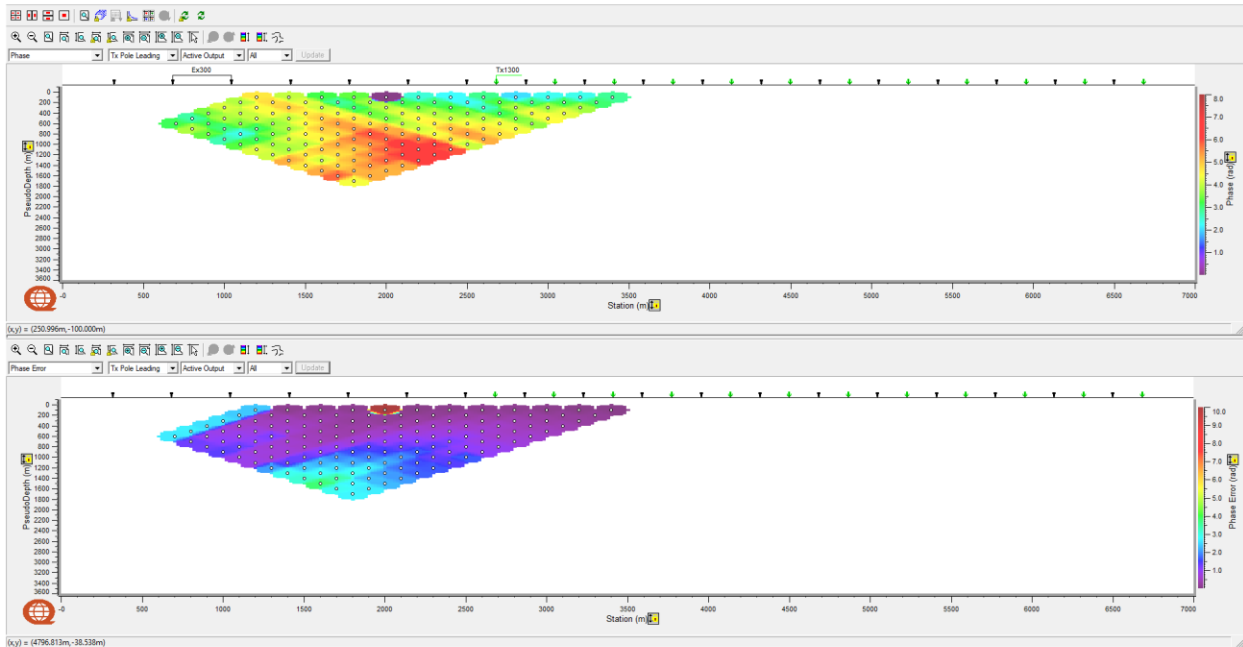


Tx pole leading receiver dipoles

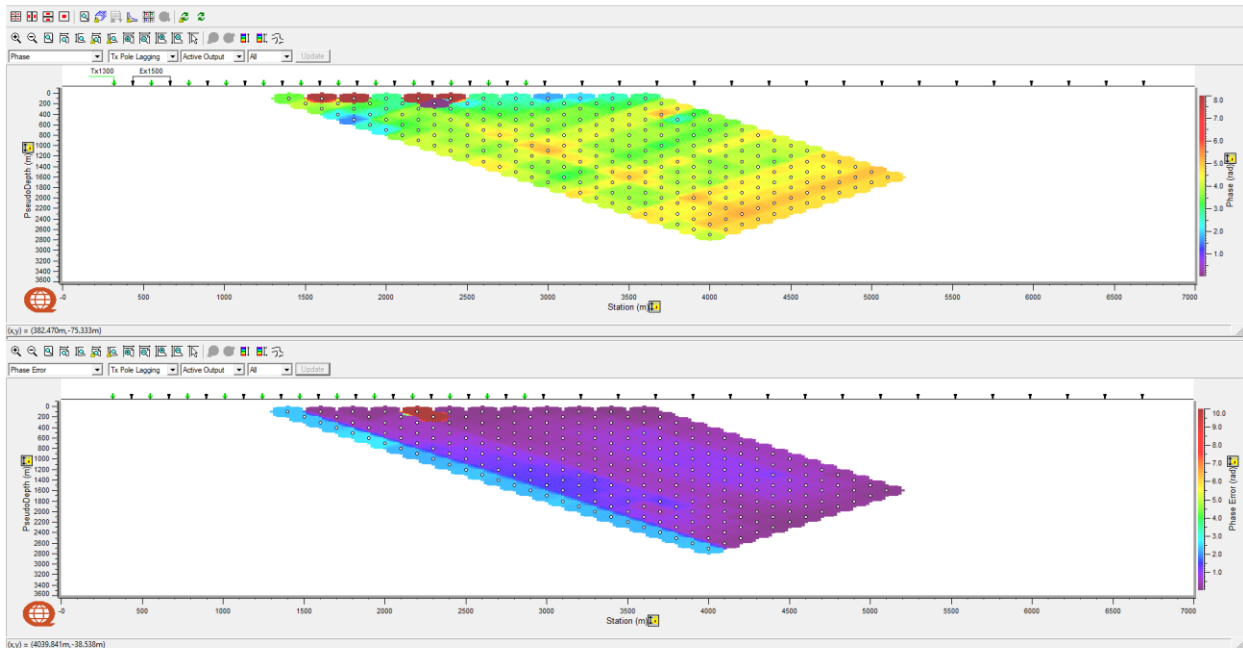


Tx pole lagging receiver dipoles

### C.1.2. Observed IP (mrad) and IP Errors (mrad)



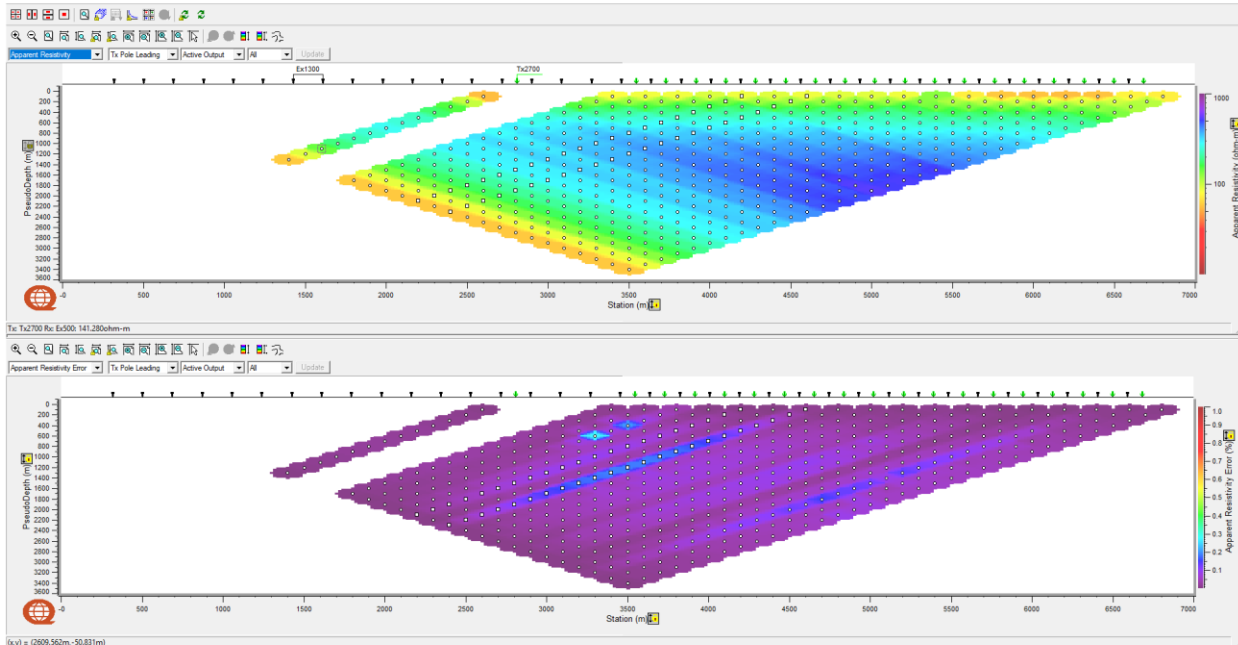
Tx pole leading receiver dipoles.



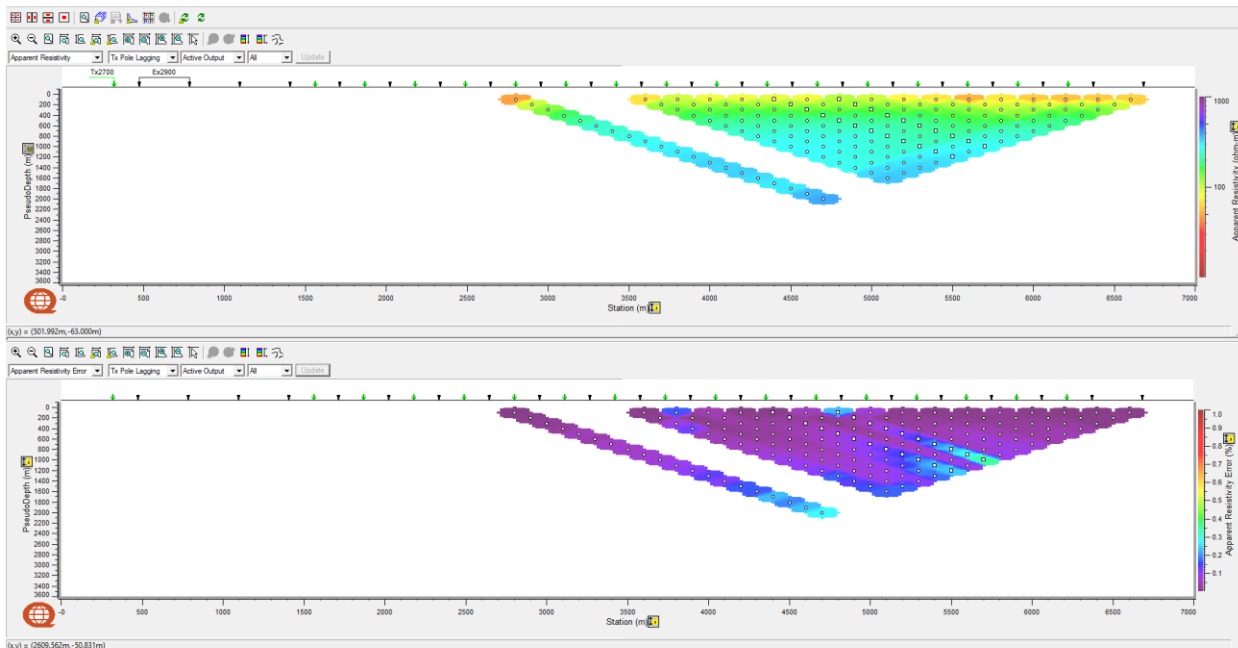
Tx pole lagging receiver dipoles.

## C.2. LINE 1000E – SOUTH INFINITE

### C.2.1. Observed Apparent Resistivity ( $\Omega\cdot m$ ) and Voltage Errors (%)

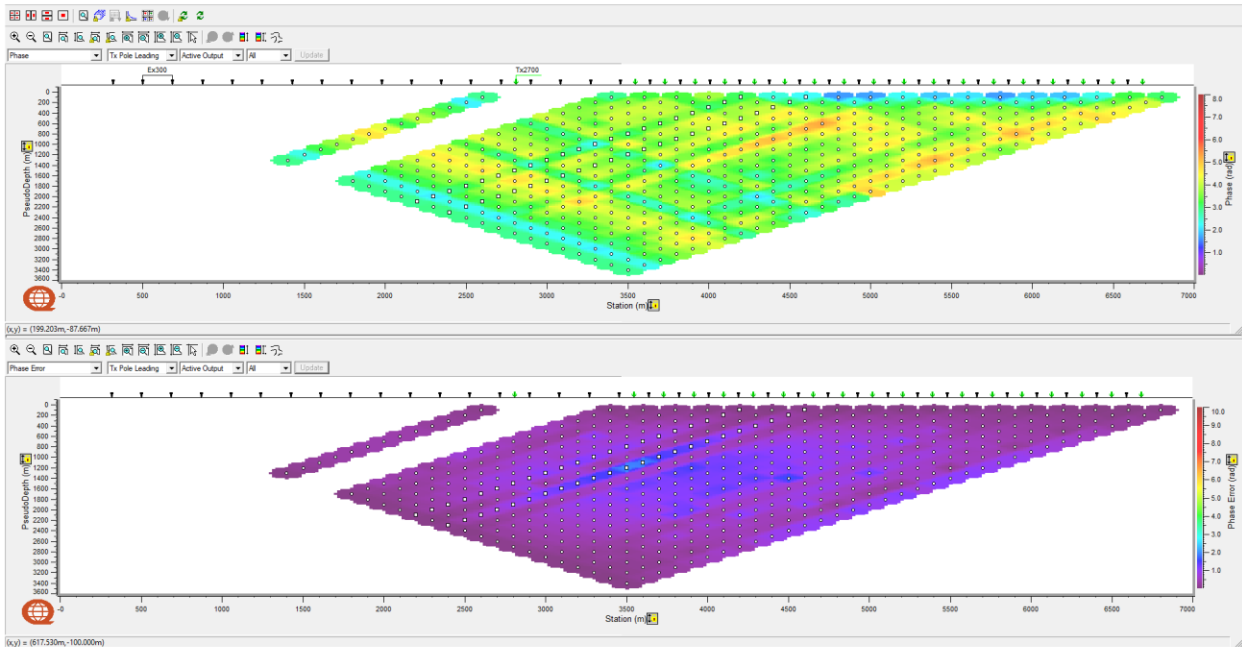


Tx pole leading receiver dipoles

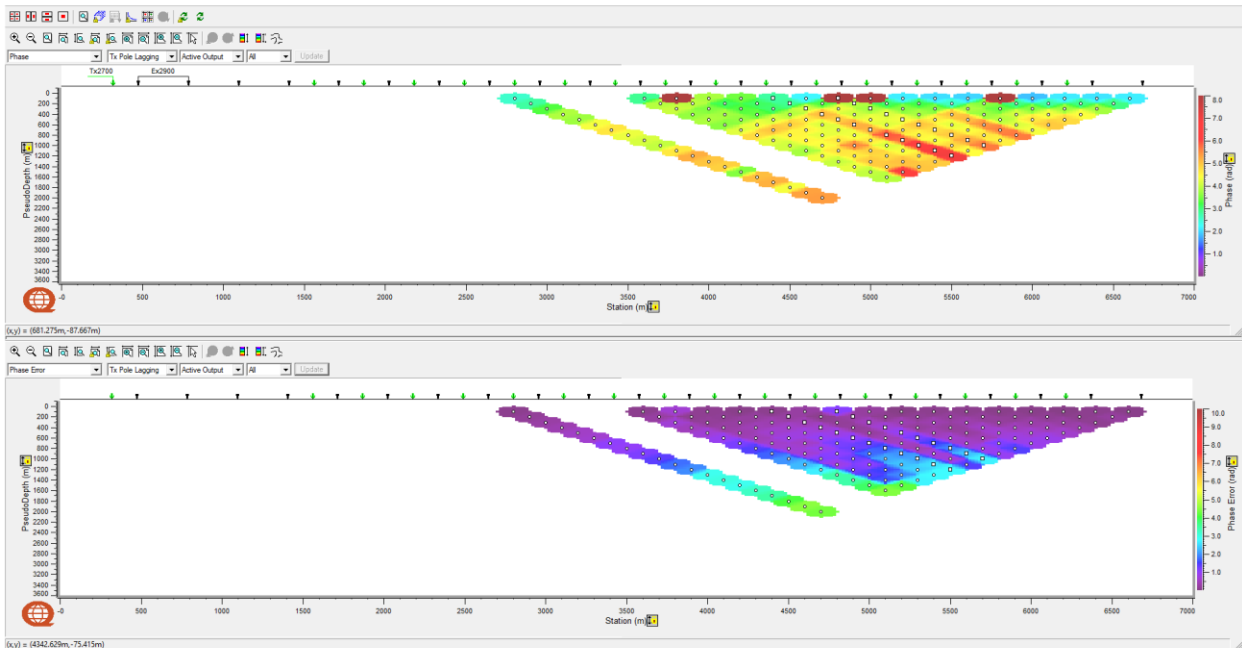


Tx pole lagging receiver dipoles

C.2.2. Observed IP (mrad) and IP Errors (mrad)



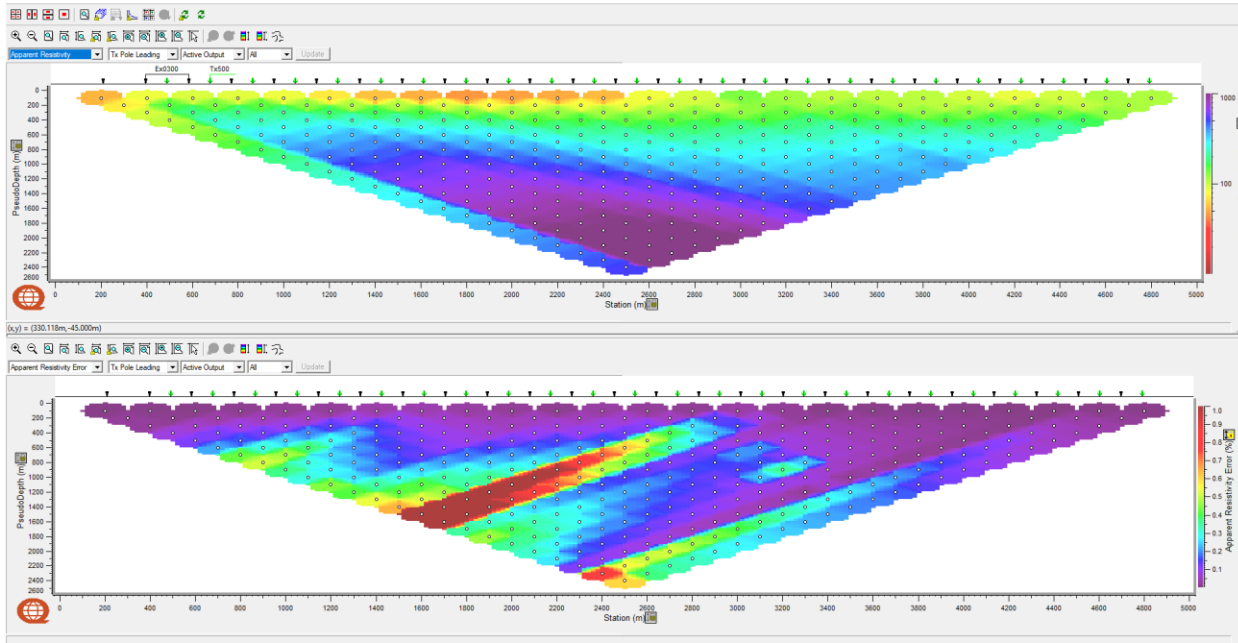
Tx pole leading receiver dipoles.



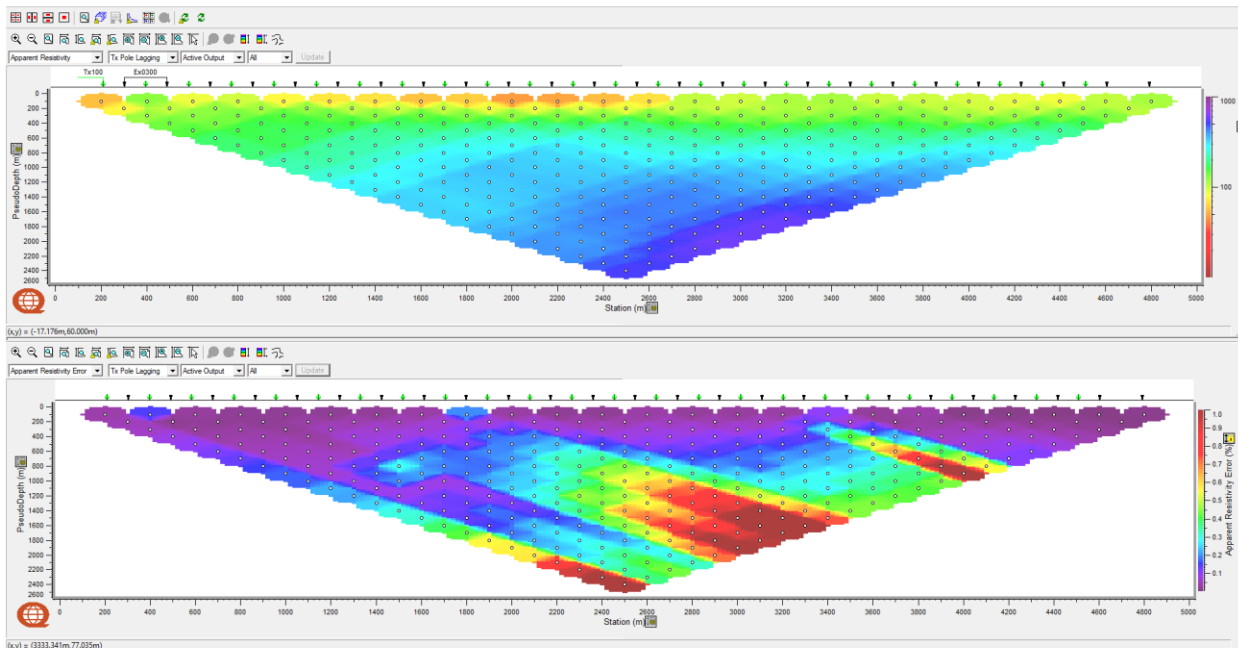
Tx pole lagging receiver dipoles.

**C.3. L2000N**

**C.3.1. Observed Apparent Resistivity ( $\Omega\text{-m}$ ) and Voltage Errors (%)**

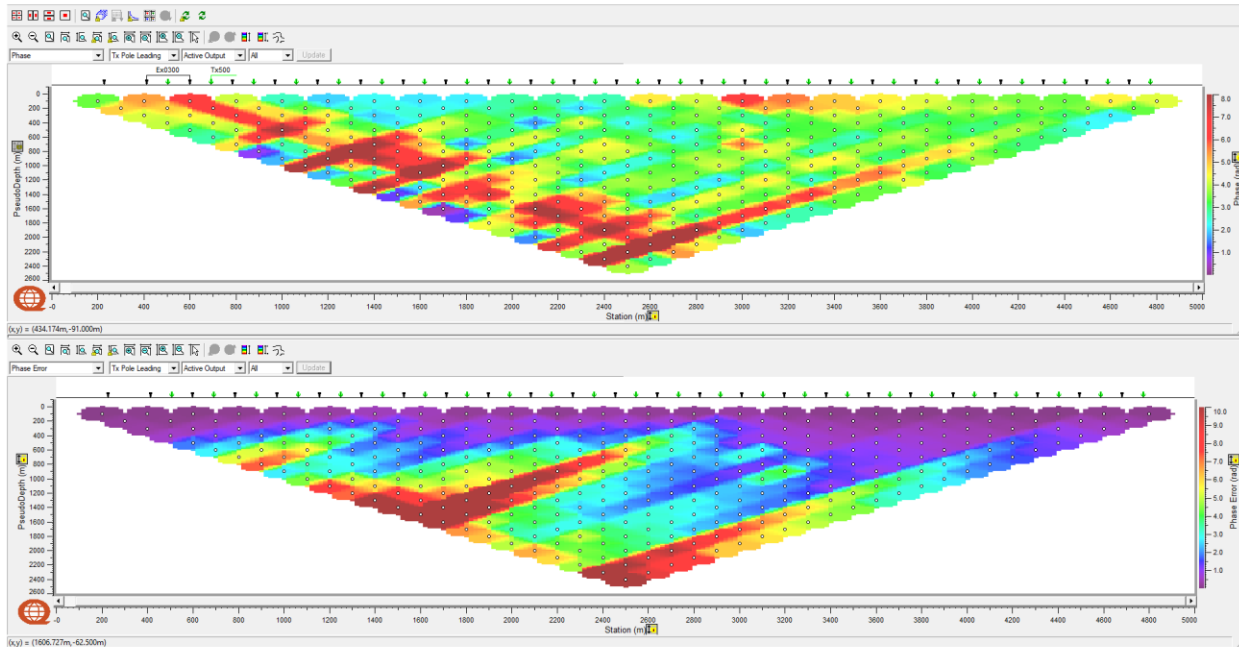


Tx pole leading receiver dipoles.

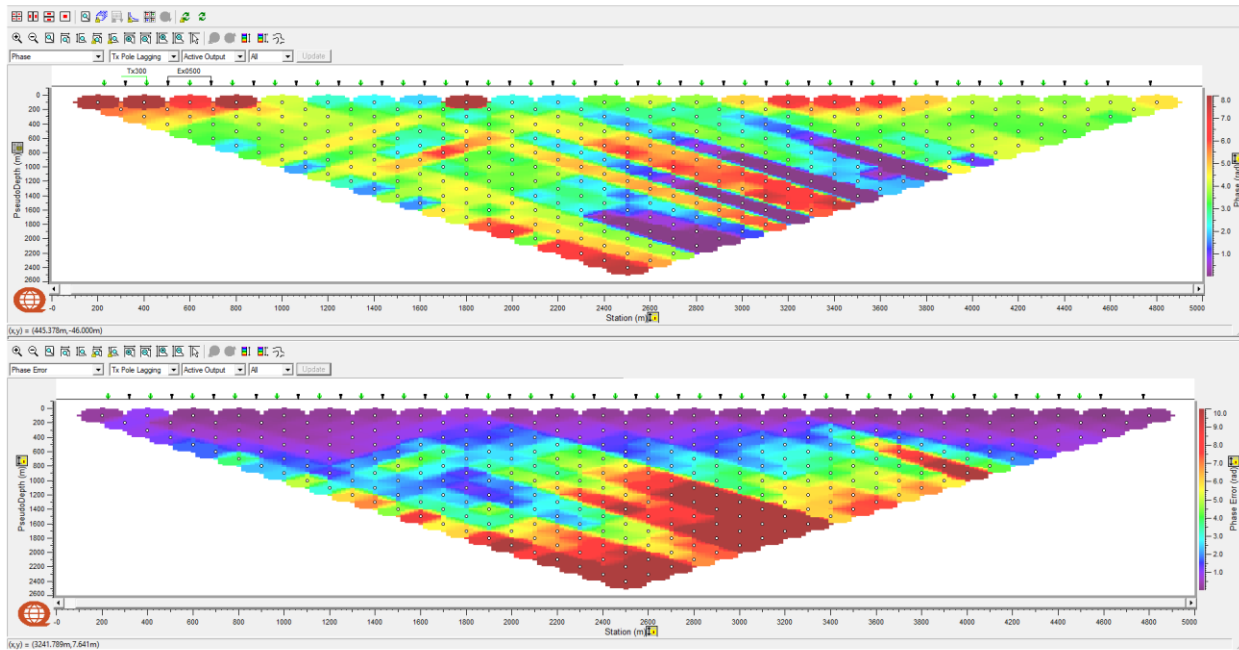


Tx pole lagging receiver dipoles.

C.3.2. Observed IP (mrad) and IP Errors (mrad)



Tx pole leading receiver dipoles.

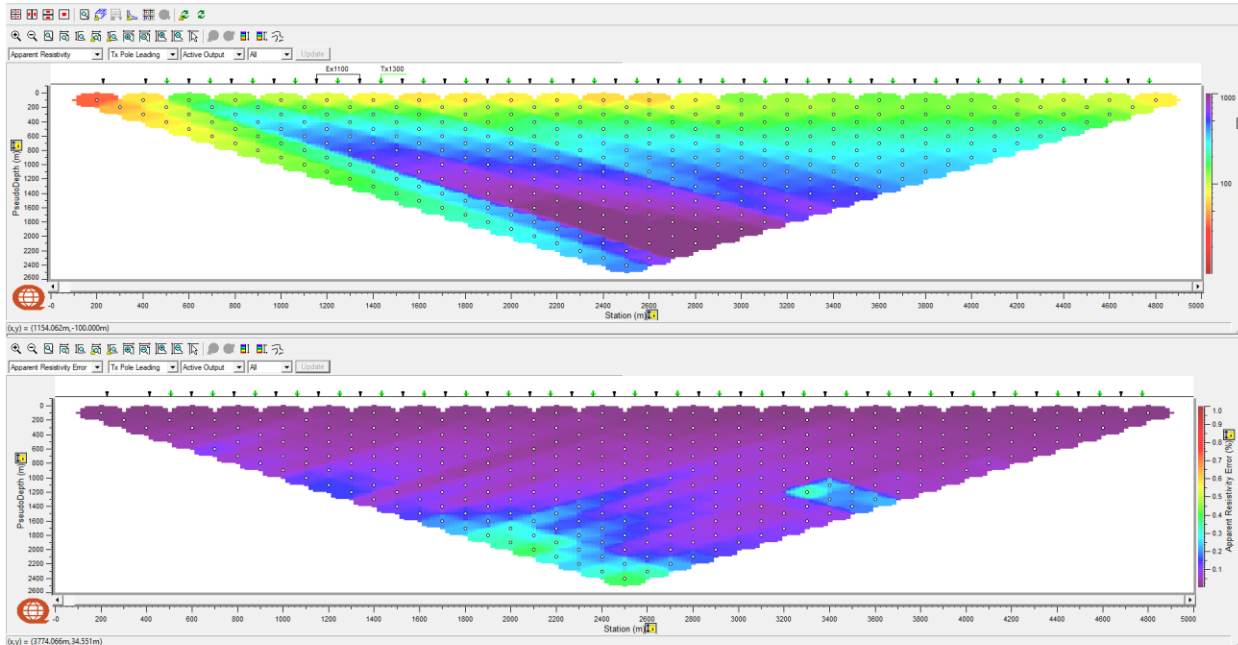


Tx pole lagging receiver dipoles.

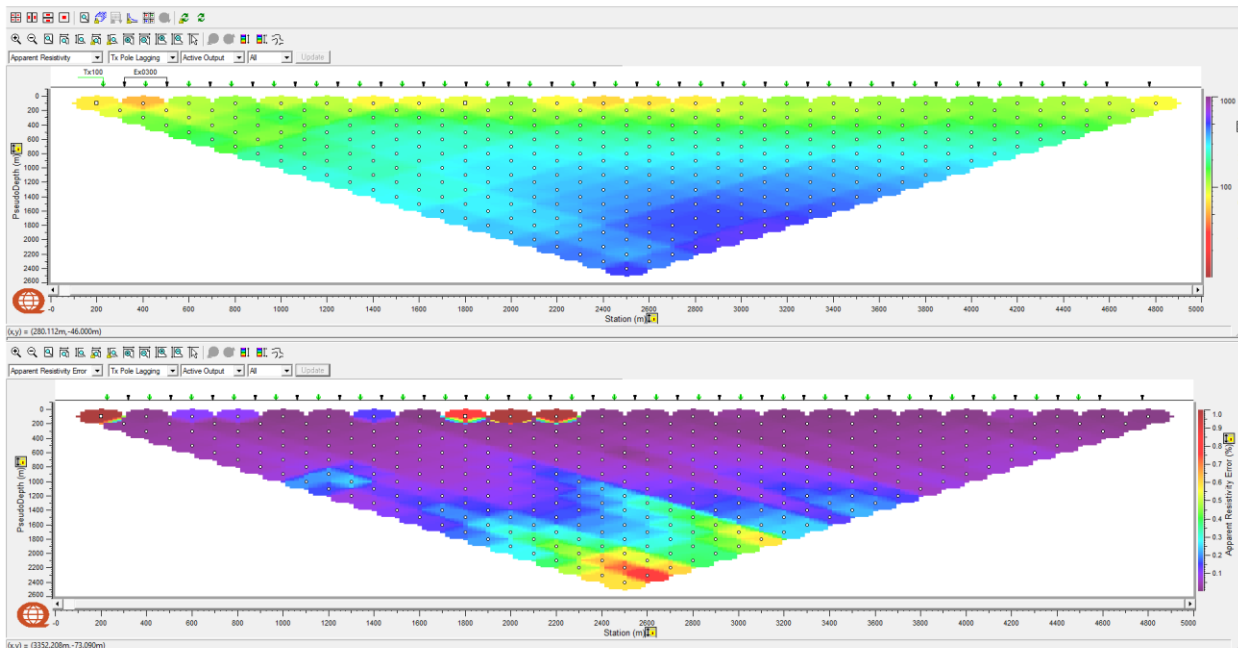


**C.4. L3000N**

**C.4.1. Observed Apparent Resistivity ( $\Omega\cdot m$ ) and Voltage Errors (%)**

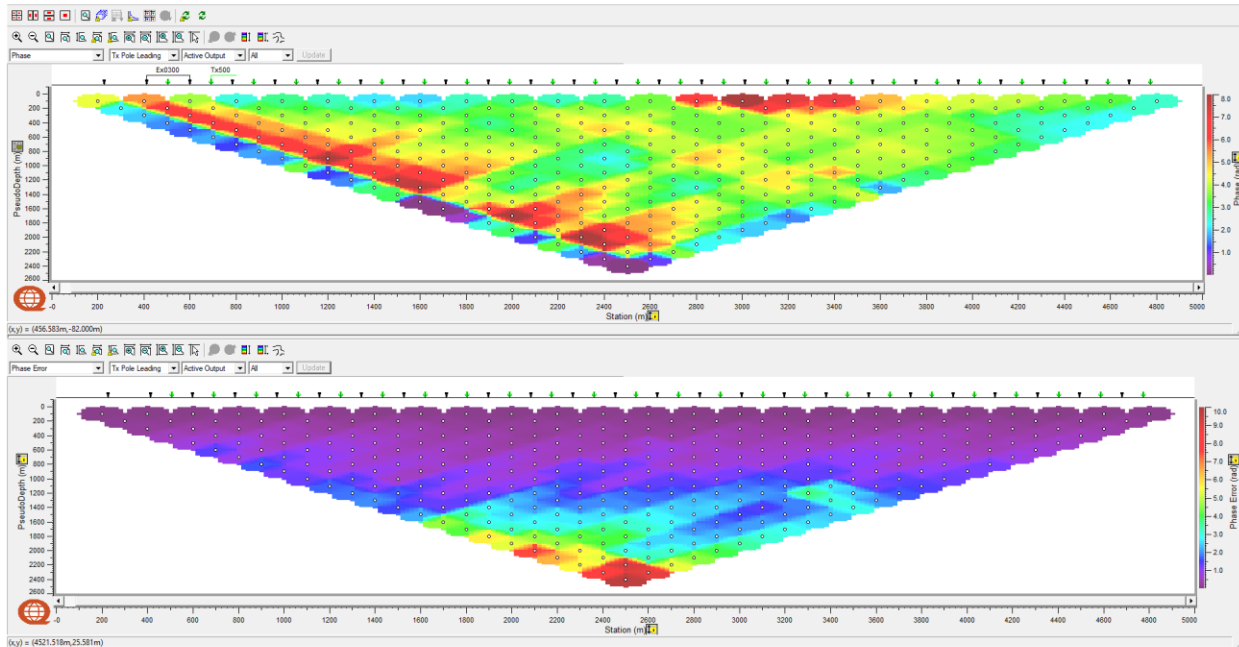


Tx pole leading receiver dipoles.

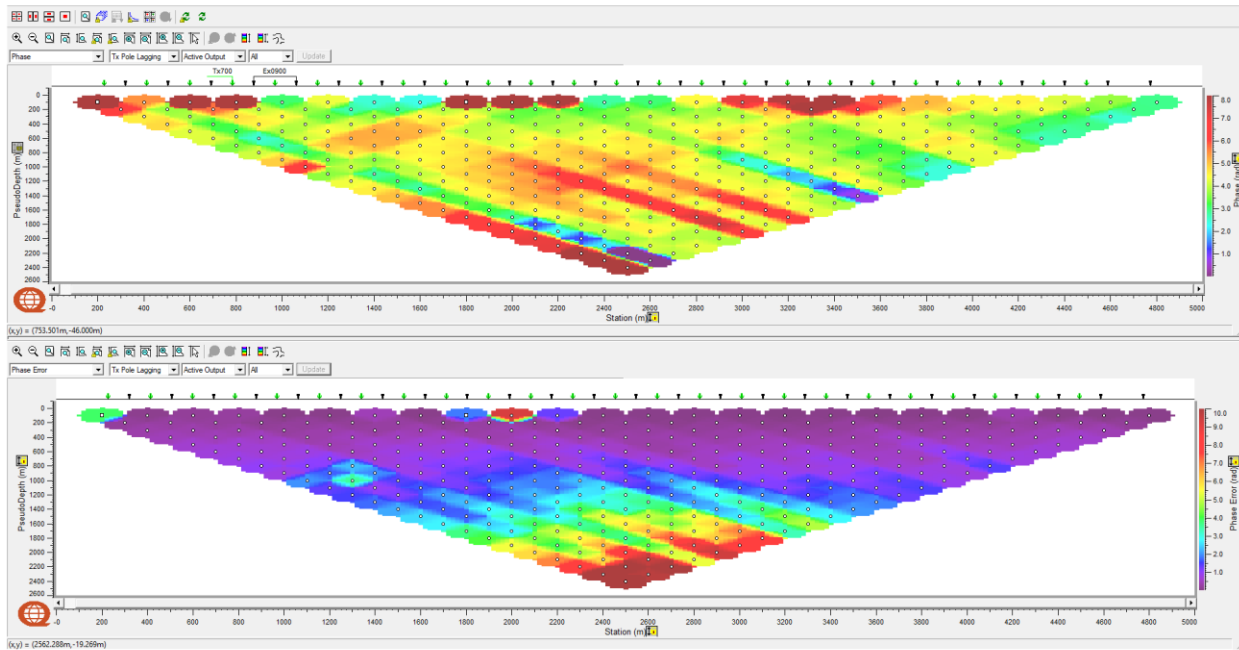


Tx pole lagging receiver dipoles.

C.4.2. Observed IP (mrad) and IP Errors (mrad)



Tx pole leading receiver dipoles.



Tx pole lagging receiver dipoles.

## APPENDIX D. INSTRUMENT SPECIFICATIONS

### A.1 REF TEK – 120 DATA ACQUISITION SYSTEM

Refraction Technology Inc. – Plano, Texas

#### Specifications:

Specification	Description
<b>Physical</b>	
Size:	267 x 248 x 184 mm / 10.5 x 9.75 x 7.25 in.
Weight:	3.7kg / 8 lbs (2-Channels maximum weight))
Temperature:	-40°C to 60°C operating range.
Environmental:	Operates in 1m of water without leaking for 48 hours. Airtight to 1.0 psi.
Shock:	Remains operational after 1m drop (any corner) onto cement floor.
<b>Connectors</b>	
Line A & Line B:	A pair of identical 10 pin U77/U style connectors. Each connector provides 3 pairs of lines (+): A (+)/B (-) Receive telemetry data and/or commands C (+)/D (-) Transmit telemetry data and/or commands E (+)/F (-) Sync
Power:	PTO7A12-8S style connector. Provides input +12 VDC supplied from battery.
Sensor:	PU283/U style connector. Provides for a direct connection from the AM to the sensor.
<b>Power Requirements</b>	
Battery:	Two 12 volt lead acid battery (7 Ah).
Input Impedance:	10 Mohm, 330 pF, differential
Broadband Dynamic Range:	130dB (noise power ratio test @ 125 sample per second [sps])
ADC Type:	Delta-sigma modulation
Sample Rate:	Multiple 50 to 48,000
Gain Settings:	Four – programmable for 1, 4, 16 and 64.

Specification		Description			
Sensor Input Signal Range:	Gain	24-Bit High Speed A/D		24-Bit Low Speed A/D	
		Actual	Reported	Actual	Reported
	1	1.192 $\mu$ V	78.12 mV	1.907 $\mu$ V	125.0 mV
	4	298.0 nV	19.53 mV	476.8 nV	31.25 mV
	16	74.51 nV	4.883 mV	119.2 nV	7.812 mV
	64	18.63 nV	1.221 mV	29.80 nV	1.953 mV
<b>Data Storage</b>					
Data Size:	32-bit two's compliment.				
Base Memory:	128K EPROM 6.5Mb SRAM				
Base Capacity:	Better than 1.5 million samples / approx. 190 min. continuous data @ 125 sps.				
<b>AM Telemetry</b>					
Protocol:	Full duplex synchronous data link control (SDLC).				
Error Correction:	Packet acknowledge with modulo 8 sliding window.				
Speed	3.072 Mb/second				
Encoding:	Bi-phase pulse = 1, missing pulse = 0				
Line Impedance:	100 Ohm				
<b>Synchronization</b>					
Timing:	Each AM on-line is timed and synchronized for simultaneous sampling within + 1.50 $\mu$ second.				
<b>Protection</b>					
Electrical Protection:	Line A and Line B signals circuits are protect by: - A surge arrester located on the RT514 board (SS1-14). - A line isolation transformer located on the RT514 board (T1-6) with over-voltage diodes (D1-4) on both sides of each secondary windings				
<b>State-of-Health</b>					
Information Provided:	The AM reports information on battery status, clock setting, gain setting, calibration mode and the communications link.				

### Sensor Calibration

The AM can source a 12.5 Hz, 50  $\mu$ A signal to the sensor input for measuring the source impedance of the attached sensor. The user can also specify frequency in amplitude of calibration signal.

### Telemetry Cable

The telemetry cable is a *Category V* specification cable and is supplied by the customer.

**Sample Rates**

The following table shows all available sample rates, based on a 12.288 Mhz oscillator. A 24-bit resolution ADC is used for sample rates 48000 through 4800 and a 24-bit resolution ADC is used for sample rates 3200 and below. The correct ADC is selected automatically by the AM, based on the sample rate.

Typically, different sample rates and transmitter frequencies are used in 50 Hz and 60 Hz power environments to minimize AC power effects on the data. In the table, the shaded areas indicate the sample rates typically used in a 60 Hz power environment. A few rates are typically used in both environments.

Sample Rate	Power Line
48000	50 & 60
24000	50 & 60
19200	60
16000	50
12000	50 & 60
9600	50 & 60
6400	50
4800	60
3200	50
1920	60
1600	50
960	60
800	50
480	60
400	50
240	60
200	50
120	60
100	50
60	60
50	50
60/2	60
50/2	50
60/4	60
50/4	50
60/8	60
50/8	50
60/16	60
50/16	50
60/32	60
50/32	50

## A.2 INSTRUMENTATION GDD MODEL TXII-5000



### 8. SPECIFICATIONS

<b>Size :</b>	TxII-5000W with a blue carrying case: 35 x 52 x 70 cm TxII-5000W only: 26 x 45 x 55 cm
<b>Weight :</b>	TxII-5000W with a blue carrying case: ~ 56kg TxII-5000W only: ~40 kg
<b>Operating Temperature :</b>	-40 °C to 65 °C (-40 °F to 150 °F)
<b>Time Base:</b>	2 s ON+, 2 s OFF, 2 s ON- Optional: 1, 2, 4 or 8 s 0.5, 1, 2 or 4 s DC
<b>Output current :</b>	0.030 A to 10 A (normal operation) 0.0 A to 10 A (cancel open loop) Maximum of 5 A in DC mode
<b>Rated Output Voltage :</b>	150V to 2400V Up to 4800V in a master/slave configuration
<b>LCD Display :</b>	<ul style="list-style-type: none"> <li>▪ Output current, 0.001 A resolution</li> <li>▪ Output power</li> <li>▪ Ground resistance (when the transmitter is turned off)</li> </ul>
<b>Power source :</b>	220-240 V / 50-60 Hz



## APPENDIX E. QUANTEC DCIP CSV FILE FORMAT

	Column headings	Description	Units
1	Event No	Event number; '*' is used for the average	
2	Tx SiteID	Transmitter site ID (e.g., 75)	
3	Rx SiteID	Receiver site ID (e.g., Rx150)	
4 to 15	C1-x, -y, -z, ...	C1-C2/P1-P2 positions	m
16	Current(A)	Current	A
17	CurrentErr(A)	Current error	A
18	Vp(mV)	Voltage	mV
19	VpErr(mV)	Voltage error	mV
20	Phz(mrad)	Phase	milliradians
21	PhzErr(mrad)	Phase Error	milliradians
22	AppRes(ohm-m)	Apparent Resistivity	$\Omega \cdot m$
23	ContactRes(ohm)	Contact Resistance	$\Omega$
24	Chargeability(mV/V)	Chargeability	mV/V
25	ChargeabilityErr(mV/V)	Chargeability Error	mV/V
26	SP(mV)	Self-Potential	mV
27	StacksKept	Number of Stacks used	
28	Tx(Hz)	Tx frequency	Hz
29	DutyCycle	Duty cycle (full or half)	
30	Event Time	Event time [yyyy.mm.dd hh.mm.ss.ssss]	
31	Duration(s)	Duration	s
32	IPWindowStart(s)	Decay window Start time	s
33	IPWindowEnd(s)	Decay window End time	s
34	Samples	Number of Samples	
35	SampleInt(ms)	Sample Interval	ms



	<b>Column headings</b>	<b>Description</b>	<b>Units</b>
<b>36</b>	Time(ms)	TAG to indicate next values on the header are the time axis values of the decays; It has "Samples" values	
<b>37-N</b>	<Double>	Y-value of the decay	mV/V

## APPENDIX F. QUANTEC IP PROCESSING

### F.1. HALVERSON-WAIT CHARGEABILITY MODEL

Quantec IP chargeability is described using the Halverson-Wait spectral model (Halverson et al., 1981) which is similar to the Cole-Cole model proposed by Pelton et al. (1978). The formulation is based on a simple relaxation model that fits complex (frequency-dependant) resistivity data.

The time domain chargeability, originally proposed by Siegel (1959), is defined (Telford et al., 1976) as:

$$M = \frac{1}{V_c} \int_{t_1}^{t_2} V(t) dt$$

where  $V(t)$  is the residual or secondary voltage at a time  $t$  that is decaying after the current is cut off, between time  $t_1$  and  $t_2$  with the steady voltage  $V_c$  during the current flow interval. The ratio  $V(t)/V_c$  is expressed in millivolts per volts (mV/V).

In the frequency domain, the “frequency effect” is defined as:

$$FE = \frac{(\rho_{DC} - \rho_{AC})}{\rho_{AC}}$$

where  $\rho_{DC}$  and  $\rho_{AC}$  are the apparent resistivity's measured at DC and “very high” frequency, usually in the 0.1 to 10 Hz range.

The Cole-Cole model for the chargeability  $m$ , as defined by Pelton et al. (1978) is given by the following:

$$Z(\omega) = R_0 \left[ 1 - m \left( 1 - \frac{1}{1 + (i\omega\tau)^c} \right) \right]$$

where  $Z(\omega)$  is the complex impedance with  $\omega$  the angular frequency in Hz,  $R_0$  the DC resistivity,  $m$  the chargeability in volts per volt,  $\tau$  the time constant in seconds, and  $c$  is the frequency dependence (unit less). The latter two physical properties describe the shape of the decay curve in time domain or the phase spectrum in frequency domain, and commonly range between 0.01s to +100s and 0.1 to +0.5, respectively (Johnson, 1984).

The Halverson-Wait model was proposed by Halverson et al. (1981) as an extension to the Wait (1959) model of the impedance of “volume loading” of spheres, given by:

$$Z(\omega) = \frac{\rho}{G} \left[ 1 - 3V \left( 1 - \frac{3\delta}{1 + 2\delta} \right) \right]$$

where  $G$  is a geometric factor,  $\rho$  the resistivity of the media,  $V$  the volume loading (the volume fraction of chargeable “spheres”),  $\delta$  the sphere surface impedance. The Wait model was designed to

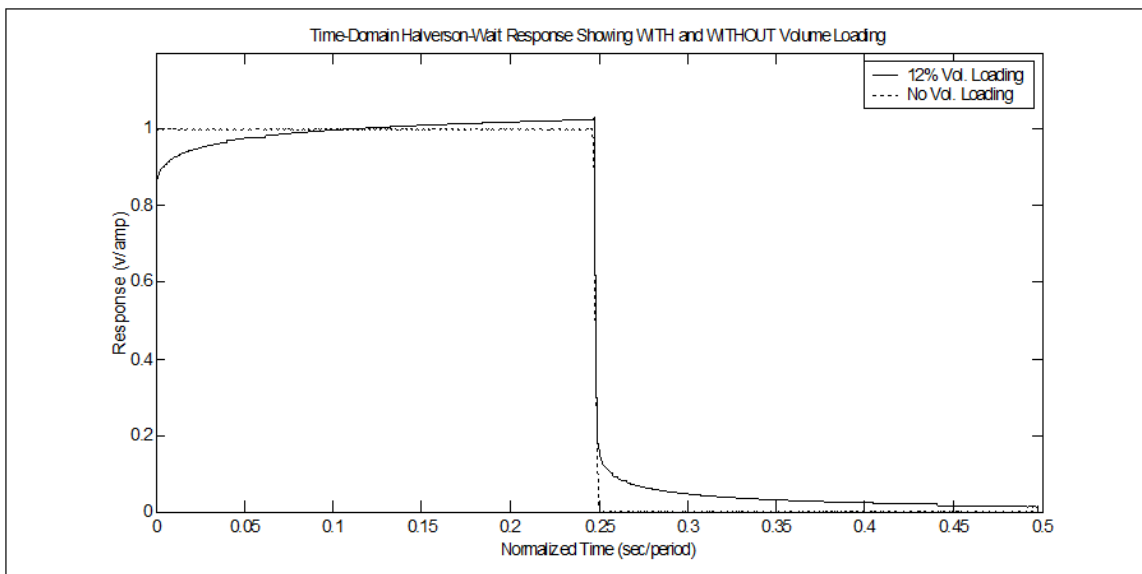
provide an explanation of the differences in the shape of decay curves from different polarisable targets but does not describe very well the physical attributes of the rocks.

The Halverson-Wait model expands the Wait coated sphere IP model to include a new formulation of the sulphide-rock interface impedance, based on field studies and laboratory tests on samples. It is closely correlated to the Pelton et al. (1978) Cole-Cole model and is given by:

$$Z(\omega) = \frac{\rho}{G} \left[ 1 - 3v \left( 1 - \frac{3/2}{1 + r[i\omega]^K} \right) \right]$$

where  $r$  is the sphere radius and is equivalent to  $\tau$  - the Cole-Cole time constant ( $r = \tau^K$ ). The volume loading  $V$  compares well to  $m$ , the Cole-Cole chargeability (see equation below), and the exponent  $K$  is equal to  $C$ , the Cole-Cole frequency dependence (Halverson et al., 1981). For sulphide systems, the  $r$ -factor reflects the size or inter-connectedness of the sulphide grains and the  $K$ -factor reflects the electrical characteristics of the sulphide surfaces.

An example of time domain Halverson-Wait model responses is shown below:



Polarisable versus Non-Polarisable TD-IP response using Halverson-Wait Model.

In the Halverson-Wait model the theoretical Percentage Frequency Effect (PFE)<sup>3</sup> (for infinite bandwidth), which equates to the theoretical chargeability in the Cole-Cole equation, is thereby defined by the volume loading:

$$\frac{PFE_0^\infty}{100} = m_0 = \frac{9v}{(2 + 3v)}$$

and  $m$  is output in units of milliradians (mrad).

<sup>3</sup> The classical definition of PFE is  $100 \times (\rho_0 - \rho_\infty) / \rho_0$ .

## F.2. QUANTEC PHASE IP UNITS

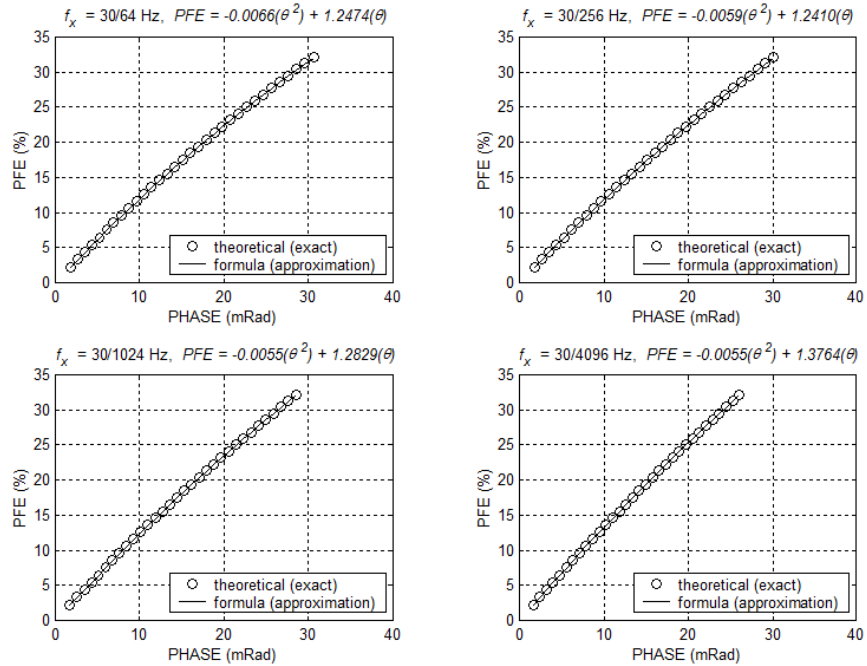
Quantec measures IP responses using a time domain half-duty square-wave excitation standard, but converts those chargeability results to units of phase. The specific procedure and algorithm is as follows:

1. Determine the earliest time for which EM coupling has died out sufficiently. This time is called the averaging or integration *start time*  $t_0$ . A typical value for  $t_0$  is 0.8 s from the start of the cycle;
2. Determine the latest charge/decay time that is minimally affected by sigma-delta and low-pass (usually Hanning window moving average) filtering, called the averaging or integration *end time*  $t_1$ . A typical value for  $t_1$  is 1.95s;
3. Adjust the *start time* ( $t_0$ ) so that  $t_1 - t_0$  (equated to number of samples) exactly spans an integer number of power-line signal periods. This can only be done for transmitted (fundamental) frequencies that are much lower than the power-line frequency;
4. Using the charge and decay sample numbers that equate to the averaging window<sup>4</sup> defined by  $t_0$  and  $t_1$ , calculate the average charge and decay voltages. This average may involve a non-uniform weighting to further improve rejection of power-line noise;
5. Calculate the theoretical Halverson-Wait half-duty time-domain response using identical filtering to that applied to the measured data response estimate, and presuming the following spectral parameters:
  - a. volume loading: 0.125 (this value is not important)
  - b. r – value: 1.0
  - c. k – value: 0.2
6. For the standard Halverson-Wait spectral parameters mentioned, the synthesized time-domain response and the  $t_1 - t_0$  averaging window, convert all estimated/measured charge and decay voltages (using the specified averaging window) to chargeability (millivolts/volt) and then to phase (milliradians).

This is the algorithm used in the data processing. The relationship between Quantec’s chargeability unit, phase in milliradians, and other frequency domain systems is straightforward; Quantec’s time-domain based phase equates to frequency domain-based phase, see figures next page.

---

<sup>4</sup> In practice this averaging window is tapered slightly to widen the stop-band notches and thereby provide enhanced power-line noise rejection.



Phase vs. PFE for various pulse lengths presuming standard Halverson-Wait spectral parameters (r-value = 1.0 and k-value = 0.2).

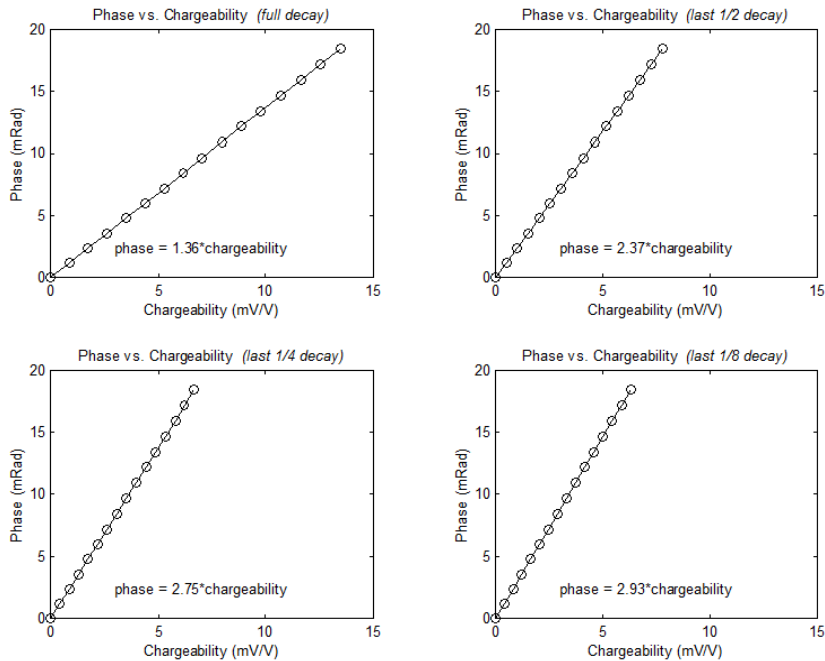


Illustration of the proportional relationship between phase (mrad) and chargeability (mV/V) for various charge/decay averaging windows

## **APPENDIX G. REFERENCES**

Telford., W.M., Geldart, L., Sheriff, R., and Keys, D., 1976. Applied Geophysics: Cambridge University Press, New York, NY.

### **G.1. DIRECT CURRENT (DC) AND INDUCED POLARISATION (IP) METHODS**

Halverson, M.O., Zinn, W.G., McAlister, E.O., Ellis, R., and Yates, W.C., 1981. Assessment of results of broad-band spectral IP field test. In: Advances in induced polarization and complex resistivity, 295-346, University of Arizona.

Johnson, I.M., 1984. Spectral induced polarization parameters as determined through time-domain measurements. *Geophysics*, 49, 1993-2003.

Pelton, W.H., Ward, S.H., Hallof, P.G., Sill, W.R., and Nelson, P.H., 1978. Mineral discrimination and removal of inductive coupling with multi-frequency IP. *Geophysics*, 43, 588-609.

Seigel, H.O., 1959. Mathematical formulation and type curves for induced polarization. *Geophysics*, 24, 547-565.

DCIP2D: A Program Library for Forward Modelling and Inversion of DC Resistivity and Induced polarization Data over 2D Structures, version 5.0. Developed under the consortium research project Joint/Cooperative Inversion of Geophysical and Geological Data, UBC-Geophysical Inversion Facility, Department of Earth and Ocean Sciences, University of British Columbia, Vancouver, British Columbia.

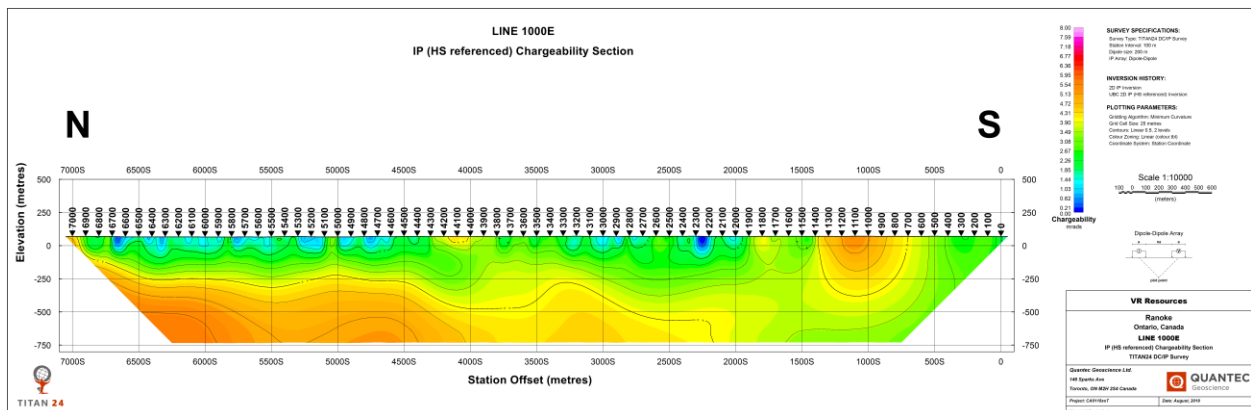
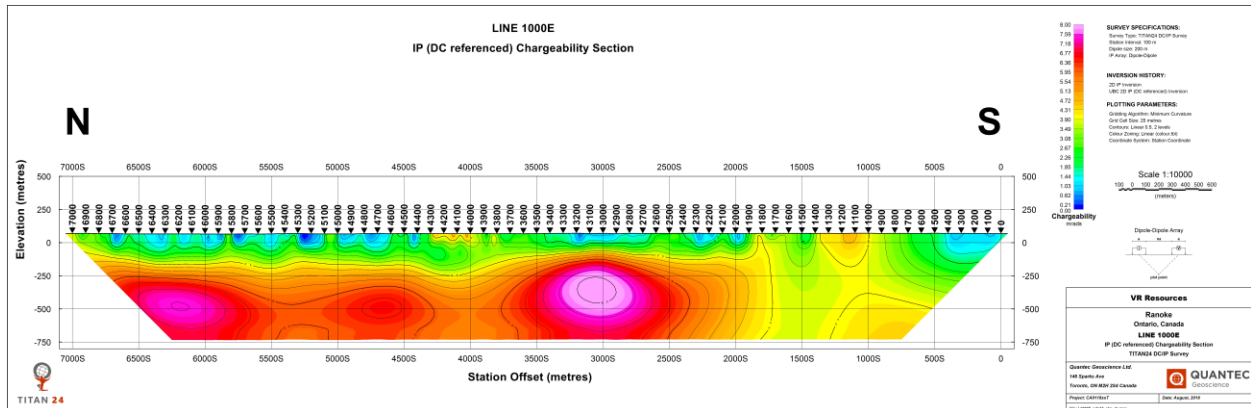
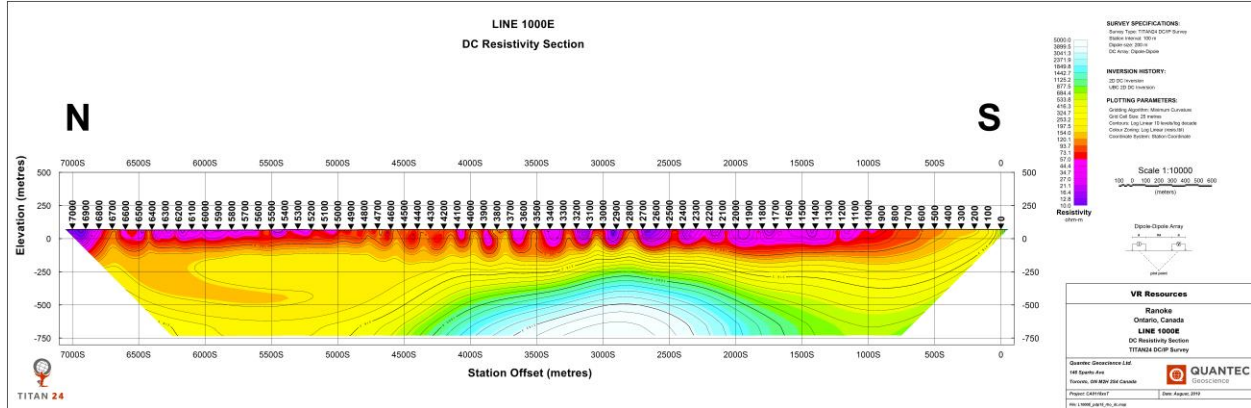
Li, Y., and Oldenburg, W., 2000. 3-D inversion of induced polarization data. *Geophysics*, v 65 (6), 1931-1945.

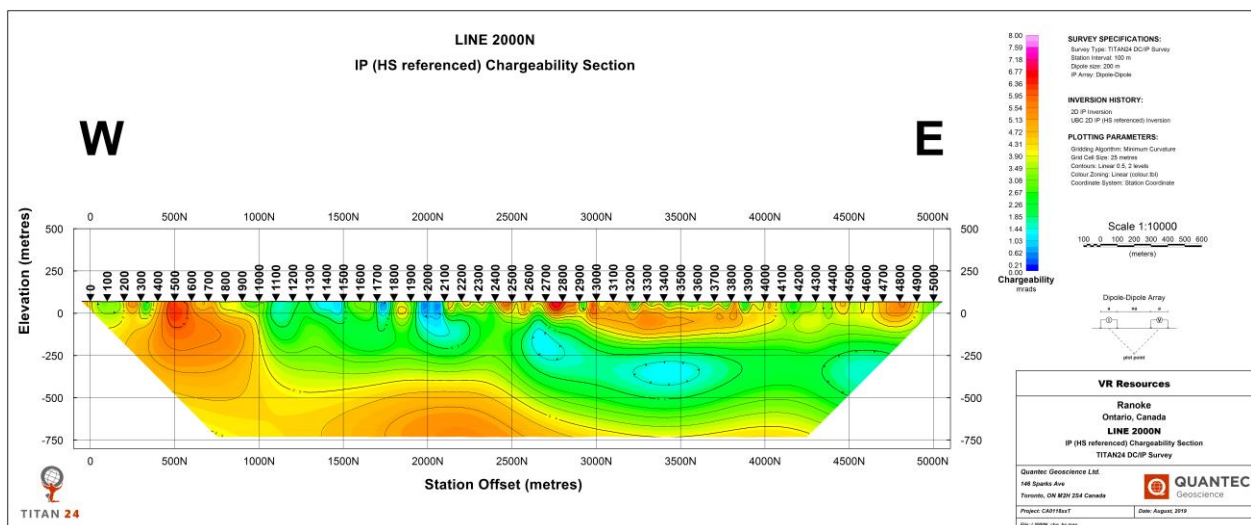
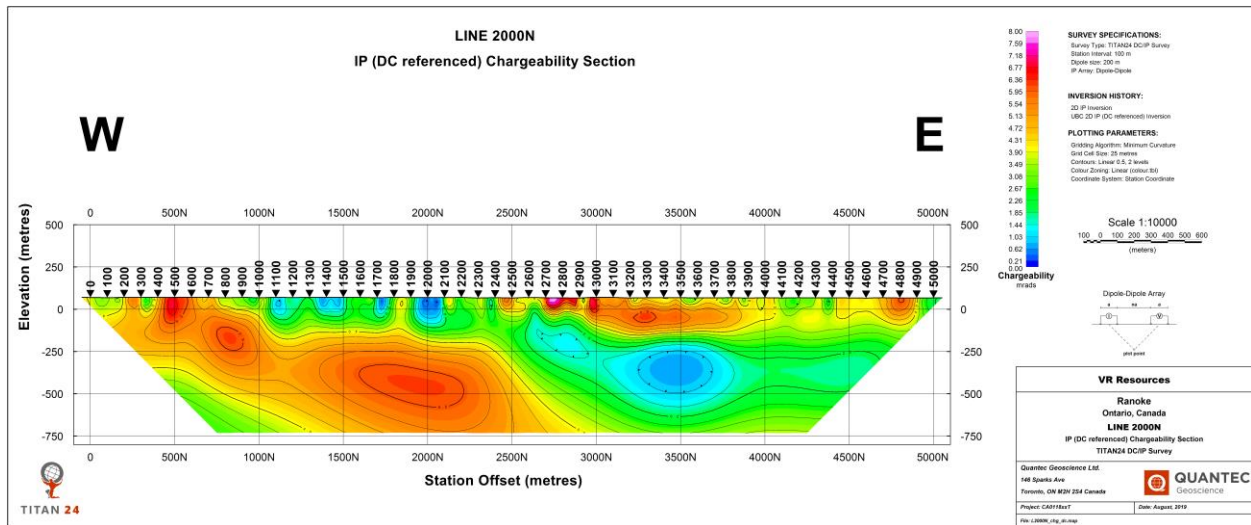
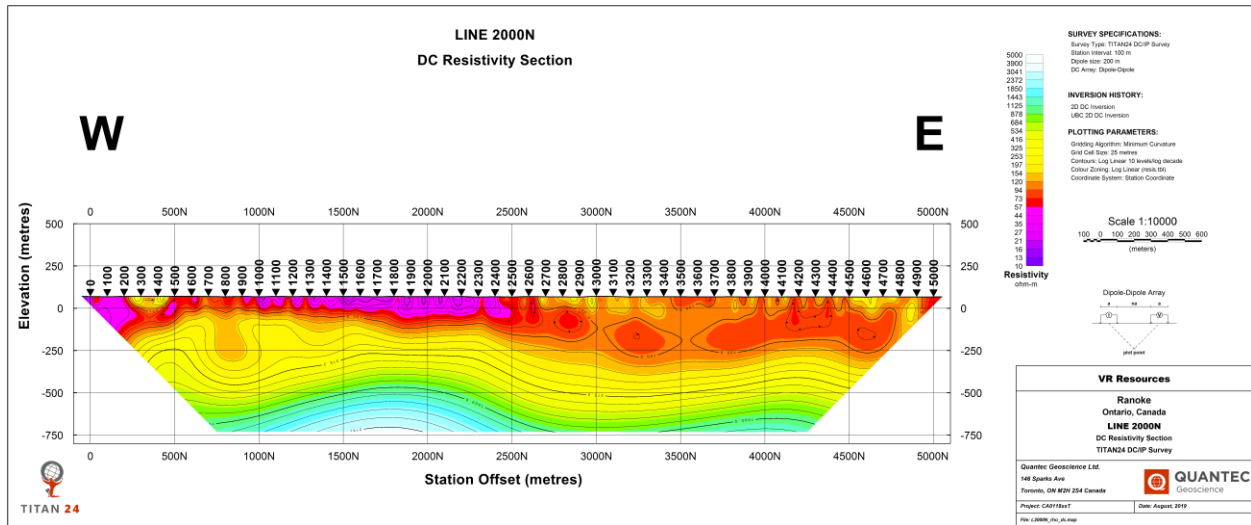
Oldenburg, D., and Li, Y., 1994. Inversion of induced polarization data. *Geophysics*, 59, 1327-1341.

Oldenburg, D., Li, Y., and Jones, F., 1998. Tutorial: Inversion (Res/IP) Methodology. In: The UBC-GIF Tutorials [<http://www.geop.ubc.ca/ubcgif>].

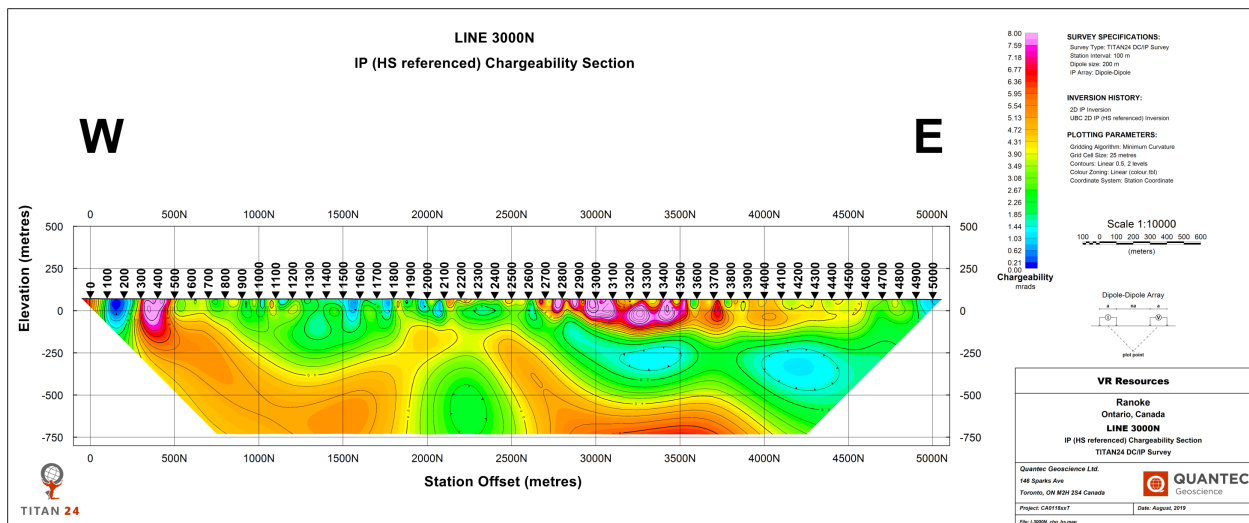
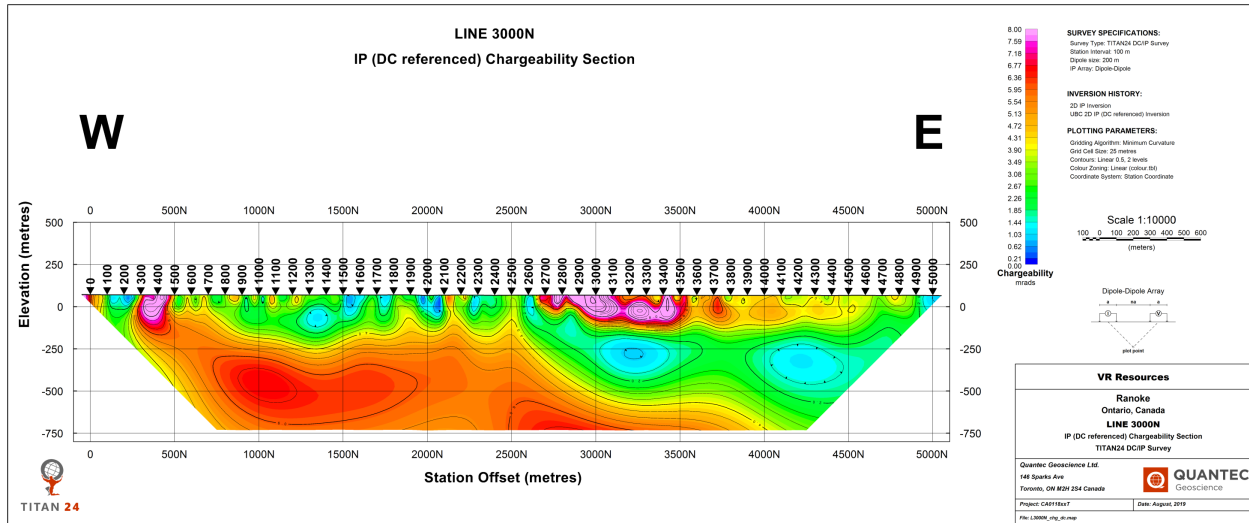
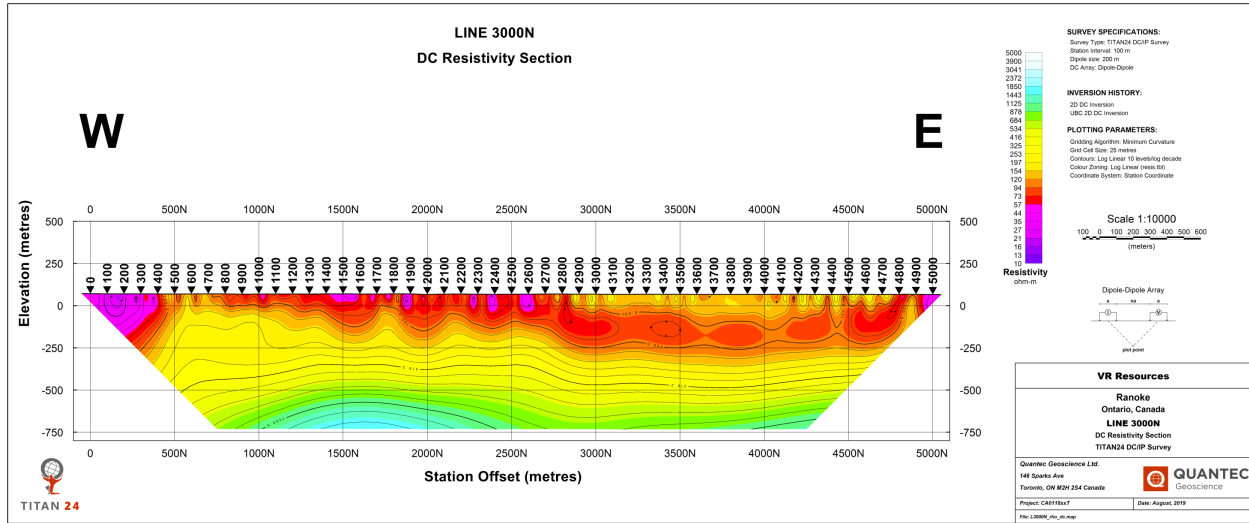
Oldenburg, D., and Li, Y., 1999. Estimating depth of investigation in DC and IP surveys. *Geophysics*, 64, 403-416.

## APPENDIX H. INVERSION SECTIONS









## SUMMARY INFORMATION

QUANTEC OFFICE INFORMATION	
Office:	Quantec Geoscience Ltd.
Address:	146 Sparks Ave., Toronto, ON, M2H 2S4, Canada
Phone:	+1-416-306-1941
Web:	<a href="http://quantecgeo.com">quantecgeo.com</a>
Email:	<a href="mailto:info@quantecgeoscience.com">info@quantecgeoscience.com</a>
PROJECT INFORMATION	
Client Name:	VR Resources
Project Name:	Ranoke Property
Project Location:	Cochrane, ON
Project Type:	Titan 24 DCIP
Project Number:	CA01199T
Project Manager:	Kevin Blackshaw
Project Period:	August 23 to September 8, 2019
Report Type:	Logistics Report
Report Author(s):	Ryan Fearon, José Antonio Rodríguez
Report date:	September 16, 2019
Revision History	N/A
Reference	<i>Summary Report for a Titan 24 DCIP survey over Ranoke Property (Cochrane, ON) on behalf of VR Resources. Quantec Geoscience Ltd.</i>
Template version	Version 3.0 – 2019/08/15